PRODUCTION AND EVALUATION OF SMOKE EMISSION COEFFICIENTS FROM MODIS MEASUREMENTS OF FIRE RADIATIVE POWER IN THE UNITED STATES

By

ANDREW PHEIFFER RENGEL

A thesis submitted in partial fulfillment of
the requirements for the degree of

MASTER OF SCIENCE IN ENVIRONMENTAL ENGINEERING

WASHINGTON STATE UNIVERSITY
Department of Civil & Environmental Engineering

MAY 2013

To the Faculty of Washington State University:

The members of the Committee appointed to examine the thesis of ANDREW PHEIFFER RENGEL find it satisfactory and recommended that it be accepted.

_____
Fok-Yan Leung, Ph.D., Chair

_____
Brian Lamb, Ph.D.

_____
Heping Liu, Ph.D.

ACKNOWLEDGEMENTS

I would like to take the opportunity to express my thanks to my advisor Dr. Fok-Yan Leung for his support and guidance during my Master's work at Washington State University. I would also like to thank Dr. Brian Lamb and Dr. Heping Liu for being on my thesis committee, and for their guidance, comments, and suggestions. Many thanks go to the outside collaborators from NASA Goddard for sharing their resources and valuable insight.

I want to thank the faculty in the Laboratory for Atmospheric Research for teaching fun and interesting classes to further my education. I also would like to thank my fellow graduate students for their insights and encouragement during my time here.

Finally, I would like to thank my family and friends for their love and support while I pursued my education thousands of miles from home.

PRODUCTION AND EVALUATION OF SMOKE EMISSION COEFFICIENTS FROM MODIS MEASUREMENTS OF FIRE RADIATIVE POWER IN THE UNITED STATES

Abstract

by Andrew Pheiffer Rengel, M.S.
Washington State University
May 2013

Chair: Fok-Yan Leung

Previous studies calculating smoke emission coefficients (C_e) from the correlation between fire radiative energy (FRE) and PM mass emission rates derived from aerosol optical thickness (AOT) measurements from the Moderate Resolution Imaging Spectroradiometer (MODIS) for wildland fires in the contiguous United States yielded poor correlation coefficients. Estimates of C_e, in kilograms per megajoule, were developed to utilize the direct linear relationship between MODIS-derived rates of release of fire radiant energy and the rate of release of smoke aerosols. To improve these smoke emission coefficients, the method for calculating C_e was modified to exclude fire pixel detections with scan angles greater than $\pm 40^o$ and to eliminate FRE and AOT retrievals that contained a cloud fraction greater than zero. This modified method was applied each year from 2003 to 2008 for the contiguous U.S., six regions, and thirteen land cover types. The average C_e for the U.S. was found to be 0.0193, ranged from 0.0092 to 0.0357 for the six regions, and from 0.0082 to 0.0435 for the thirteen land cover types. Average correlation coefficient values improved significantly from the previous studies. Uncertainties still remain as annual variability and outliers related to high FRE measurements are prevalent.

Evaluation of MODIS FRE-derived particulate matter ($PM_{2.5}$) emissions was performed through a comparison with $PM_{2.5}$ emissions from the BlueSky framework. Ten large fires from 2007 in the northwest were selected for comparison because of their size, duration, and primary land cover type. The comparison utilized Classification and Regression Trees (CART) to explore the influence of meteorology, fuel characteristics, and geographic factors on the difference between the $PM_{2.5}$ estimates from both methods. The classification tree showed that the fuel loadings and soil moisture drove the over or under estimation of the MODIS $PM_{2.5}$ emissions by BlueSky. A separate regression tree showed that the numeric difference between these two $PM_{2.5}$ emissions estimates is driven by the maximum planetary boundary layer height and soil moisture. The presence of soil moisture in both CART results suggests it is a critical factor in the value of the emissions.

TABLE OF CONTENTS

Page

LIST OF TABLES

CHAPTER 2

CHAPTER 3

APPENDIX

LIST OF FIGURES

CHAPTER 2

ATTRIBUTION

This thesis consists of three chapters. Chapter 1 contains an overview of the research, an introduction to the effects of biomass burning on the atmosphere, and an overview of the MODIS sensor package. Chapter 2 presents the production of smoke aerosol emission coefficients for the United States and Chapter 3 presents an evaluation of the smoke aerosol emission coefficients through a comparison of particulate matter emissions from the BlueSky Framework. While I am the primary author of the entire thesis, I received assistance from my advisor, Dr. Fok-Yan Leung, and other committee members in preparing this thesis.

CHAPTER 1

INTRODUCTION

1.1 Overview of the research

This thesis includes the top-down calculation of smoke aerosol emission coefficients derived from Moderate Resolution Imaging Spectroradiometer (MODIS) measurements of the rate of release of fire radiant energy (FRE) and the rate of release of smoke aerosols for estimating the emitted particulate matter from biomass burning events such as wildfires, prescribed burning, and agricultural waste burning in the contiguous United States. This thesis also includes an evaluation of estimates of daily particulate matter (PM) emissions using fire radiative power (FRP) measurements from MODIS and modeled emissions from the BlueSky Framework. A top-down approach to calculating emission coefficients directly relates the mass emission rate of PM from the fire to the rate of release of radiant energy from the fire, eliminating the need for external parameters such as burned area, biomass density, fraction of above-ground biomass, and burn efficiency (Ichoku and Kaufman, 2005). The emission coefficients are calculated for the contiguous United States, which has been divided into six regions to assess regional dependencies, and are calculated for each year from 2003 to 2008 to assess temporal dependencies. Also investigated is the impact of the vegetation type burned on the emission coefficients and subsequent PM emissions. Using the daily measurements of FRP by MODIS, a daily profile of PM emissions was generated for specific fires in the Pacific Northwest region. These profiles were used to evaluate the performance of the BlueSky Framework-modeled PM emissions for those same fires.

The BlueSky Framework and the Satellite Mapping Automatic Reanalysis Tool for Fire Incident Reconciliation (SMARTFIRE) (BSF-SF) facilitates connections between modeling steps responsible for fire consumption, smoke emissions, transport, and chemistry. BSF-SF is used by scientists, air quality managers, policy adopters, land managers, and incident command teams to support decisions regarding fire suppression efforts, go/no-go permits for prescribed burning, and public health warnings for smoke impacts. In 2008, the FRP Emissions Module was proposed to produce biomass burning emissions estimates using satellite data to be included in BSF-SF. This module will provide supplemental estimates of emissions for various types of fires in the United States. Critical to this module is the development of emission coefficients derived from FRP data from MODIS. The process used to generate these emission coefficients and the results is the subject of Chapter 2.

The motivation of this research came from the need to reduce the large uncertainties in the method for calculating emission coefficients from FRP measurements in the contiguous United States. Very diverse geographic features, complex meteorological conditions, and numerous vegetation types characterize the contiguous United States. Each of those factors influence fire behavior and emissions, resulting in high uncertainty in the calculated emission coefficients. Ichoku and Kaufman (2005) reported emission coefficients with very poor fits between the rate of emission of fire radiant energy and the rate of emission of smoke aerosols with r^2 values less than 0.2 for the contiguous U.S. and regional fits within the U.S. with r^2 values less than 0.6. Jordan et al. (2008) reported emission coefficients with improved fits with r^2 values of 0.645 and 0.752 for the U.S. Southern Great Plains region. Improvement of these coefficients is

necessary to produce accurate emissions estimates from biomass burning events for use with BSF-SF. Therefore, the research outcomes were aimed at a better understanding of the sources of uncertainty in calculating emission coefficients for all types of fires and developing a solution to reduce them.

1.2 Effects of biomass burning on the atmosphere

Biomass burning releases significant amounts of trace gases and PM to the atmosphere and has a direct impact on air quality. During an October 2003 wildfire event, the Los Angeles Basin experienced statistically significant increases in CO, NO, and PM_{10} concentrations for a fire less than 100 km from the sample locations (Phuleria et al., 2005). Wildfires in the Western United States have been shown to enhance summer-long mean $PM_{2.5}$ concentrations throughout the region (Jaffe et al., 2008). Many of the observation sites in the Jaffe et al. (2008) study showed enhancement from regional transport of emissions from fires. Emissions from biomass burning can travel beyond the local and regional scale, as evidenced by long-range transport events in the United States and Europe. Extraordinary concentrations of PM_{10} and $PM_{2.5}$ were observed in Finland from the transport of emissions from wildfires in Russia, Ukraine, Belarus, and the Baltic countries (Niemi et al., 2005). In the Northeastern United States, extremely high concentrations of CO and condensation nuclei were observed due to transport of emissions from wildfires in Quebec, Canada (DeBell et al., 2004). These long-range transport events show that wildfires can influence air quality conditions many hundreds of kilometers from the source. Whether the result of short- or long-range transport, increased PM concentrations are the principal impact of wildfires on air quality. Other

impacts on air quality can include both inhibition of ozone formation due to increased light scattering by the high levels of PM (Phuleria et al., 2005) or the enhancement of ozone formation through increased levels of ozone precursors (DeBell et al., 2004).

Wildfires are connected with the atmosphere through the emission of PM and surface changes. PM emissions can influence precipitation processes, cloud formation and dissipation, and change the scattering and absorption characteristics of aerosols (Ichoku et al., 2012; Gyawali et al., 2009). The evolution of the daily boundary layer can be delayed due to wildfire PM reducing solar forcing at the surface (Gyawali et al., 2009). In addition to these short-term influences on the atmosphere, wildfires also influence the atmosphere on climatic scales. Changes in surface albedo, cloud albedo, and the absorption and scattering properties of the atmosphere can affect the warming and cooling of the atmosphere, contributing to climatic change (Ichoku et al., 2012). These changes in climate can create conditions favorable for more wildfire activity (Ichoku et al., 2012), providing a positive feedback to climate change.

In the United States, wildfires and other biomass burning events such as the burning of agriculture residues and prescribed burns for forest management occur in every state. Estimated total carbon emissions, using the Global Fire Emissions Database version 3, from biomass burning in the contiguous United States averaged 9 Tg (1 Tg = 10^{12} g) per year from 1997 to 2010 (van der Werf et al., 2010). This accounts for approximately 0.4% of the mean global emissions of carbon from biomass burning (GFED3; van der Werf et al., 2010). Biomass burning emissions are still important contributors to U.S. total carbon emissions as about 50% of the total carbonaceous aerosol mass concentrations and 30% (west) and 20% (east) of the total fine aerosol

concentrations were attributed to biomass burning in 2001-2004 (Park et al., 2007). A recent study has shown that the amount of biomass consumed by wildfires is increasing in the Western United States (Westerling et al., 2006). Westerling et al. (2006) provided evidence that the earlier melting of the winter snow pack and prolonged hot and dry summer conditions is contributing to the increase in biomass consumed. With warmer, dryer summers expected to occur as a result of climate change, wildfire activity is expected to increase in the future (Field et al., 2007). Therefore accurate estimation of emissions from wildfires is important for future air quality assessments.

1.3 Overview of MODIS

MODIS rides aboard the National Aeronautics and Space Administration's (NASA) Terra and Aqua Earth Observing System (EOS) satellites. Launched on December 18, 1999 (Terra) and May 4, 2002 (Aqua), the two satellites orbit the earth every 98 minutes, crossing the equator at 10:30 am (Terra) and 1:30 pm (Aqua) local time. These orbits, combined with an across track swath width of 2330 kilometers, enable MODIS to achieve global coverage every one to two days. Global coverage is achieved at three resolutions: 250, 500, and 1000 meters utilizing thirty-six spectral bands. These spectral bands start in the visible range at 0.4 microns and end in the infrared at 14 microns. This wide spectral range enables scientists to study a multitude of atmospheric, oceanic, and terrestrial processes in an effort to understand how they interact (Lindsey and Herring, 2001).

Through the use of EOS instruments such as MODIS, scientists seek to answer questions about global change by understanding the interactions between atmospheric,

oceanic, and terrestrial processes. To study changes in the Earth's surface, MODIS measures surface reflectance, albedo, land surface temperature, and vegetation indices. The oceans are studied through measurements of ocean color and sea surface temperatures by MODIS. The understanding of atmospheric processes focuses on measurements of the radiative forcing properties of clouds, water vapor, and aerosols. The simultaneous measurements of these global processes help scientists build an understanding of changing global dynamics (Lindsey and Herring, 2001). In this study, measurements by MODIS of atmospheric aerosols and thermal anomalies related to biomass burning are used to investigate the impacts of biomass burning on air quality.

References

DeBell, L. J., Talbot, R. W., Dibb, J. E., Munger, J. W., Fischer, E. V., Frolking, S. E., 2004. A major regional air pollution event in the northeastern United States caused by extensive forest fires in Quebec, Canada. Journal of Geophysical Research, 109, D19305.

Field, C.B., L.D. Mortsch, M. Brklacich, D.L. Forbes, P. Kovacs, J.A. Patz, S.W. Running and M.J. Scott, 2007: North America. Climate change 2007: impacts, adaptation and vulnerability. Contribution of working group II to the Fourth Assessment Report of the Intergovernmental Panel on Climate Change, M.L. Parry, O.F. Canziani, J.P. Palutikof, P.J. van der Linden and C.E. Hanson, Eds., Cambridge University Press, Cambridge, UK, 617-652.

Gyawali, M., Arnott, W. P., Lewis, K., Moosmüller, H., 2009. In situ aerosol optics in Reno, NV, USA during and after the summer 2008 California wildfires and the influence of absorbing and non-absorbing organic coating on spectral light absorption. Atmospheric Chemistry and Physics, 9, 8007-8015.

Ichoku, C., Kaufman, Y.J., 2005. A method to derive smoke emission rates from MODIS fire radiative energy measurements. IEEE Transactions on Geoscience and Remote Sensing, 43(11), 2626-2649.

Ichoku, C., Kahn, R., Chin, M., 2012. Satellite contributions to the quantitative characterization of biomass burning for climate modeling. Atmospheric Research, 111, 1-28.

Jaffe, D., Hafner, W., Chand, D., Westerling, A., Spacklen, D., 2008. Interannual variations in PM2.5 due to wildfires in the western United States. Environmental Science and Technology, 42, 2812-2818.

Jordan, N.S., Ichoku, C., Hoff, R.M., 2008. Estimating smoke emissions over the US Southern Great Plains using MODIS fire radiative power and aerosol observations. Atmospheric Environment, 42, 2007-2022.

Lindsey, R., Herring, D., 2001. Moderate-Resolution Imaging Spectroradiometer, Abott, M., Conboy, B., Esaias, W., Justice, C., King, M., Murphy, B., Salomonson, V., Eds. NASA. 1-25.

Niemi, J. V., Tervahattu, H., Vehkamäki, Martikainen, J., Laakso, L., Kulmala, M., Aarnio, P., Koskentalo, T., Sillanpää, M., Makkonen, U., 2005. Characterization of aerosol particle episodes in Finland caused by wildfires in Eastern Europe. Atmospheric Chemistry and Physics, 5, 2299-2310.

Park, R. J., Jacob, D. J., Logan, J. A., 2007. Fire and biofuel contributions to annual mean aerosol mass concentrations in the United States. Atmospheric Environment, 41, 7389-7400.

Phuleria, H. C., Fine, P. M., Zhu, Y., Sioutas, C., 2005. Air quality impacts of the October 2003 Southern California wildfires. Journal of Geophysical Research, 110, D07S20.

van der Werf, G. R., Randerson, J. T., Giglio, L., Collatz, G. J., Mu, M., Kasibhatla, P. S., Morton, D. C., DeFries, R. S., Jin, Y., van Leeuven, T. T., 2010. Global fire emissions and the contribution of deforestation, savanna, forest, agricultural, and peat fires (1997-2009). Atmospheric Chemistry and Physics, 10, 11707-11735.

Westerling, A. L., Hidalgo, H. G., Cayan, D. R., Swetnam, T. W., 2006. Warming and earlier spring increase western U.S. forest wildfire activity. Science, 313, 940-943.

CHAPTER 2

CALCULATION OF EMISSION COEFFICIENTS FROM MODIS OBSERVATION OF FIRES FOR THE CONTIGUOUS UNITED STATES

Abstract

Poor correlation values characterized previous calculations of emission coefficients (C_e) for smoke aerosols in the United States from measurements of fire radiative energy (FRE) and aerosol optical thickness (AOT) by the Moderate Resolution Imaging Spectroradiometer (MODIS). The calculation of C_e relies on the direct linear relationship between the rate of emission of FRE and the rate of emission of smoke aerosols. Limiting the scan angle for measuring FRE to $\pm 40^o$ and eliminating any FRE and AOT retrievals that had a cloud fraction greater than zero were two modifications made to the method for deriving C_e. This modified method was applied for each year from 2003 to 2008 and generates C_e values for the contiguous U.S., six regions, and thirteen land cover types. The average C_e for the U.S. was found to be 0.0193, ranged from 0.0092 to 0.0357 for the six regions, and ranged from 0.0082 to 0.0435 for the thirteen land cover types. Average correlation values improved significantly from the previous C_e calculations, with the average improvement for the U.S. being 0.286 and the improvement for the six regions ranging from 0.008 to 0.399. Uncertainties still remain as annual variability and outliers related to high FRE measurements are prevalent.

2.1 Introduction

Estimation of the emission of gaseous species from biomass burning was inspired by the need to understand the global atmospheric carbon dioxide cycle as it related to increasing levels of global carbon dioxide and other trace gases in the atmosphere (Sieler and Crutzen, 1980). At the time of Sieler and Crutzen's work, the impact of biomass burning was difficult to estimate and more difficult to quantify. Using the available data, the total amount of biomass burned annually in a biome was estimated by the following equation:

$$M = A \times B \times \alpha \times \beta \tag{1}$$

where A = total land area burned annually (m^2/yr), B = the average organic matter per unit area in the individual biomes (g dm/m^2), α = the fraction of the average above-ground biomass relative to the total average biomass B, and where β = the burning efficiency of the above-ground biomass (Sieler and Crutzen, 1980). Another method for estimating emissions utilizes this equation:

$$M_x = EF_x * M_{biomass} \tag{2}$$

where M_x is the mass of emitted species *x*, EF_x is the emission factor for the emitted species *x*, and $M_{biomass}$ is the mass of dry biomass burned (Andreae and Merlet, 2001). This method is better suited for laboratory experiments as measuring the mass of biomass before and after burning is more easily achieved in the lab than in the field. To improve the data quality used in estimating emissions, these methods began using data derived from satellites.

A number of satellites, currently and historically, provide data for estimating emissions from biomass burning. The Geostationary Operational Environmental

Satellites (GOES) and the Meteosat Spinning Enhanced Visible and Infra-Red Imager (SEVRI) are two geosynchronous satellites that are used for fire detection and measurement. Several instruments aboard polar orbiting satellites, such as the Advanced Very High Resolution Radiometer (AVHRR), the Along Track Scanning Radiometer (ATSR-2), the Moderate Resolution Imaging Spectroradiometer (MODIS), and the Visible Infrared Imaging Radiometer Suite (VIIRS), have been and will continue to be used to estimate emissions from biomass burning. Fire pixel counts from AVHRR (Kaufman et al., 1990) and GOES-8 Automated Biomass Burning Algorithm (ABBA) (Prins et al., 1998) were among the first satellite data products used to estimate emissions. Saturation of the fire detection channel in the AVHRR (Kaufman et al., 1990) and coarse spatial resolution of GOES (Prins et al., 1998) motivated advancements in both the satellite technology and in the detection algorithms. Burned area estimates from ASTR-2 and MODIS have been used to generate global and regional estimates of emissions from biomass burning (Simon et al., 2004; van der Werf et al., 2010). While estimates using burned area data have reduced uncertainty by approximately 20% (van de Werf et al., 2010), they are most effective when used to compile post burn emission inventories. To generate near real time estimates of emissions from biomass burning, measurements of the rate of release of fire radiative energy (FRE) are made by MODIS, GOES, and SEVRI (Kaufman et al., 1998; Xu et al., 2010; Roberts and Wooster, 2008).

Most methods for estimating emissions from biomass burning using today's satellites can be classified as either "top down" or "bottom up." Emission estimates using the bottom up method utilize Equation 1, which requires estimation of B, α, and β in addition to the burned area measurement. A top down approach using measurements

of FRE virtually eliminates the need for all of the variables in Equation 1 because it is a measure of fire strength, the fire's size and intensity (Ichoku and Kaufman, 2005). Modifying Equation 2, Ichoku and Kaufman (2005) derived the following equation to estimate emissions from biomass burning using MODIS:

$$M_x = C_e * R_{fre} \quad (3)$$

where M_x is the rate of emission of species x (kg/s), R_{fre} is the rate of release of fire radiative energy (MJ/s), and C_e is the FRE-based emission coefficient (kg/MJ). In order to estimate emissions using Equation 3, an appropriate C_e must be derived using MODIS measured FRE and smoke aerosols.

2.2 MODIS data products for estimating emission coefficients from biomass burning

Fire detection by MODIS was designed to build upon and augment fire datasets based on GOES ABBA and AVHRR. The MODIS active fire product detects fires by their output of infrared radiant energy, reported as a brightness temperature. Two infrared wavelengths spanning three channels were specifically included to detect and characterize fires and their emitted energy (Kaufman et al., 1998; Giglio et al., 2003). Two channels detect at 4-μm and saturate at brightness temperatures of 500 K and 331 K respectively (Giglio et al., 2003). The third channel detects at 11-μm and saturates at 340 K for Aqua and 400 K for Terra (Giglio et al., 2003). Using these three channels, Kaufman et al. (1998) developed the original fire detection algorithm, which was refined later by Giglio et al. (2003) to eliminate persistent false detections and to detect relatively smaller fires.

The fire detection algorithm utilizes the significant difference between the blackbody radiation emitted at 4-μm and 11-μm during combustion (Giglio et al., 2003). During the daytime overpasses, a pixel is identified as a potential fire pixel if the brightness temperature at 4-μm exceeds 310 K, the difference between the brightness temperatures at 4-μm and 11-μm is greater than 10 K, and the reflectance is less than 0.3. During the nighttime overpasses, the required brightness temperature is reduced to 305 K at 4-μm and the reflectance test is omitted but the difference between the two wavelengths must still be greater than 10 K. Once identified as a potential fire pixel, two tests are performed to confirm that a potential fire pixel contains fire. The absolute threshold test requires the pixel brightness temperature at 4-μm to exceed 360 K during the day and 320 K at night (Kaufman et al., 1998). This test identifies fire pixels that are very unlikely to be a false alarm. The second test is the contextual test, which seeks to identify the remaining potential fire pixels. The contextual test begins with computing the respective mean and the mean absolute deviation of the 4-μm, 11-μm, and the difference between the 4-μm and 11-μm brightness temperatures for the pixels surrounding the potential fire pixel. These values are then used in five tests outlined by Giglio et al. (2003) to tentatively classify a pixel as a fire pixel. If during a nighttime overpass, these tests are the final step in identifying the pixel as a fire pixel. During the daytime, three more tests are performed to determine if the pixel is a false detection due to sun glint, proximity to a desert boundary, and proximity to a coastline.

Under typical conditions, this algorithm detects flaming and smoldering fires that are approximately 1000 m^2 in size (Giglio, 2010). Under very good and pristine observing conditions, flaming fires that are approximately 100 m^2 and 50 m^2 in size can

be detected (Giglio, 2010). All fire detects are reported on a 2340 by 2030 km grid, with each grid cell representing a 1-km pixel. These results are what are known as the Level 2 Thermal Anomalies product, which represent about five minutes of data.

Retrieval of aerosol optical thickness (AOT) by MODIS is split into two algorithms, one algorithm for retrievals over the ocean and one algorithm for retrievals over land. The land algorithm originally required the direct use of five spectral channels to make an AOT measurement. Reflectance was measured at 0.47-, 0.66-, 2.1-, 3.8-, and 11-μm to take advantage of relationships between reflectance measurements in the visible and infrared spectrums (Kaufman and Tanré, 1998). Remer et al. (2005) modified the algorithm to eliminate the use of the 3.8-μm and 11-μm channels and to include brighter surfaces by increasing the maximum surface reflectance allowed at 2.1-μm to 0.25 from 0.15. The remaining reflectance measurements are grouped into 10-km boxes of 20 by 20 pixels, or 400 500-m resolution pixels. Each of the 400 pixels is evaluated to determine if the pixel contains clouds, water, or snow or ice. This evaluation is achieved through the MODIS cloud mask (Levy et al., 2009) and use of the normalized difference vegetation index (NDVI). The cloud fraction is reported as the percentage of the 500-m pixels that are reported as cloud pixels. After the pixels that contain cloud, water, or snow or ice have been screened out, the remaining pixels are screened based on the new criteria that their reflectance value at 2.13-μm must be greater than 0.01 but less than 0.25 (Remer et al., 2005). The pixels that remain after the 2.13-μm reflectance test are then ordered by their 0.66-μm reflectance, from which 20% of the least reflective and 50% of the most reflective are eliminated. Based on the number of remaining pixels, the

algorithm proceeds with either the dark target retrieval path or the bright surfaces retrieval path.

The dark target retrieval path is the more accurate of the two retrieval pathways (Remer et al., 2005). The mean measured reflectance for each of the three wavelengths is calculated from the remaining pixels. Using the mean measured reflectance at 2.13-μm, surface reflectances at 0.47-μm and 0.66-μm are calculated using empirical relationships (Kaufman et al., 1997b). The mean measured reflectance and the surface reflectance values at 0.47-μm and 0.66-μm are then used to retrieve the AOT, single scattering albedo, and phase function values from the continental aerosol model look up table for their respective wavelengths. The values from the look up table are used to determine if the aerosol is pure dust, nondust, or mixed (Kaufman et al., 1997a). If the aerosol is found to be dust or nondust, the AOT is retrieved from the appropriate look up table for the dust or nondust model (Remer et al., 2005). The final step in the process is to interpolate the AOT at 0.55-μm from the 0.47-μm and 0.66-μm values using an Ångström law. This is necessary because 0.55-μm is an important wavelength of global climate modeling and analysis (Remer et al., 2005).

The bright surfaces retrieval path was created to increase the number of aerosol retrievals without introducing suspicious artifacts (Remer et al., 2005). If a land surface is too bright to satisfy the requirement of twelve dark pixels for the dark target path, the maximum reflectance at 2.13-μm is allowed to increase as a function of the slant path to a value of 0.40. Twelve pixels must satisfy this new requirement to proceed, otherwise no aerosol retrieval is made and fill-in values are output. If there are twelve or more pixels, aerosol is retrieved from the 0.47-μm channel only due to the increased atmospheric

signal and decreased surface reflectance. Because only the 0.47-μm channel is used, only the continental aerosol model can be applied. The resulting AOT is then extrapolated to 0.55-μm and 0.66-μm using the spectral dependence of the continental model and reported as "poor quality" (Remer et al., 2005).

2.3 Study domains and period

The area of study for this thesis is the contiguous United States of America, which will hereto be referred to as the U.S or the United States. Because of the diversity in both the land cover and geography, the U.S. was divided into six regions (Table 2.1) for analysis.

Table 2.1: Latitude and longitude boundaries in decimal degrees for the U.S. and the six regions of study.

Area	North Edge	South Edge	East Edge	West Edge
Northeast	48.90	36.60	-66.75	-91.00
Northern Plains	49.30	39.00	-91.00	-111.00
Northwest	49.00	39.00	-111.00	-125.00
Southeast	36.60	25.00	-75.35	-91.00
Southern Plains	39.00	25.70	-91.00	-106.00
Southwest	39.00	31.00	-106.00	-125.00
United States	49.30	25.00	-66.75	-125.00

Regionalization of a large area can be effective in improving estimates of emission coefficients from MODIS (Ichoku and Kaufman, 2005; Jordan et al., 2008; Pereria et al., 2009). Thirteen land cover types (Figure 2.1) as described by the Fuel Characteristic Classification System Version 2 (FCCS 2) were applied to the U.S. to derive vegetation-specific emission coefficients at the U.S. and regional level. Laboratory studies by Wooster et al. (2005) showed that FRE was not dependent on fuel type; however, it remains among the uncertainties of interest (Ichoku et al., 2012). Previous works on

MODIS-derived emission coefficients have been limited to a single year of study (Ichoku and Kaufman, 2005; Jordan et al., 2008; Pereria et al., 2009). In this study, emission coefficients were calculated annually from 2003 to 2008 to assess temporal changes in fire activity.

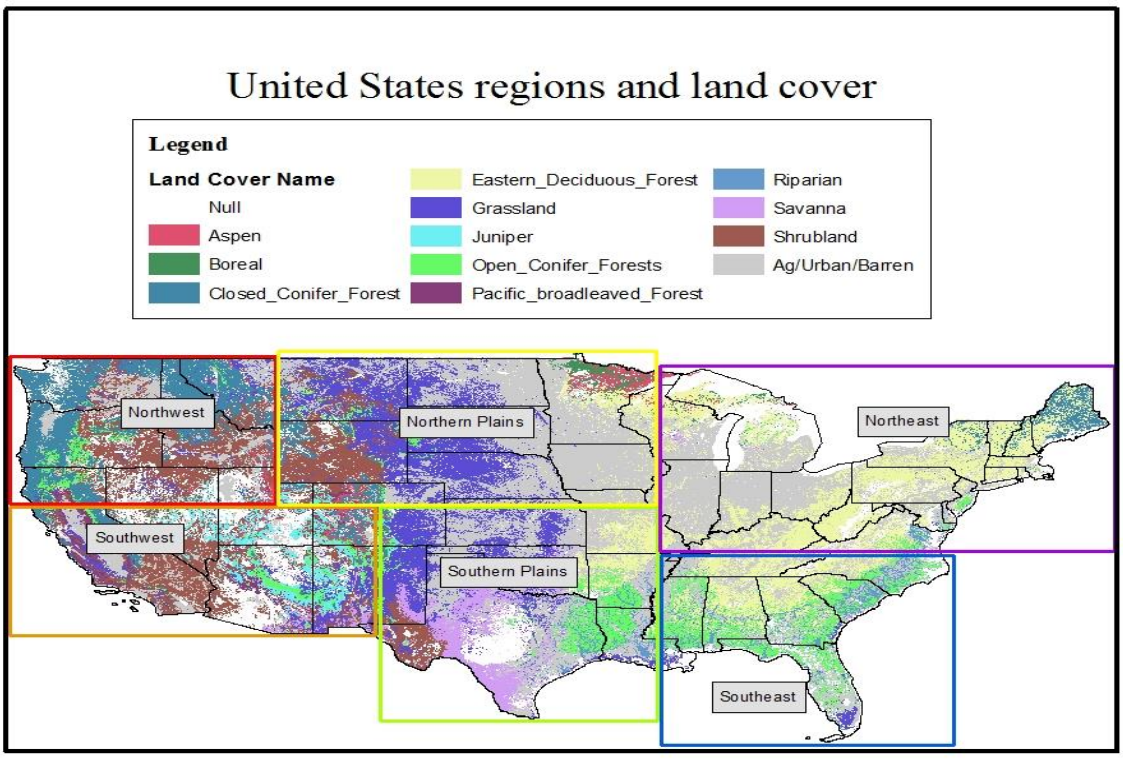

Figure 2.1: A map showing the six study regions overlaying the thirteen FCCS 2 land cover types. Fires are detected in varying amounts in every land cover type.

2.4 Methods for calculating emission coefficients

MODIS-based biomass burning emission coefficients are calculated using a swath-based approach, following Ichoku and Kaufman (2005), which total the FRP and smoke emissions over the entire 5-minute MODIS swath. This method is also used in a second additional process, which includes land cover type in the calculation of the

emission coefficient. This method is applied to calculate the emission coefficients for the entire U.S. and for each of the six study regions.

In order to calculate the emission coefficient, M_x and R_{fre} from Equation 3 must first be calculated from the MODIS data for a selected area. The data for the selected area is grouped by the 5-minute MODIS swath in which it was observed. R_{fre} is calculated as the sum of all of the fire pixels that contain a measurement of the FRP, which has units of MJ/s, which is given by

$$R_{fre} = \sum_{i=1}^{N_{af}} R_{fre}^{i} . \quad (4)$$

It is in this step that a quality assurance technique of limiting retrievals to those between scan angles of $\pm 40^{o}$ can be applied to limit off-nadir bias caused by overlapping measurements of FRP at large scan angles (Giglio et al., 2006). Limiting the scan angle to $\pm 40^{o}$ still captured 77% of the fire pixel detections in Africa and the loss of detections is compensated for by the omission of fire pixels that are less than 40 MW (Freeborn et al., 2011). M_x requires multiple steps to calculate, starting with the conversion from AOT to smoke mass density. For a given aerosol pixel that contains a fire pixel with a FRP return, the AOT values at 550 nm for the given aerosol pixel and its eight neighbors are extracted.

$$\tau_{a550}^{f} = \tau_{a550}^{t} - \tau_{a550}^{b} \quad (5)$$

For each of the aerosol pixels retrieved, the cloud fraction value is simultaneously retrieved. From those nine AOT values, the smallest value, or background value (τ^{b}_{a550}), and largest value (τ^{t}_{a550}) are determined. The difference between those two values is calculated to be the AOT of emitted smoke (τ^{f}_{a550}). If fewer than two of the nine pixels

contain AOT values, the pixel will not return an AOT value of emitted smoke. A quality assurance technique that can be applied at this step excludes all AOT pixels and its associated FRP returns if the sum of the cloud fraction is greater than zero (L. Ellison, personal communication, 2012). This eliminates fire pixels that are underestimated due to blocking of the thermal radiation by clouds and AOT retrievals influenced by clouds. When there is a successful AOT return, the next step is to convert the AOT to smoke mass density (M_d g/m^2) by dividing the AOT by the smoke mass extinction efficiency (β_e).

$$M_d = \tau^f_{a550} / \beta_e \tag{6}$$

The smoke mass extinction efficiency is the sum of the smoke mass scattering and absorption efficiencies of the smoke aerosols emitted into the atmosphere. Its value is wavelength dependent and varies for different aerosol types. In this work, the value of 4.6 m^2/g is used (Ichoku and Kaufman, 2005).

The next step is to calculate the period of emission for the aerosol pixel, which is the amount of time it would take for all of the smoke to exit the target pixel. To make this calculation requires an assumption about the injection height of the smoke plume. The global average injection height for smoke plumes from wildfires is 1.5 kilometers (Ichoku and Kaufman, 2005), therefore it is assumed that the smoke plumes in the United States reach the global average height. This assumption allows for the use of wind vectors at 850 mb (approximately 1.5 km above the surface) to calculate the wind speed at the injection height as follows:

$$WS = \sqrt{u^2 + v^2} \, . \tag{7}$$

These wind vectors are extracted from the National Center for Environmental Prediction/Nation Center for Atmospheric Research (NCEP/NCAR) reanalysis dataset, which has a spatial resolution of one degree. The next step is to calculate the distance over which the wind must blow (L) to clear the smoke from the aerosol pixel:

$$L = \sqrt{A^{ap}} \tag{8}$$

where A^{ap} is the area of the aerosol pixel. That distance is then divided by the wind speed, giving the period of emission for that aerosol pixel (T^{ap})

$$T^{ap} = L/WS \tag{9}$$

The final step in calculating M_x shifts from individual pixel-based calculations to swath-based calculations. The total area of influence of fire (A_T) is calculated as the sum of the areas of all aerosol pixels that contain fire pixel retrievals, even if the aerosol pixel does not contain a retrieval of AOT, which is given by

$$A_T = \sum_{i=1}^{N_{af}} A_i^{ap} \tag{10}$$

where N_{af} is the number of all the aerosol pixels that contain fire pixel retrievals. The overall mean aerosol mass density (M_D) is calculated as the average of the smoke mass densities from the aerosol pixels that returned an AOT value. M_D is given by

$$M_D = \left(\sum_{i=1}^{N_{aa}} \left(M_d\right)_i \right) / N_{aa} \tag{11}$$

where N_{aa} is the number of only the aerosol pixels that contain both an AOT return and fire pixel retrievals. The actual total mass of smoke aerosol emitted is the product of the mean aerosol mass density and total area, given by

$$M_{sa} = M_D * A_T. \tag{12}$$

The average period of emission of the smoke is given by

$$T = \left(\sum_{i=1}^{N_{aa}} \left(T^{ap} \right)_i \right) / N_{aa}. \quad (13)$$

Finally, the rate of emission of smoke aerosols (M_x) in kilograms per second is given by

$$M_x = M_{sa} / T. \quad (14)$$

The standard error is calculated the same as M_x – replacing the overall mean mass density with the standard deviation of the overall mean mass density.

Plotting M_x versus R_{fre} (Figure 2.2) gives a relationship that allows for the estimation of the rate of emission of smoke aerosols for a given rate of emission of fire radiant energy. A linear regression line with the intercept constrained to zero is used to derive the emission coefficient (kg/MJ) from a plot. The intercept of the regression line is constrained to zero to emphasize the direct relationship between the fire radiant energy and the emission of smoke aerosols – smoke is not present without fire radiant energy. The correlation coefficient from the regression is used to evaluate the quality of the fit.

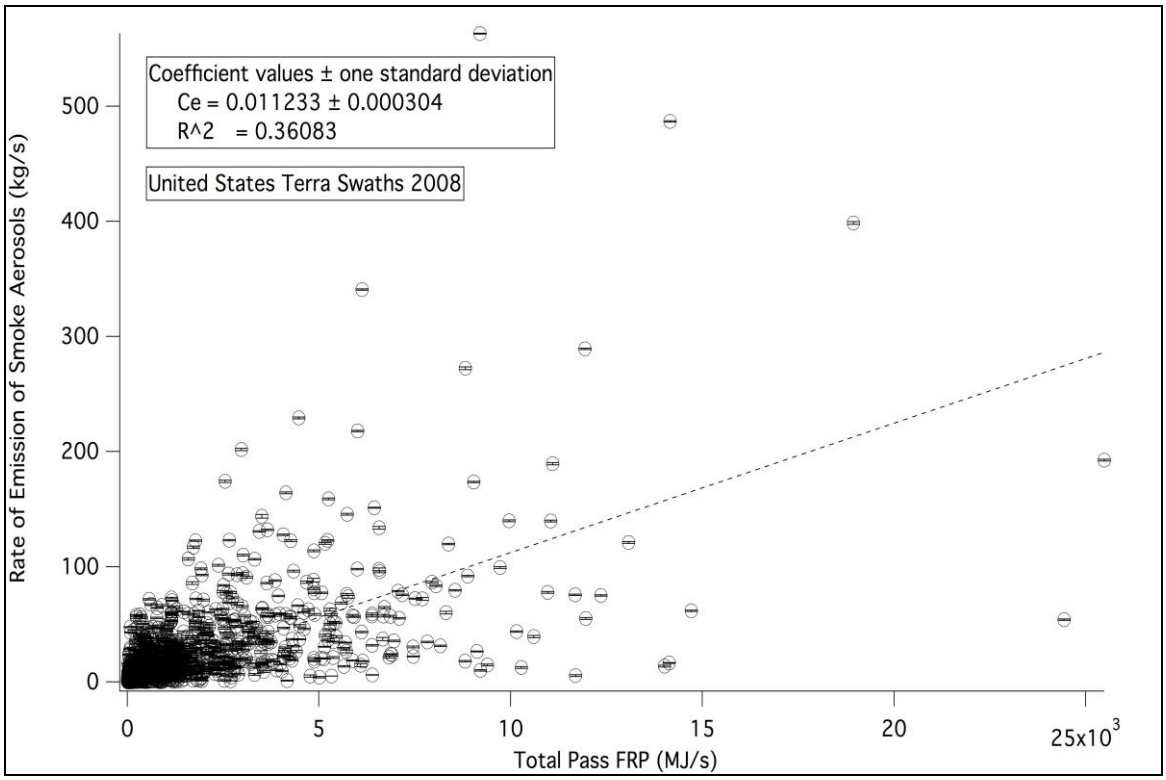

Figure 2.2: A plot showing the relationship between the rate of release of smoke aerosols and the rate of release of fire radiant energy. The linear fit line is the emission coefficient (kg/MJ) for the Terra satellite for 2008. No QA was used to screen out questionable data points. The error bars represent the standard error of the rate of release of smoke aerosols.

The inclusion of land cover type in the calculation of the emission coefficients is a simple grouping process. FRP points from a MODIS are grouped by one of the thirteen land cover types, seen in Figure 2.1. Then for each individual land cover type, the emission coefficient is calculated following the swath-based approach.

There are several sources of error in the calculation of R_{fre} and M_x that propagate into the uncertainty of the emission coefficient. In North America, AOT from MODIS is overestimated by 50% against ground-based Aerosol Robotic Network (AERONET) measurements (Ichoku and Kaufman, 2005). For M_x, smoke aerosol hygroscopicity effects on β_e can cause overestimation of M_x by up to 25% (Ichoku and Kaufman, 2005). R_{fre} has been found to be overestimated by 18% (Wooster et al., 2005). For WS, the

internal root mean square difference in both the u- and v-direction winds is 0.4 m s^{-1} and the external root mean square difference is 1.0 m s^{-1} at 850 mb (Kalnay et al., 1996). The uncertainty generated by these variables is separate from the uncertainty reported by the correlation coefficient from the linear regression analysis. Assuming a typical wind speed of 10 m s^{-1} at 850 mb and using a simple propagation of errors yields an estimated uncertainty of approximately 60% in the PM mass emission rate for a given wildfire.

2.5 Results and discussions

Emission coefficients were calculated for the U.S. and regionally for each year of the study. The average coefficients were calculated for each satellite using both the scan angle and cloud fraction QA methods and are shown in Figure 2.3.

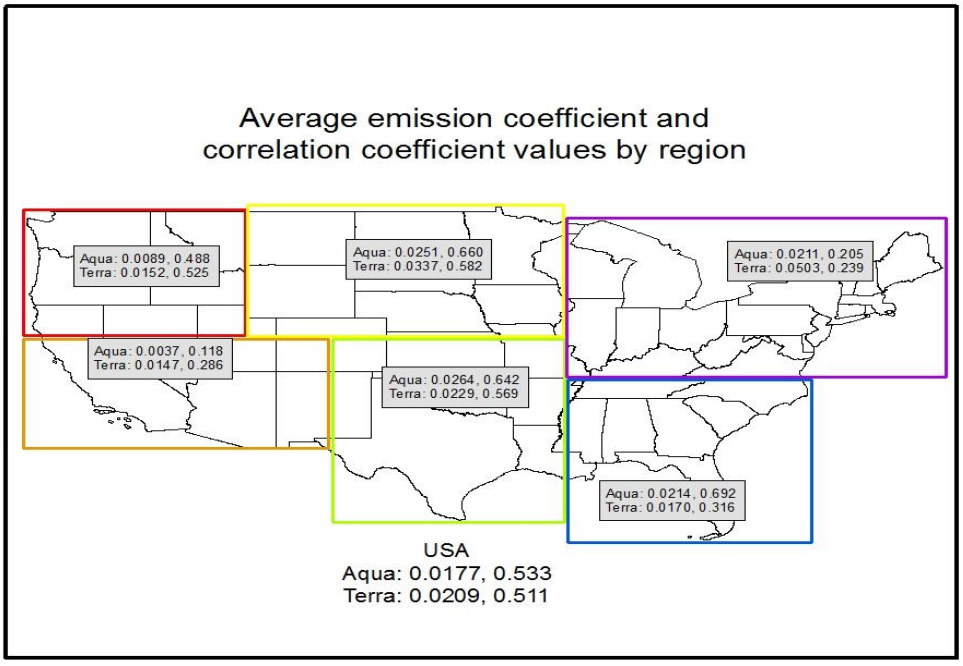

Figure 2.3: A map of the average emission coefficients for the entire United States and each region's average emission coefficients. The emission coefficients in the two western regions are considerably lower than the central and eastern regions.

In four of the regions, the emission coefficient for Terra is greater than the emission coefficient for Aqua. This occurrence is against expectations because of the assumed direct relationship between fire radiant energy and smoke aerosol emissions and the assumed diurnal cycle of fires being more intense in the afternoon. The emission coefficients for the Northwest and Southwest are considerably lower than the other four regions. This indicates that the radiative intensity of the fires in the region is much higher relative to the smoke aerosol emissions than the other regions and that the fire behavior is similar. The correlation coefficients for the Northeast and Southwest are poor for both satellites suggesting that there are some other factors influencing the fire behavior in those regions. There is fairly good agreement between the Southeast and Southern Plains, suggesting that the fire behavior is similar in the two regions. While there is some agreement between regions, each region has unique characteristics that require further inspection.

A FRE-based emission coefficient was found to be 0.03 ± 0.013 kg/MJ from laboratory studies for smoke aerosols (Ichoku et al., 2008). This value was determined through experiments that burned different biomass types and measured the FRE output and the amount of aerosols released at the Fire Sciences Laboratory of the United States Forest Service Rocky Mountain Research Station in Missoula, Montana (Ichoku et al., 2008). The emission coefficients for the U.S. in Figure 2.3 fall within the range established by the laboratory study. Only seven of the twelve regional emission coefficient values fall within that range.

United States

As seen in Figure 2.1, the U.S. is characterized by diverse land cover types and covers a large area. Wildfires and other biomass burning events occur to some degree in every part of the U.S. and in each land cover type. Due to the diverse land cover types and burning events, calculating an emission coefficient for the U.S. typically results in poor correlation coefficient values. The emission coefficients in Table 2.2 are coupled with correlation coefficients that average 0.233 for Aqua and 0.240 for Terra. Ichoku and Kaufman (2005) reported correlation coefficients of less than 0.2. Additionally, ten of the twelve emission coefficients are less than 0.01, which are less than the reported range in Ichoku and Kaufman (2005). To improve both the emission and correlation coefficients, the QA techniques described in Section 2.4 were applied.

Table 2.2: Emission coefficient, in kilograms of smoke aerosols per megajoule, and correlation coefficient (C_e, R^2) values for the United States before any QA screening was applied. N is the total number of MODIS overpasses (Aqua, Terra) included in the analysis and the Fire Pixels (Aqua, Terra) are the total number of fire pixels detected that year. The emission coefficient values are below the expected values from the literature.

Year	Aqua (C_e, R^2)	Terra (C_e, R^2)	N (A, T)	Fire Pixels (A, T)
2003	0.0039, 0.144	0.0031, 0.095	1364, 1289	80302, 28738
2004	0.0083, 0.230	0.0101, 0.241	1370, 1300	64863, 22061
2005	0.0083, 0.244	0.0072, 0.232	1439, 1369	81410, 30301
2006	0.0042, 0.197	0.0045, 0.152	1476, 1429	86401, 33662
2007	0.0028, 0.296	0.0038, 0.360	1443, 1413	91427, 34756
2008	0.0082, 0.288	0.0112, 0.361	1448, 1379	86947, 32418

Using the QA techniques resulted in improved emission and correlation coefficients for each year and satellite, seen in Table 2.3. With the exception of Aqua 2007, the correlation coefficients have improved to values greater than 0.4, which is in the acceptable range for the U.S. The emission coefficients have also improved to meet with values reported in the literature, with all years and both satellites having values

greater than 0.01. One reason for the increase in the emission coefficient values is the scan angle QA technique excluding FRP pixel values that are overestimated due to overlaps in the scanning process.

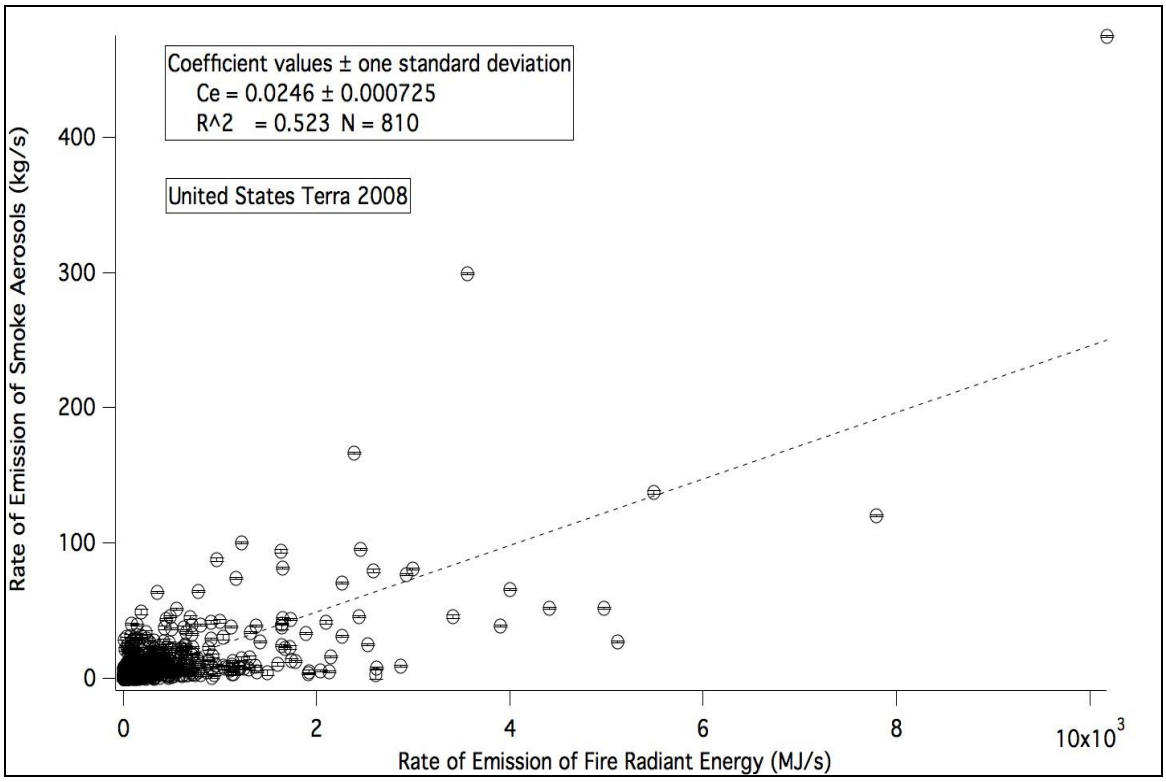

Figure 2.4: A plot of M_x versus R_{fre} for Terra 2008 with the QA techniques applied. The emission coefficient has more than doubled from Figure 2.2 and the correlation coefficient has also increased significantly. The error bars represent the standard error of the rate of release of smoke aerosols.

This technique reduces both the total number of fire pixels and the amount of radiant energy reported. When compared to Figure 2.2, Figure 2.4 shows a reduction in the maximum value of R_{fre} of approximately 15,000 MJ/s, which when coupled with a minimal decrease in the maximum M_x results in an increased emission coefficient. Also evident in Figure 2.4 is the reason for the increase in the correlation coefficient value: the amount of spread in the data points is reduced.

Table 2.3: Emission coefficient, in kilograms of smoke aerosols per megajoule, and correlation coefficient (C_e, R^2) values for the United States with the QA techniques applied. N is the total number of MODIS overpasses (Aqua, Terra) included in the analysis and the Fire Pixels (Aqua, Terra) are the total number of fire pixels detected that year. The annual variability in the emission and correlation coefficient values is not a factor of the number of data points or number of detected fire pixels.

Year	Aqua (C_e, R^2)	Terra (C_e, R^2)	N (A, T)	Fire Pixels (A, T)
2003	0.0193, 0.532	0.0161, 0.407	711, 731	28809, 11691
2004	0.0213, 0.629	0.0216, 0.444	666, 732	24668, 10062
2005	0.0187, 0.623	0.0262, 0.777	761, 797	26963, 14025
2006	0.0142, 0.481	0.0204, 0.459	739, 777	27070, 13890
2007	0.0117, 0.284	0.0163, 0.456	697, 812	28522, 14417
2008	0.0208, 0.650	0.0246, 0.523	731, 810	31181, 14316

In Tables 2.4 and 2.5, the emission coefficients were calculated for each land cover type in the U.S. Doing so achieved varied success as both correlation coefficients and emission coefficients showed high annual variability. For Aqua, emission and correlation coefficients for the eastern deciduous forest and open coniferous forest showed the most consistency over the study period. The greatest number of all fire detections occurs in the agriculture/urban/barren (42%) land type, followed by open coniferous forests (16%). The fewest number of fire detections occur in the boreal (0.07%) and aspen (0.10%) land types, which is responsible for the low correlation coefficient values and the extreme annual variability. For the savanna and grassland land types, the emission coefficients were similar in value to those reported in other areas of the globe (Ichoku and Kaufman, 2005). Overall, these emission coefficients for Aqua provide insight into the regional variability seen in Figure 2.3. The emission coefficients for the closed coniferous forest and shrubland land types are similar to those seen in the two western regions. This shows that the dominant fire activity in those regions is in those land types.

Table 2.4: Emission coefficient, in kilograms of smoke aerosols per megajoule, and correlation coefficient (C_e, R^2) values for Aqua for the United States with the QA techniques applied. Each land type is characterized by moderate to high annual variability in both its emission and correlation coefficient values. If a value is underlined, it indicates that the correlation coefficient was calculated from a negative R-value.

Land Type	2003 (C_e, R^2)	2004 (C_e, R^2)	2005 (C_e, R^2)	2006 (C_e, R^2)	2007 (C_e, R^2)	2008 (C_e, R^2)
Null	0.0140, 0.240	0.0222, 0.221	0.0209, 0.332	0.0292, 0.366	0.0173, 0.340	0.0177, 0.302
Aspen	0.0068, 0.071	0.0165, 0.025	0.0339, 0.124	0.0099, 0.049	0.0012, 0.115	0.0062, 0.023
Boreal	0.0016, 0.064	0.0147, 1.000	0.0664, 0.199	0.0398, 0.592	0.0127, 0.567	0.0438, 1.000
Closed Coniferous Forest	0.0066, 0.203	0.0071, 0.133	0.0123, 0.644	0.0081, 0.675	0.0047, 0.509	0.0220, 0.524
Eastern Deciduous Forest	0.0272, 0.797	0.0141, 0.508	0.0190, 0.470	0.0195, 0.634	0.0177, 0.535	0.0137, 0.640
Grassland	0.0323, 0.724	0.0298, 0.886	0.0269, 0.981	0.0204, 0.727	0.0448, 0.564	0.0367, 0.764
Juniper	0.0091, 0.945	0.0150, 0.543	0.0035, 0.136	0.0075, 0.014	0.0015, 0.036	0.0053, 0.003
Open Coniferous Forest	0.0149, 0655	0.0127, 0.285	0.0167, 0.440	0.0165, 0.445	0.0185, 0.691	0.0217, 0.569
Pacific Broadleaved Forest	0.0102, 0.636	0.0041, 0.136	0.0018, 0.744	0.0110, 0.479	0.0034, 0.249	0.0054, 0.057
Riparian	0.0183, 0.257	0.0357, 0.623	0.0254, 0.393	0.0269, 0.453	0.0135, 0.155	0.0188, 0.415
Savanna	0.0610, 0.889	0.0448, 0.734	0.0109, 0.136	0.0149, 0.147	0.0338, 0.558	0.0308, 0.420
Shrubland	0.0048, 0.032	0.0017, 0.049	0.0091, 0.521	0.0112, 0.449	0.0107, 0.680	0.0089, 0.111
Ag/Urban/ Barren	0.0305, 0.589	0.0345, 0.755	0.0271, 0.543	0.0231, 0.384	0.0211, 0.348	0.0355, 0.593

For Terra, the land type with the most consistent emission coefficient and best correlation coefficient values is grassland. As with Aqua, the greatest number of fire detections is in the agriculture/urban/barren (40.4%) land type and the fewest occur in the

aspen (0.10%) and boreal (0.06%) land types. Contrary to the trend seen in Table 2.3, the emission coefficients for Terra for the dominant land types in Table 2.5 are not consistently greater than the emission coefficients for Aqua. For example, the emission coefficients for Terra for the open coniferous forest land type are less than those for the same land type for Aqua. This appears to be against expectations as the second most (19.01%) fire occurrences are in the open coniferous forest land type. It is possible that the fire radiant energy and subsequent emissions in this land type are highly dependent on time of day. However, certain land types, particularly those that are dominant in the western regions, consistently exceed their Aqua counterpart. Those land types, namely the closed coniferous forest and pacific broadleaved forest, appear to be the leading factor for the U.S. emission coefficient for Terra exceeding the value for Aqua. This will be explored further in the regional analyses.

Table 2.5: Emission coefficient, in kilograms of smoke aerosols per megajoule, and correlation coefficient (C_e, R^2) values for Terra for the Contiguous United States with QA applied. For most land cover types, the value of the emission coefficient is greater than its Aqua counterpart; however, it is not true for all years within a land cover type. Not enough data points were returned to calculate an emission coefficient for the boreal land cover type in 2008.

Land Type	2003 (C_e, R^2)	2004 (C_e, R^2)	2005 (C_e, R^2)	2006 (C_e, R^2)	2007 (C_e, R^2)	2008 (C_e, R^2)
Null	0.0173, 0.086	0.0266, 0.245	0.0169, 0.289	0.0292, 0.366	0.0325, 0.135	0.0102, 0.126
Aspen	0.0435, 0.007	0.0102, 0.525	0.0315, 0.552	0.0052, 0.845	0.0051, 0.071	0.0028, 0.859
Boreal	0.0453, 0.619	0.0845, 0.930	0.0892, 1.000	0.0443, 0.989	0.0797, 0.962	
Closed Coniferous Forest	0.0140, 0.717	0.0051, 0.244	0.0229, 0.639	0.0137, 0.490	0.0229, 0.690	0.0299, 0.490
Eastern Deciduous Forest	0.0220, 0.299	0.0183, 0.250	0.0145, 0.190	0.0176, 0.247	0.0160, 0.140	0.0139, 0.183
Grassland	0.0228, 0.352	0.0283, 0.604	0.0282, 0.932	0.0283, 0.885	0.0248, 0.411	0.0504, 0.926
Juniper	0.0132, 0.079	0.0177, 0.151	0.0233, 0.429	0.0093, 0.017	0.0073, 0.584	0.0038, 0.010
Open Coniferous Forest	0.0095, 0.442	0.0131, 0.317	0.0128, 0.356	0.0097, 0.285	0.0109, 0.226	0.0146, 0.151
Pacific Broadleaved Forest	0.0065, 0.262	0.0237, 0.923	0.0108, 0.803	0.0164, 0.050	0.0046, 0.015	0.0164, 0.528
Riparian	0.0158, 0.325	0.0251, 0.418	0.0102, 0.112	0.0151, 0.161	0.0072, 0.362	0.0120, 0.232
Savanna	0.0488, 0.687	0.0621, 0.679	0.0445, 0.438	0.0414, 0.372	0.0242, 0.170	0.0265, 0.245
Shrubland	0.0094, 0.071	0.0051, 0.001	0.0075, 0.338	0.0093, 0.503	0.0069, 0.256	0.0133, 0.292
Ag/Urban/ Barren	0.0273, 0.366	0.0395, 0.374	0.0370, 0.713	0.0367, 0.387	0.0250, 0.177	0.0292, 0.297

Northeast United States

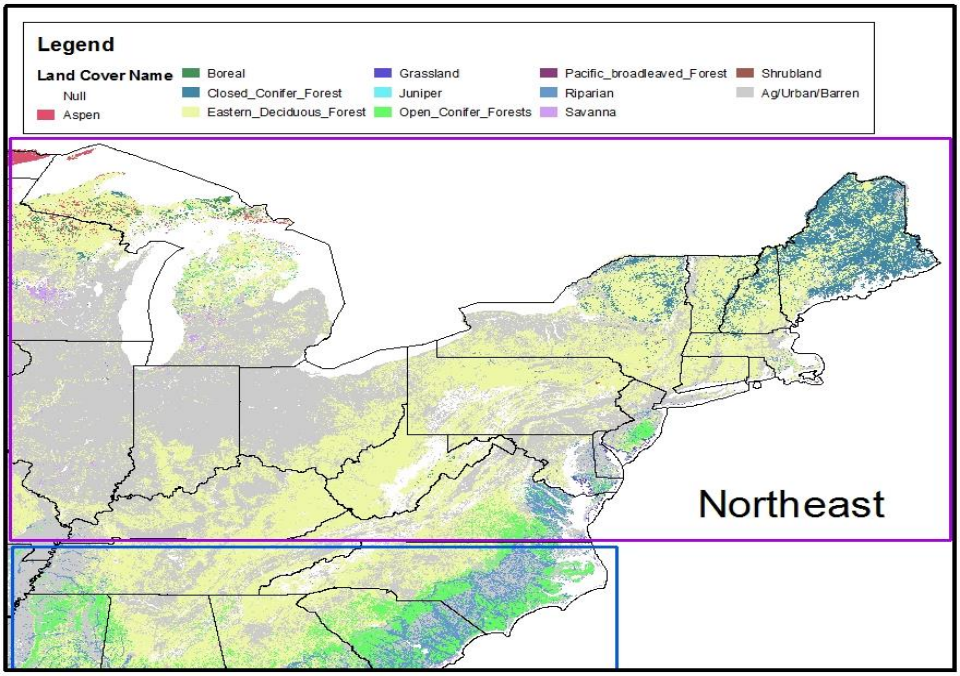

Figure 2.5: A map of the land cover types for the Northeast. Most of the land area is classified as eastern deciduous forest or agriculture/urban/barren.

As seen in Figure 2.5, two land cover types dominate the Northeast: eastern deciduous forest and agriculture/urban/barren. This region contains the fewest number of fire pixel detections of all the regions (6.43%) and has the lowest average correlation coefficient. With the exception of 2007, the emission coefficients in Table 6 for both Aqua and Terra are greater than 0.01, which puts them in line with literature values. For all of the years, the correlation coefficients are poor, with 0.277 as the highest value. Aside from 2003, the emission coefficients for Terra are greater than Aqua, highlighting this region's effect on Terra's higher U.S. emission coefficient. Annual variability is prevalent for both satellites, which when combined with the poor correlation coefficient values led to applying the previously described QA techniques.

Table 2.6: Emission coefficient, in kilograms of smoke aerosols per megajoule, and correlation coefficient (C_e, R^2) values for the Northeast before any QA screening was applied. N is the total number of MODIS overpasses (Aqua, Terra) included in the analysis and the Fire Pixels (Aqua, Terra) are the total number of fire pixels detected that year. The 2007 emission coefficients are extreme outliers for the region.

Year	Aqua (C_e, R^2)	Terra (C_e, R^2)	N (A, T)	Fire Pixels (A, T)
2003	0.0372, 0.261	0.0274, 0.168	257, 257	1995, 1498
2004	0.0164, 0.152	0.0221, 0.035	255, 265	1661, 1380
2005	0.0155, 0.169	0.0275, 0.112	291, 297	2241, 2229
2006	0.0130, 0.168	0.0224, 0.119	300, 290	1925, 1883
2007	0.0023, 0.068	0.0024, 0.004	308, 315	2307, 2255
2008	0.0210, 0.277	0.0343, 0.201	290, 274	2065, 1909

The application of the QA techniques yielded mixed results. For both satellites, the average correlation coefficient values increased; however, the annual variability increased, with the increases found in some years negated by decreases in others. This is most prevalent for Aqua, as the high value of 0.431 is brought down by multiple years of less than 0.1. As seen in Table 2.7, the emission coefficients for Terra significantly exceed those for Aqua, with the exception for 2008.

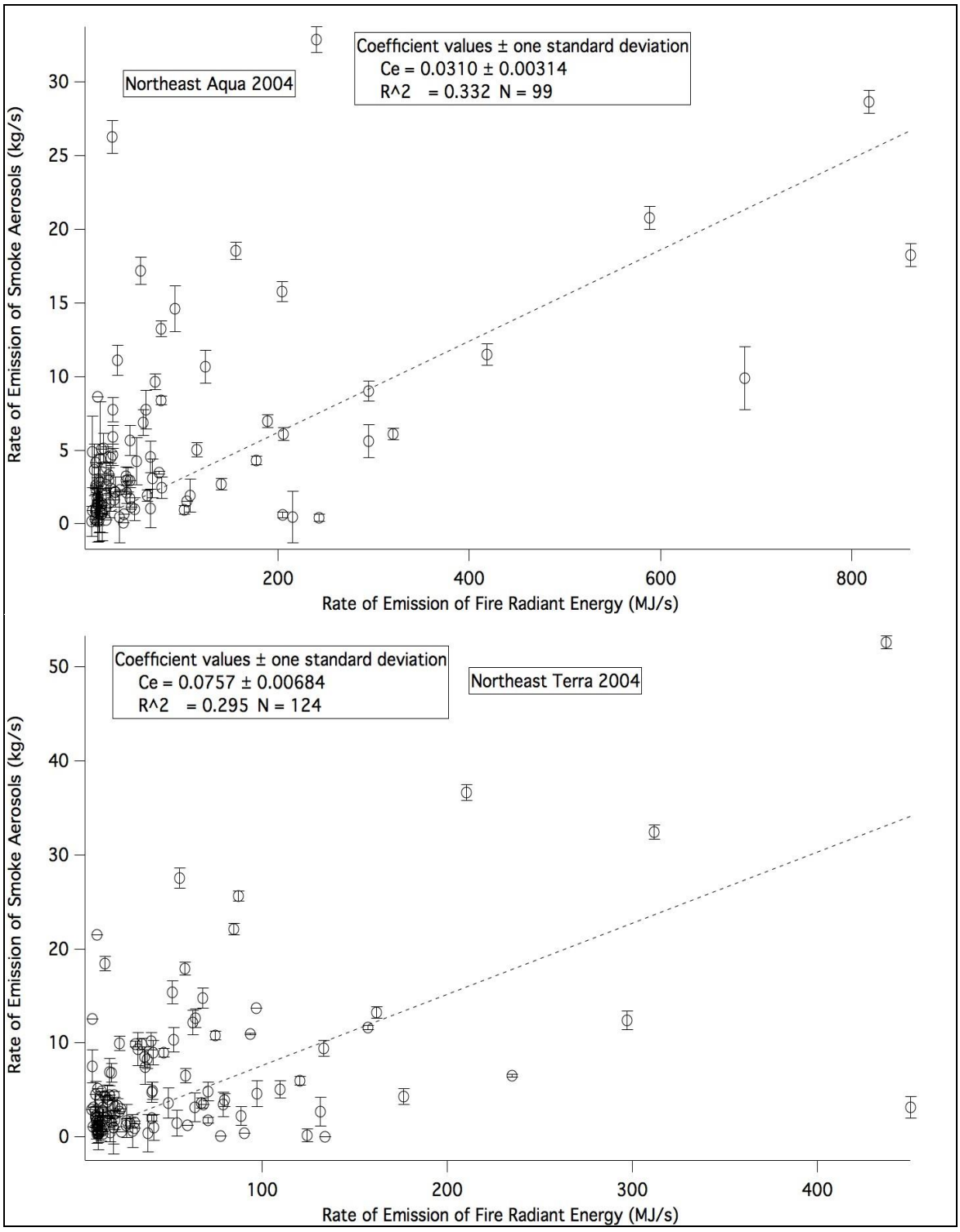

Figure 2.6: Plots of M_x versus R_{fre} for 2004. Relative to R_{fre}, the values for M_x are quite large; however, Terra's emission coefficient value is comparable to the cropland emission coefficients observed in other parts of the world (Ichoku and Kaufman, 2005). The error bars represent the standard error of the rate of release of smoke aerosols.

For both satellites, the total number of data points and fire pixel returns decreased by approximately half due to the QA techniques. While the correlation coefficient values are still poor, these emission coefficients are a fair representation for most of the fires in the region. As seen in Figure 2.6, the radiant energy outputs of these fires are quite low and are coupled with moderate rates of emission of smoke aerosols. This combination leads to the higher observed emission coefficients in this region.

Table 2.7: Emission coefficient, in kilograms of smoke aerosols per megajoule, and correlation coefficient values for the Northeast with the QA screening techniques applied. N is the total number of MODIS overpasses (Aqua, Terra) included in the analysis and the Fire Pixels (Aqua, Terra) are the total number of fire pixels detected that year. 2007 continues to be an outlier as data points with unusually high R_{fre} for this region are influencing the emission coefficients.

Year	Aqua (C_e, R^2)	Terra (C_e, R^2)	N (A, T)	Fire Pixels (A, T)
2003	0.0197, 0.087	0.0717, 0.392	112, 128	894, 707
2004	0.0310, 0.332	0.0757, 0.295	99, 124	605, 656
2005	0.0156, 0.090	0.0483, 0.300	128, 155	934, 1231
2006	0.0187, 0.190	0.0609, 0.287	110, 133	679, 959
2007	0.0088, 0.098	0.0205, 0.059	124, 151	840, 1125
2008	0.0329, 0.431	0.0245, 0.100	110, 149	725, 1131

To determine if the higher observed emission coefficients in this region are a product of a certain land cover type, the emission coefficients were calculated for the major land cover types in the region. Most of the fire pixel detections by Aqua occur in the eastern deciduous forest (21.23%) and agriculture/urban/barren (68.89%) land types, which follows with Figure 2.5 as most of the land area in this region is classified as one of those two types. The annual variability in those land types, seen in Table 2.8, provides insight into the annual variability observed in Table 2.7. Despite the relatively few fire pixel returns by the other land cover types, their influence on the correlation coefficient is likely significant as their values are very inconsistent and range from 0.009 to 0.991. As seen in Figure 2.6, a single outlying data point, which may represent burning in a land

cover type outside the two main types for this region, can strongly influence the regression line.

Table 2.8: Emission coefficient, in kilograms of smoke aerosols per megajoule, and correlation coefficient (C_e, R^2) values for Aqua for the Northeast with the QA techniques applied. Underlined coefficients represent those calculated from a negative R-value and missing coefficients are the result of too few observations in that land cover type for that year.

Land Type	2003 (C_e, R^2)	2004 (C_e, R^2)	2005 (C_e, R^2)	2006 (C_e, R^2)	2007 (C_e, R^2)	2008 (C_e, R^2)
Null	0.0143, 0.044	0.0396, 0.007	0.0273, 0.063	0.0623, 0.339	0.0179, 0.133	0.0381, 0.499
Eastern Deciduous Forest	0.0257, 0.351	0.0431, 0.580	0.0207, 0.283	0.0147, 0.327	0.0331, 0.355	0.0128, 0.510
Open Coniferous Forest	0.0130, 0.021	0.0097, 0.081	0.0164, 0.039	0.0129, 0.090	<u>0.0047,</u> <u>0.009</u>	0.0551, 0.687
Riparian	0.0861, 0.141	0.0322, 0.679	0.0388, 0.244	0.0157, 0.643		0.0269, 0.899
Savanna	0.0811, 0.936	0.0525, 0.955	<u>0.0478,</u> <u>0.568</u>		0.1320, 0.991	0.0976, 0.741
Ag/Urban/ Barren	0.0354, 0.153	0.0338, 0.388	0.0407, 0.272	0.0185, 0.176	0.0323, 0.252	0.0416, 0.503

Like Aqua, the land cover types where most of the fires are detected are the eastern deciduous forest (11.71%) and agriculture/urban/barren (79.85%). Using the emission coefficient values from Table 2.9, the land cover type that appears to be the most dominant in influencing the regional emission coefficient is the agriculture/urban/barren land cover type. Contrary to Aqua, the other land types that return observed fires contain too few observations to have significant influence on the regional emission coefficient value.

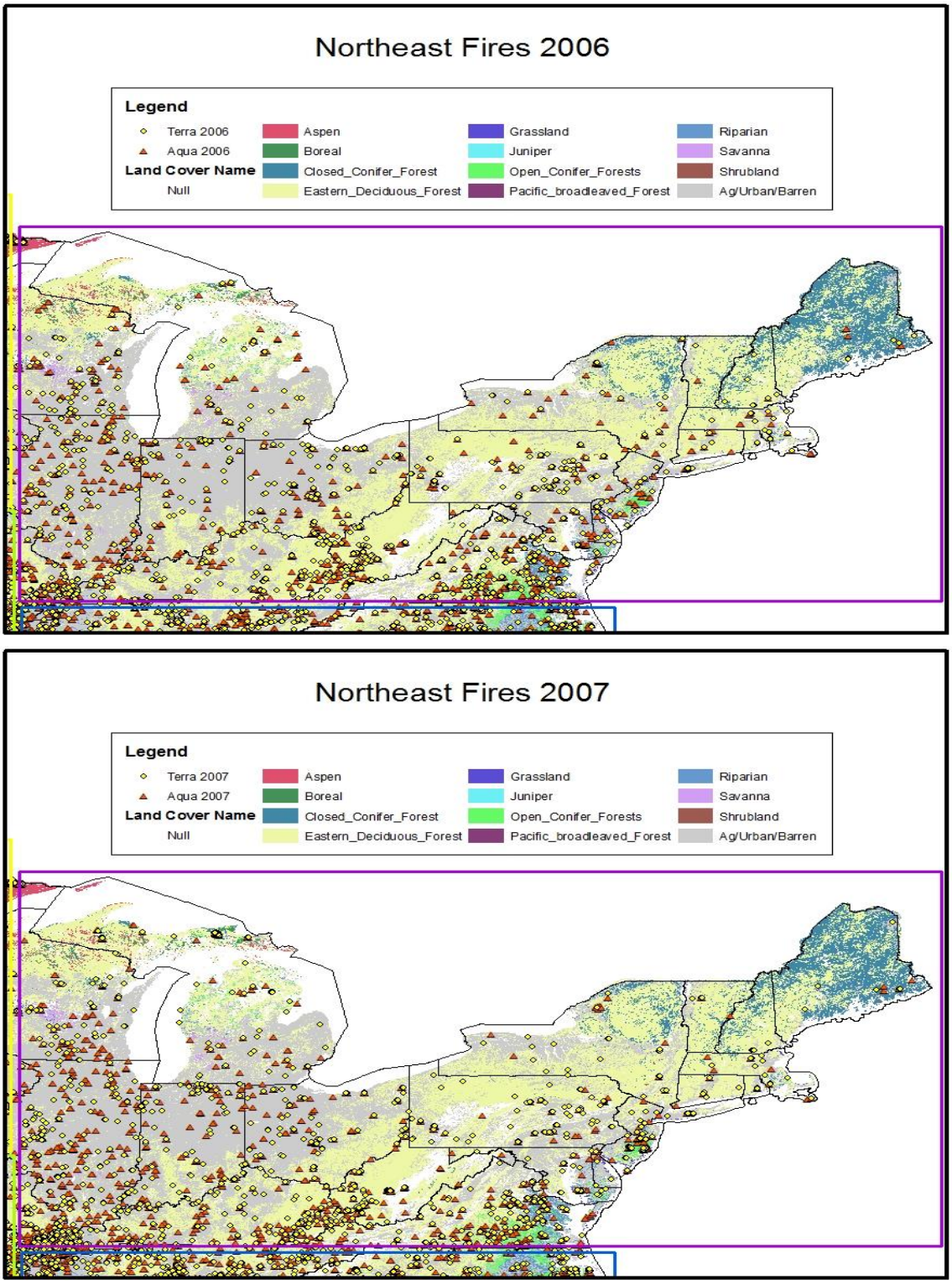

Figure 2.7: Observed fire pixel detections for the Northeast for 2006 and 2007. Most fire detections occur in the western half of the region in the agriculture/urban/barren land cover type. The most active areas in the region are consistently active in each year.

As seen in Figure 2.7, annual variability is difficult to assess due to many of the observed fires occurring in similar locations each year. However, because most fires occur in the agriculture/urban/barren land type and are for land management, the annual variability could be a product of when the fires are observed by the satellites relative to the fire ignition time. The fires in this land type have a strong influence on the regional emission coefficient value.

Table 2.9: Emission coefficient, in kilograms of smoke aerosols per megajoule, and correlation coefficient (C_e, R^2) values for Terra for the Northeast with the QA techniques applied. Underlined coefficients represent those calculated from a negative R-value and missing coefficients are the result of too few observations in that land cover type for that year.

Land Type	2003 (C_e, R^2)	2004 (C_e, R^2)	2005 (C_e, R^2)	2006 (C_e, R^2)	2007 (C_e, R^2)	2008 (C_e, R^2)
Null	0.0686, 0.004	0.0375, 0.065	0.0140, 0.013	0.0697, 0.004	0.145, 0.033	0.0207, 0.003
Eastern Deciduous Forest	0.0286, 0.533	0.0451, 0.044	0.0384, 0.075	0.0496, 0.331	0.0610, 0.073	0.0123, 0.010
Open Coniferous Forest	0.0177, 0.609	0.1190, 0.007	0.0083, 0.162	0.0115, 0.881	0.0372, 0.179	0.0053, 0.189
Riparian	0.0715, 0.154		0.0217, 0.354	0.0031, 0.011	0.0065, 0.062	0.0127, 0.002
Savanna	0.0586, 0.019			0.0546, 0.003	0.0843, 0.682	
Ag/Urban/ Barren	0.1339, 0.563	0.0786, 0.262	0.0671, 0.314	0.0724, 0.281	0.0270, 0.115	0.0373, 0.122

Northern Plains United States

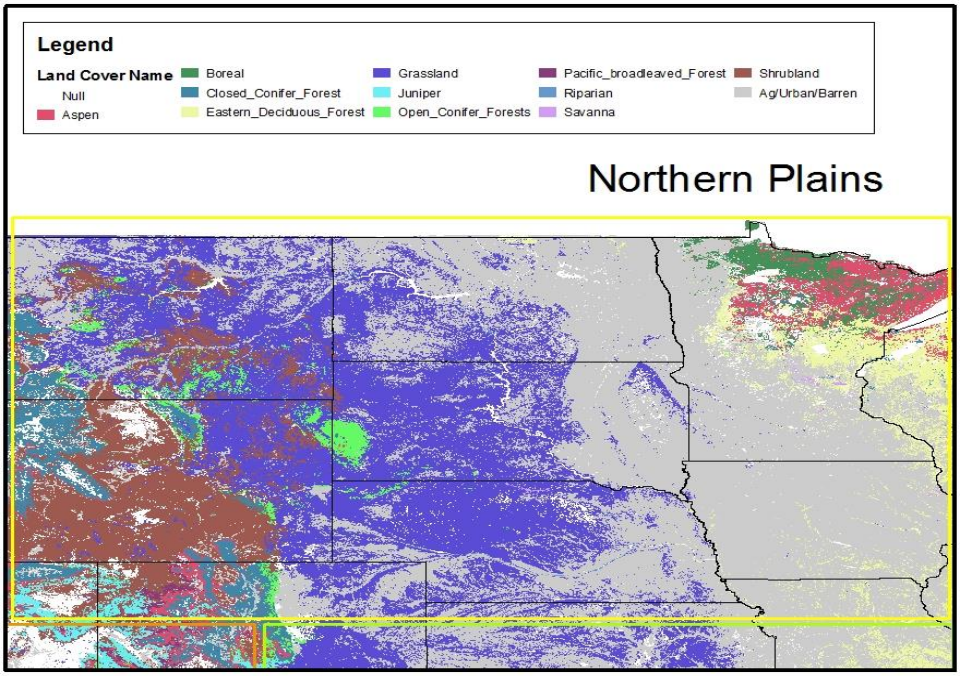

Figure 2.8: A map of the land cover types for the Northern Plains. Most of the land in this region is categorized as grassland and agriculture/urban/barren with significant contributions from other land types.

The diversity in the land cover types for the Northern Plains region is shown in Figure 2.8. On average, this region contains the third fewest observations (8.53%) of active fire pixels of the six regions. As seen in Table 2.10, most of the emission coefficients for the region are less than 0.01 and are coupled with poor correlation coefficients. Prior to any QA process, this region does not show a consistent trend of which satellite has the greater emission coefficient. This variability, along with the observed strong annual variability highlights the need for QA in this region.

Table 2.10: Emission coefficient, in kilograms of smoke aerosols per megajoule, and correlation coefficient (C_e, R^2) values for the Northern Plains before any QA screening was applied. N is the total number of MODIS overpasses (Aqua, Terra) included in the analysis and the Fire Pixels (Aqua, Terra) are the total number of fire pixels detected that year. Both satellites exhibit significant range between the maximum and minimum coefficient values.

Year	Aqua (C_e, R^2)	Terra (C_e, R^2)	N (A, T)	Fire Pixels (A, T)
2003	0.0093, 0.206	0.0060, 0.105	312, 296	6140, 3016
2004	0.0032, 0.071	0.0516, 0.253	285, 237	3996, 1815
2005	0.0243, 0.616	0.0250, 0.522	288, 259	4684, 2404
2006	0.0048, 0.440	0.0039, 0.166	370, 330	6223, 3512
2007	0.0017, 0.091	0.0064, 0.088	324, 307	4122, 2167
2008	0.0029, 0.025	0.0053, 0.078	307, 270	4206, 2166

Once the QA techniques were applied, the emission coefficient and correlation coefficient values increased into acceptable ranges, as shown in Table 2.11. On average, the emission coefficients for Terra exceeded those for Aqua but for 2005 and 2008, Aqua exceeds Terra. The annual variability observed in Table 2.10 remains prevalent in Table 2.11, but mostly in the emission coefficients. The correlation coefficients are relatively consistent from year to year compared to the non-QA values.

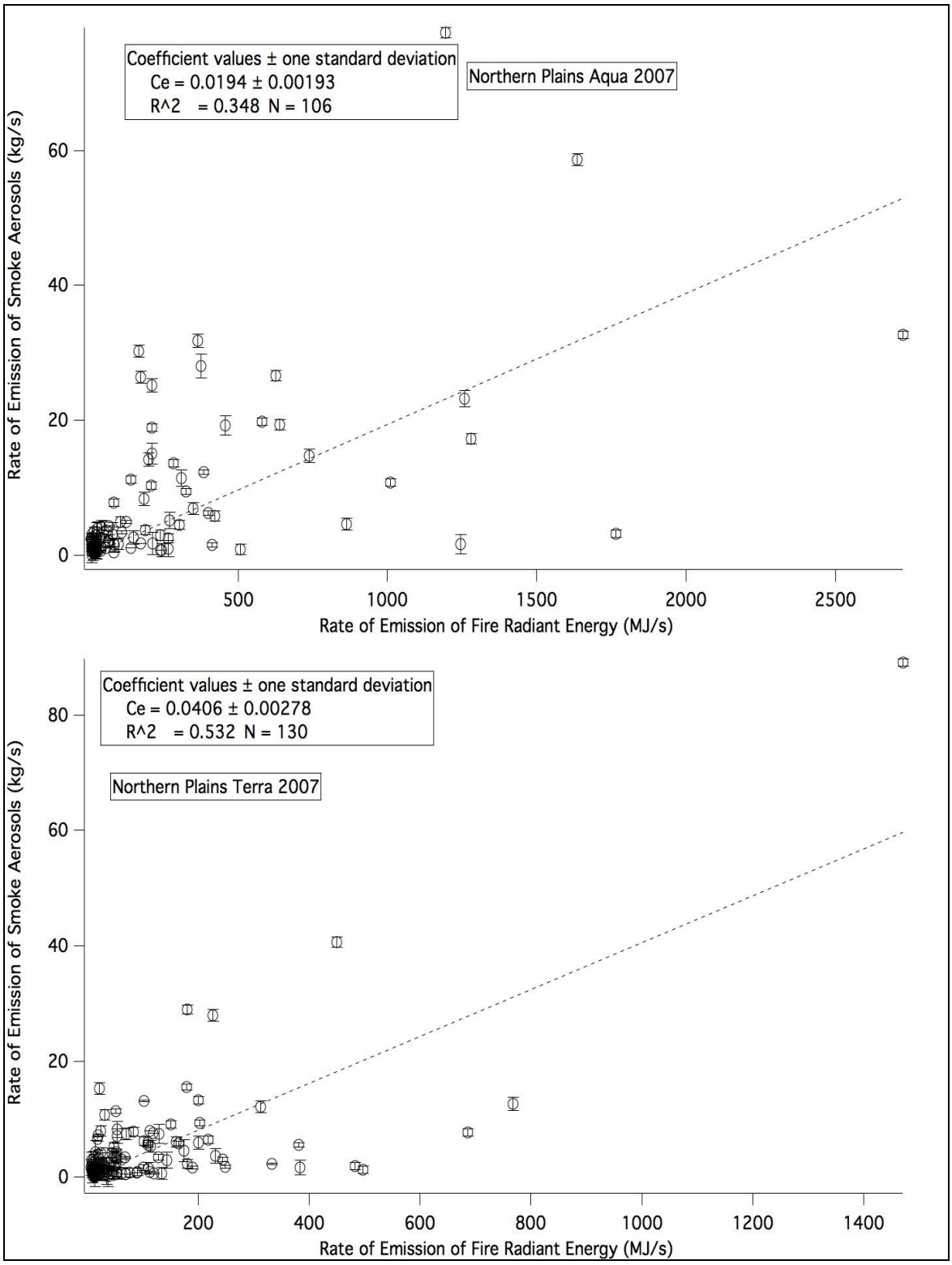

Figure 2.9: Plots of M_x versus R_{fre} for 2007. On average, R_{fre} for Aqua is much higher than for Terra, but M_x is higher for Terra at lower R_{fre}'s, which drives the higher emission coefficient value for Terra. The error bars represent the standard error of the rate of release of smoke aerosols.

The QA techniques reduced the number of observed active fire pixels to approximately a third of the previous values. As seen in Figure 2.9, the rates of emission of both fire radiant energy and smoke aerosols have increased from what is observed in the Northeast, particularly the fire radiant energy. These plots are a fair representation of the fire characteristics in the region with mostly low intensity fires coupled with low to moderate emissions of smoke aerosols. Also in this region are fires of moderate intensity coupled with moderate rates of emission of smoke aerosols. Because of the varied fire intensities and annual variability, the influence of the land cover types in the region requires investigation.

Table 2.11: Emission coefficient, in kilograms of smoke aerosols per megajoule, and correlation coefficient (C_e, R^2) values for the Northern Plains with the QA techniques applied. N is the total number of MODIS overpasses (Aqua, Terra) included in the analysis and the Fire Pixels (Aqua, Terra) are the total number of fire pixels detected that year. The correlation coefficient values show a significant increase from the QA techniques. While the emission coefficients have increased, their annual variability is still significant.

Year	Aqua (C_e, R^2)	Terra (C_e, R^2)	N (A, T)	Fire Pixels (A, T)
2003	0.0133, 0.583	0.0233, 0.506	125, 122	2287, 1014
2004	0.0217, 0.749	0.0456, 0.536	104, 100	1624, 720
2005	0.0354, 0.697	0.0303, 0.722	120, 97	1555, 925
2006	0.0187, 0.793	0.0248, 0.509	130, 109	1898, 1193
2007	0.0194, 0.348	0.0406, 0.532	106, 130	1219, 808
2008	0.0422, 0.793	0.0376, 0.691	101, 106	1125, 609

As seen in Figure 2.8, the dominant land cover types in the region are grassland and agriculture/urban/barren. The greatest number of fire pixel detections occurs in those two land cover types – 72.21% for agriculture/urban/barren and 17.60% for grassland. Similar to the emission coefficients in Table 2.11, the emission coefficients in Table 2.12 show considerable annual variability. This variability occurs in conjunction with differing numbers of fire detections in each year. Despite the annual variability, most of

the emission coefficients for Aqua show moderate to good correlation coefficient values. Even though most of the fire detections occur in the two dominant land cover types, their influence on the regional emission coefficient is inconclusive as the values for one of the land cover types varies significantly from the regional value each year.

Table 2.12: Emission coefficient, in kilograms of smoke aerosols per megajoule, and correlation coefficient (C_e, R^2) values for Aqua for the Northern Plains with the QA techniques applied. Underlined values represent those calculated from a negative R-value. While the grassland and agriculture/urban/barren land cover types contain the most fire pixel detections, their influence on the regional emission coefficient is inconclusive.

Land Type	2003 (C_e, R^2)	2004 (C_e, R^2)	2005 (C_e, R^2)	2006 (C_e, R^2)	2007 (C_e, R^2)	2008 (C_e, R^2)
Null	0.0216, 0.771	0.0597, 0.009	0.0418, 0.448	0.0282, 0.121	0.0309, 0.019	0.0696, 0.728
Eastern Deciduous Forest	0.0345, 0.606	0.0320, 0.497	0.0641, 0.833	0.0730, 0.859	0.0749, 0.243	0.0109, 0.707
Grassland	0.0121, 0.792	0.0207, 0.613	0.0411, 0.840	0.0201, 0.879	0.0484, 0.645	0.0469, 0.896
Open Coniferous Forest	0.0089, 0.418	0.0370, 0.880	0.0027, 0.884	0.0279, 0.429	0.0249, 0.005	0.0165, 0.050
Shrubland	0.0245, 0.343	0.0076, 0.288	0.0013, 0.015	0.0249, 0.932	0.0027, 0.245	0.0080, 0.570
Ag/Urban/ Barren	0.0227, 0.747	0.0228, 0.695	0.0433, 0.428	0.0350, 0.563	0.0209, 0.382	0.0509, 0.718

The number of fires detected by Terra is similarly distributed by land cover type to the number detected by Aqua, but with fewer total detections by Terra. Also similar to Aqua, the emission coefficient values for Terra in Table 2.13 show significant annual variability. Unlike the Northeast, the other land cover types may contain enough fire detections by Terra to influence the regional emission coefficients and not just as outlier data points.

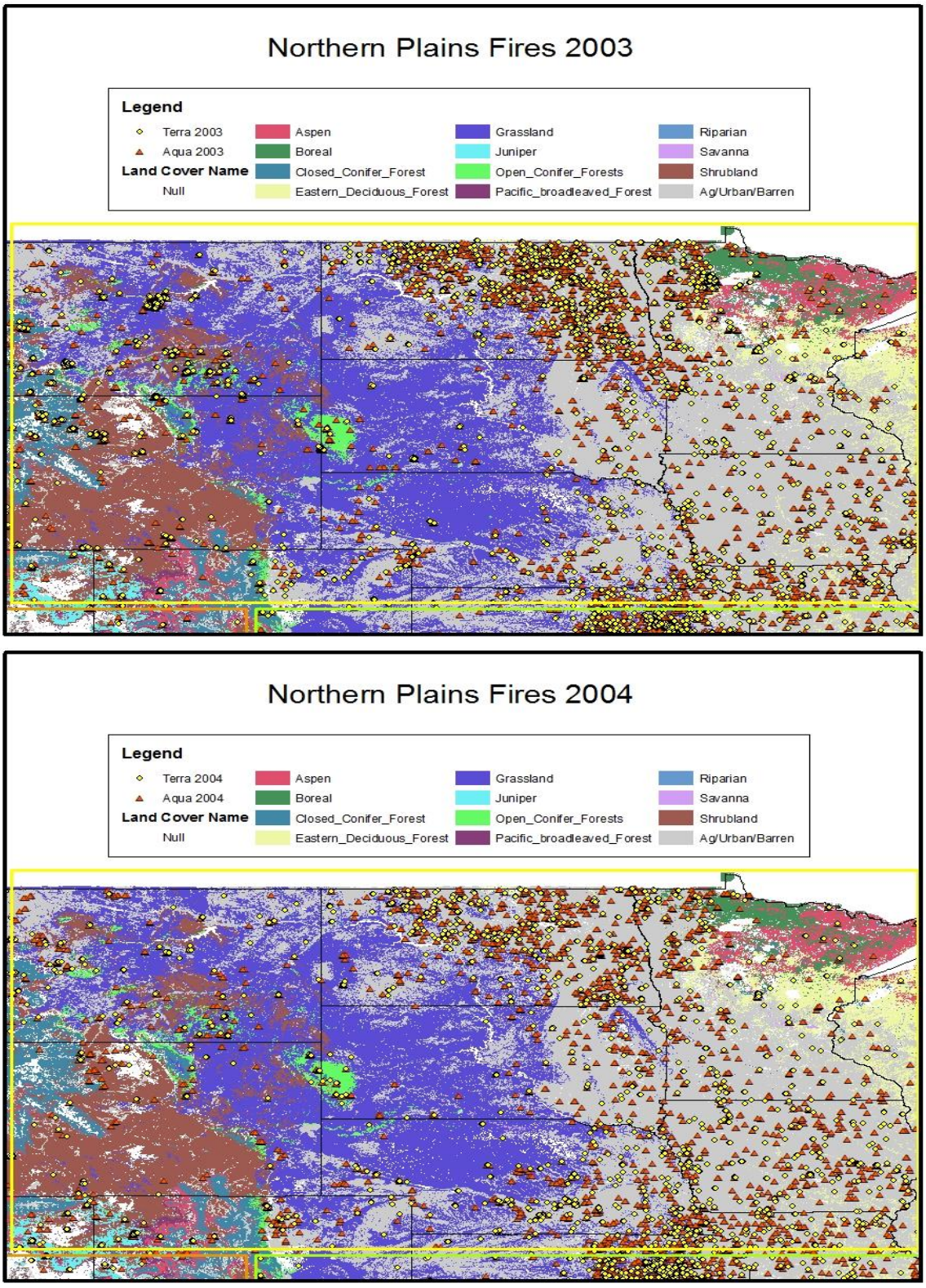

Figure 2.10: Observed fire pixel detections for the Northern Plains for 2003 and 2004. The most significant fire activity in the region occurs each year in eastern and northern North Dakota.

As seen in Figure 2.10, most of the fires in this region occur in the agriculture/urban/barren land on the eastern half of the region. The number and location of those fire detections are fairly consistent each year. In the western half of the region, fires are detected in enough numbers in the grassland, shrubland, and open coniferous forest land types to have a significant impact on the regional emission coefficient value for that year. As with in the Northeast, the annual variability in the emission coefficients for the agriculture/urban/barren land time is likely a function of the time of day of observation and fire ignition time. The annual variability in the other land cover types is likely a function of location in the region and number of occurrences.

Table 2.13: Emission coefficient, in kilograms of smoke aerosols per megajoule, and correlation coefficient (C_e, R^2) values for Terra for the Northern Plains with the QA techniques applied. Underlined values represent those calculated from a negative R-value and missing coefficients are the result of too few observations for that year.

Land Type	2003 (C_e, R^2)	2004 (C_e, R^2)	2005 (C_e, R^2)	2006 (C_e, R^2)	2007 (C_e, R^2)	2008 (C_e, R^2)
Null	0.0290, 0.315	0.0269, 0.622	0.0133, 0.083	0.0413, 0.855	0.1007, 0.972	0.0132, 0.326
Eastern Deciduous Forest	0.0723, 0.291	0.0440, 0.604	0.0657, 0.625	0.1451, 0.614	0.1119, 0.972	0.0059, 0.025
Grassland	0.0218, 0.149	0.0623, 0.563	0.0456, 0.658	0.0227, 0.591	0.0232, 0.058	0.0797, 0.980
Open Coniferous Forest	0.0156, 0.782	0.0229, 0.108		0.0060, 0.089	<u>0.0370, 0.014</u>	
Shrubland	0.0153, 0.116	0.0342, 0.430	0.0050, 0.022	0.0248, 0.976	0.0498, 0.048	<u>0.0055, 0.006</u>
Ag/Urban/ Barren	0.0300, 0.589	0.0708, 0.687	0.0311, 0.733	0.0578, 0.723	0.0375, 0.168	0.0427, 0.332

Northwest United States

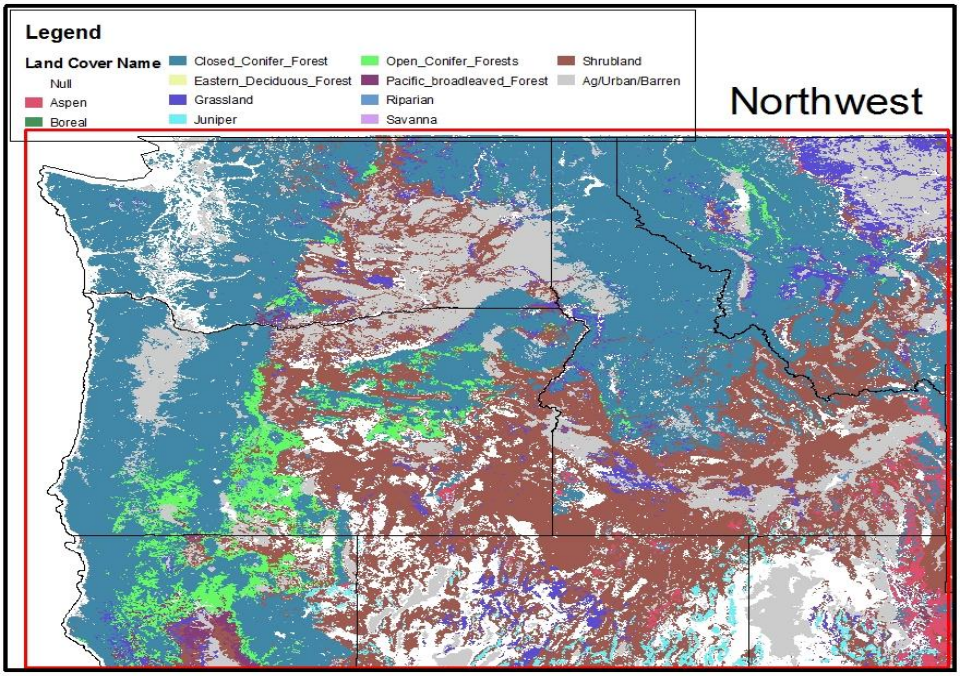

Figure 2.11: A map of the land cover types in the Northwest. The fire activity in this resides mostly in the closed coniferous forests but significant contributions from the other land types vary annually.

In addition to the diversity in the land cover types in the region, seen in Figure 2.11; the Northwest is also quite diverse geographically. On average, the Northwest contains the third most fire pixel detections of the six regions (15.96%). Despite the high fire activity in the region, the Northwest has the second lowest average emission coefficients. As seen in Table 2.14, all of the emission coefficients for both satellites are less than 0.01 except for Terra 2008. This suggests that this region is prone to fires with high to very high R_{fre} coupled with relatively low M_x. Unique to this region is the relative agreement between the emission coefficients calculated for each satellite. The prevalence of more natural fires in this region could lead to this agreement between satellites; however, the agreement does not hold after the QA techniques are applied.

Table 2.14: Emission coefficient, in kilograms of smoke aerosols per megajoule, and correlation coefficient (C_e, R^2) values for the Northwest before any QA screening was applied. N is the total number of MODIS overpasses (Aqua, Terra) included in the analysis and the Fire Pixels (Aqua, Terra) are the total number of fire pixels detected that year. Most of the emission coefficients are well correlated between the two satellites, with Terra having the greatest value on average.

Year	Aqua (C_e, R^2)	Terra (C_e, R^2)	N (A, T)	Fire Pixels (A, T)
2003	0.0039, 0.423	0.0040, 0.299	359, 329	9173, 4687
2004	0.0053, 0.219	0.0059, 0.298	319, 298	4465, 2656
2005	0.0029, 0.523	0.0022, 0.350	324, 287	6259, 3058
2006	0.0023, 0.533	0.0026, 0.254	355, 335	11892, 6158
2007	0.0028, 0.587	0.0051, 0.606	376, 361	19013, 8540
2008	0.0070, 0.296	0.0128, 0.381	362, 324	10107, 5481

The application of the QA techniques led to a significant improvement in the emission and correlation coefficient values for Terra. For Aqua, there was limited improvement in both the emission and correlation coefficient values. The agreement between the two satellites that was observed before the QA is limited to 2005, with the other years showing Terra having a significantly higher emission coefficient value than Aqua.

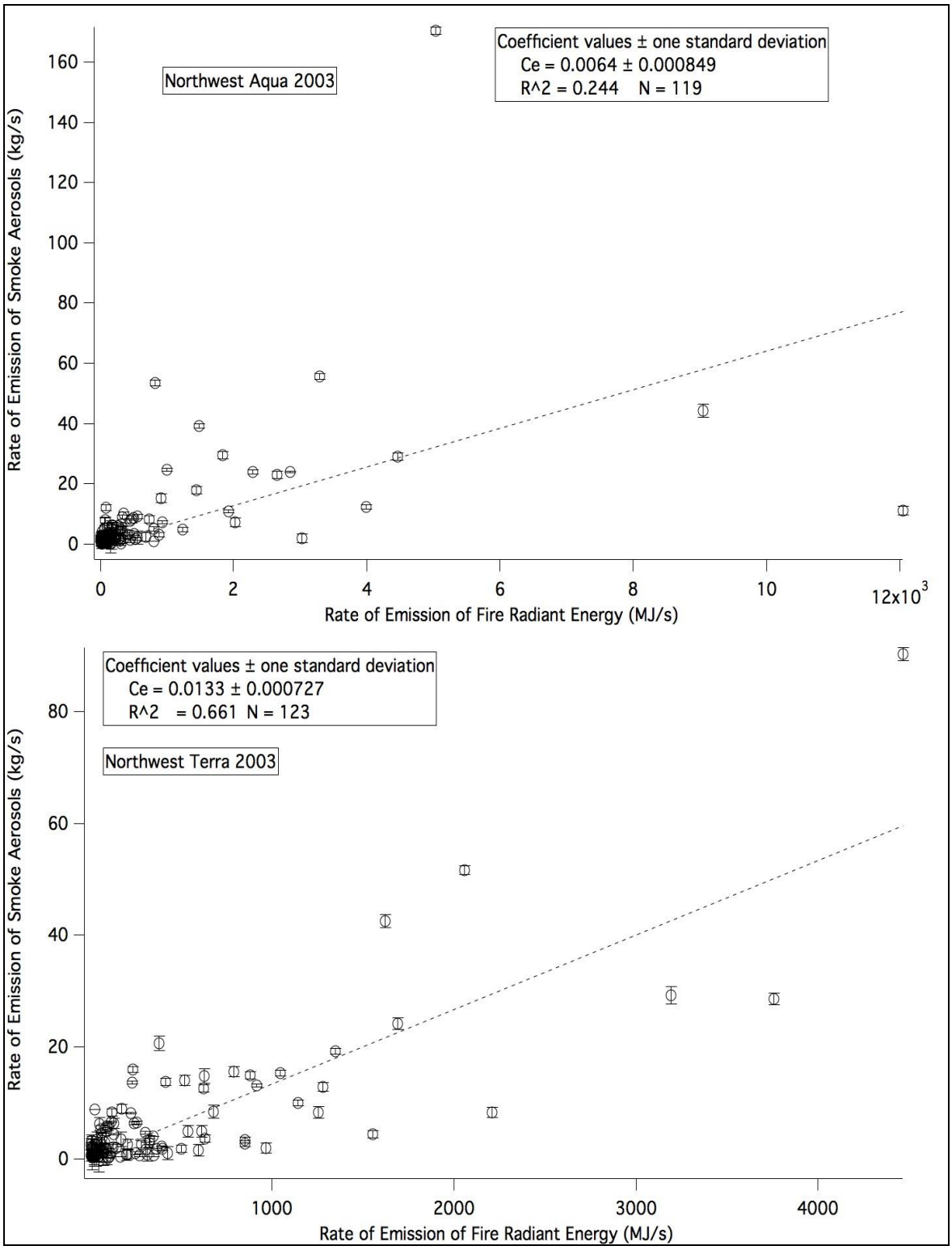

Figure 2.12: Plots of M_x versus R_{fre} for 2003. The data points with high R_{fre} values drive the emission coefficient value for Aqua as their M_x values are relatively low. The error bars represent the standard error of the rate of release of smoke aerosols.

As seen in Figure 2.12, the distribution of most of the data points is quite similar between the two satellites. What causes the difference in the emission coefficient value are the data points with high R_{fre} coupled with relatively low M_x. Looking back at Figures 2.7 and 2.9 for the Northeast and Northern Plains, the maximum R_{fre} values are significantly lower than in those regions than in the Northwest. These high R_{fre} data points are likely associated with large wildfires, which occur frequently in this region. Looking at a visible image (Figure A13) of an overpass containing high R_{fre}, it is not obvious why the value for M_x for that overpass is so low relative to R_{fre}. The number of overpasses or number of fire pixel detections per year does not provide conclusive evidence for the occurrence of these data points.

Table 2.15: Emission coefficient, in kilograms of smoke aerosols per megajoule, and correlation coefficient (C_e, R^2) values for the Northwest with the QA techniques applied. N is the total number of MODIS overpasses (Aqua, Terra) included in the analysis and the Fire Pixels (Aqua, Terra) are the total number of fire pixels detected that year. The emission coefficients for Terra experienced significant increases but the increase in the emission coefficients for Aqua were not as significant.

Year	Aqua (C_e, R^2)	Terra (C_e, R^2)	N (A, T)	Fire Pixels (A, T)
2003	0.0064, 0.244	0.0133, 0.661	119, 123	2606, 1811
2004	0.0058, 0.211	0.0093, 0.478	102, 116	1340, 1007
2005	0.0104, 0.671	0.0118, 0.343	100, 107	1375, 986
2006	0.0071, 0.649	0.0108, 0.497	107, 114	3310, 2022
2007	0.0055, 0.532	0.0202, 0.657	107, 117	4442, 2590
2008	0.0180, 0.620	0.0258, 0.512	119, 116	3912, 2256

In the Northwest, the majority of the fire pixel detections occur in the closed coniferous forest land cover type (61.28%). The other land types that make a significant contribution to the burning in the region are the open coniferous forest (6.38%), shrubland (8.21%), and agriculture/urban/barren (18.84%) land types. Because most of the fires occur in the closed coniferous forests, the regional emission coefficient follows

the trend of the emission coefficient for that land type as seen in Table 2.16. This holds in years such as 2004 and 2005 where the number of fire pixels detected in that land cover type do not greatly exceed the number of pixels detected in the other land cover types. With the QA techniques applied, the likelihood of this being the over-measurement of FRE or the influence of clouds is minimal. From the data available, a definitive reason is not apparent, as the emission and correlation coefficient values are not connected to the number of overpasses or fire pixel detections for that year.

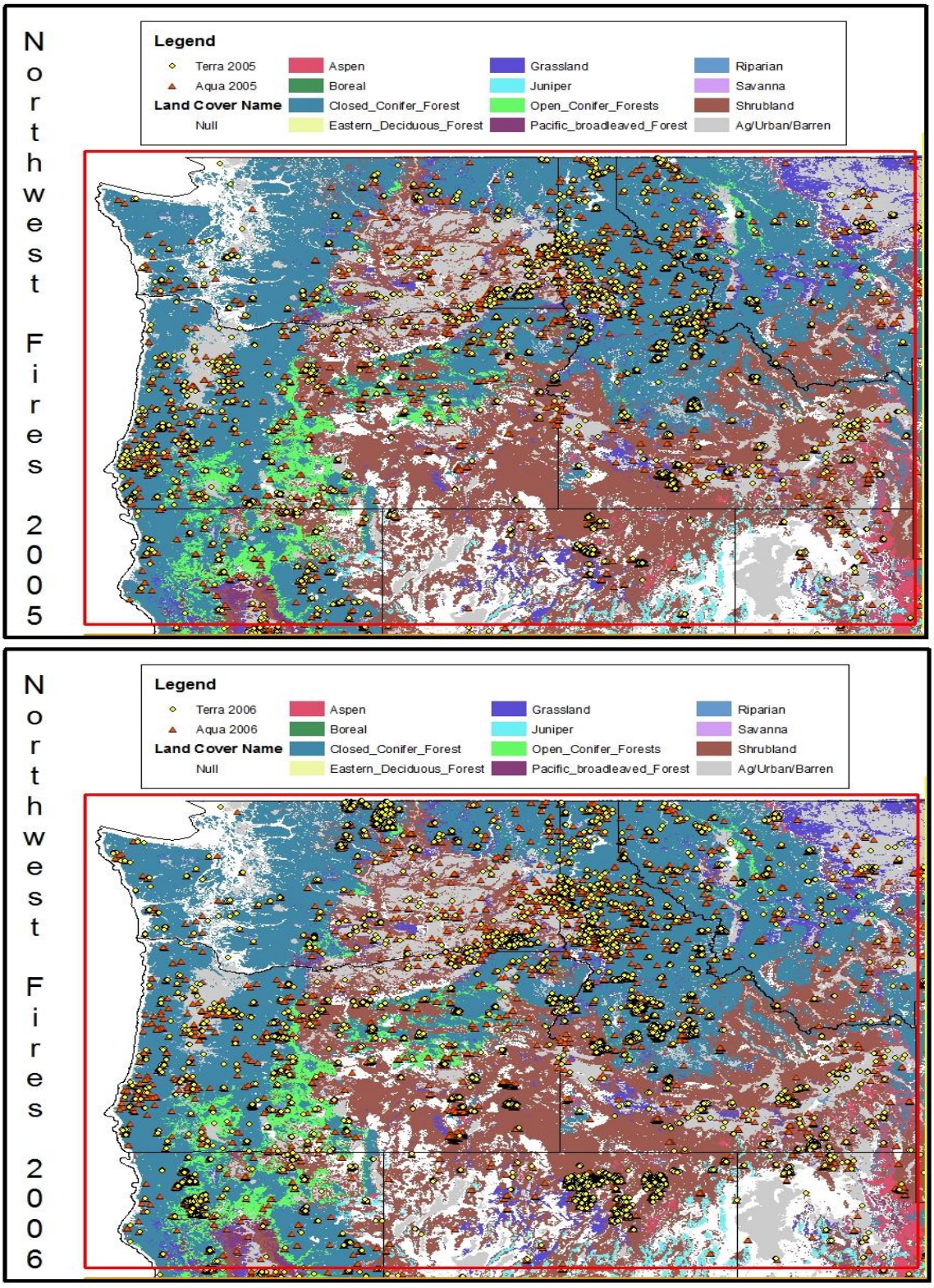

Figure 2.13: Observed fire pixel detections of an active fire year (2006) versus a relatively inactive fire year (2005) for the Northwest.

Compared to the other two northern regions, the areas of high fire activity are much more dynamic in the Northwest. As seen in Figure 2.13, there are some areas of consistent fire detection such as the area around the southeast Washington and Idaho border and southwest Oregon. Depending on the year, areas of high fire activity can be found in the forested mountains of Idaho and western Montana, in the Washington Cascades, in Northern California, or in the shrublands of Nevada and Idaho. Using the emission coefficients in Table 2.16 and plots like those in Figure 2.13, the value of the emission coefficient is not conclusively related to the location of highest fire activity.

Table 2.16: Emission coefficient, in kilograms of smoke aerosols per megajoule, and correlation coefficient (C_e, R^2) values for Aqua for the Northwest with the QA techniques applied. For all years, the emission coefficient for the region follows that of the closed coniferous forest land type. Underlined values represent those calculated from a negative R-value and missing coefficients are the result of too few observations for that year.

Land Type	2003 (C_e, R^2)	2004 (C_e, R^2)	2005 (C_e, R^2)	2006 (C_e, R^2)	2007 (C_e, R^2)	2008 (C_e, R^2)
Null	0.0380, 0.174	0.0128, 0.000	0.0042, 0.042	0.0129, 0.190	0.0058, 0.570	<u>0.0108, 0.025</u>
Closed Coniferous Forest	0.0065, 0.194	0.0081, 0.293	0.0129, 0.664	0.0081, 0.662	0.0047, 0.495	0.0221, 0.507
Grassland	0.0225, 0.046	0.0157, 0.194	0.0391, 0.181	0.0117, 0.168	0.0053, 0.002	0.0114, 0.358
Open Coniferous Forest	0.0044, 0.140	0.0028, 0.220	0.0118, 0.160	0.0058, 0.023	0.0098, 0.631	0.0373, 0.754
Pacific Broadleaved Forest	<u>0.0057, 0.009</u>	0.0092, 0.879		<u>0.0154, 0.024</u>		0.0357, 0.791
Shrubland	0.0032, 0.086	0.0124, 0.119	0.0115, 0.551	0.0068, 0.255	0.0160, 0.883	0.0056, 0.091
Ag/Urban/ Barren	0.0261, 0.474	0.0094, 0.265	0.0103, 0.161	0.0055, 0.424	0.0054, 0.411	0.0094, 0.615

In the Northwest, nearly all of the emission coefficients for Terra are greater than those for Aqua for each land cover type. For the closed coniferous forest land type, the

correlation coefficient is also greater for Terra than Aqua for four of the six years. The correlation coefficients for Terra for that land type are all in the moderate to satisfactory range so there is confidence in these values. Looking at the year 2005 in Table 2.17, the influence of the shrubland on the regional emission coefficient is fairly clear. Because of the low numbers of fire detections in the closed coniferous forest and the increased number of fire detections in the shrublands for that year, the emission coefficient for the region is brought down to account for the increased shrubland burning in the region. Using this example, the annual variability in the Northwest is a product of the amount of fire activity in the closed coniferous forests and shrublands.

Table 2.17: Emission coefficient, in kilograms of smoke aerosols per megajoule, and correlation coefficient (C_e, R^2) values for Terra for the Northwest with the QA techniques applied. While the emission coefficient for the region tends to follow the emission coefficient for the closed coniferous forest land type, in some years, the other land types have a raising or lowering influence on the regional value. Underlined values represent those calculated from a negative R-value and missing coefficients are the result of too few observations for that year.

Land Type	2003 (C_e, R^2)	2004 (C_e, R^2)	2005 (C_e, R^2)	2006 (C_e, R^2)	2007 (C_e, R^2)	2008 (C_e, R^2)
Null	0.0216, 0.311	0.0618, 0.708	0.0045, 0.023	0.0117, 0.150	0.0116, 0.197	0.0174, 0.035
Closed Coniferous Forest	0.0141, 0.691	0.0062, 0.339	0.0232, 0.632	0.0143, 0.481	0.0229, 0.679	0.0326, 0.527
Grassland	0.0142, 0.004	0.0048, 0.067	0.0458, 0.484	0.0190, 0.007	0.0079, 0.064	0.0502, 0.551
Open Coniferous Forest	0.0064, 0.256	0.0179, 0.200	0.0222, 0.132	0.0139, 0.043	0.0094, 0.064	0.0413, 0.232
Pacific Broadleaved Forest	0.0449, 0.983	0.0177, 0.324		0.0223, 0.001		0.0179, 0.073
Shrubland	0.0130, 0.111	0.0057, 0.011	0.0033, 0.317	0.0068, 0.762	0.0053, 0.199	0.0084, 0.481
Ag/Urban/ Barren	0.0205, 0.571	0.0149, 0.219	0.0144, 0.261	0.0076, 0.120	0.0164, 0.063	0.0370, 0.409

Southeast United States

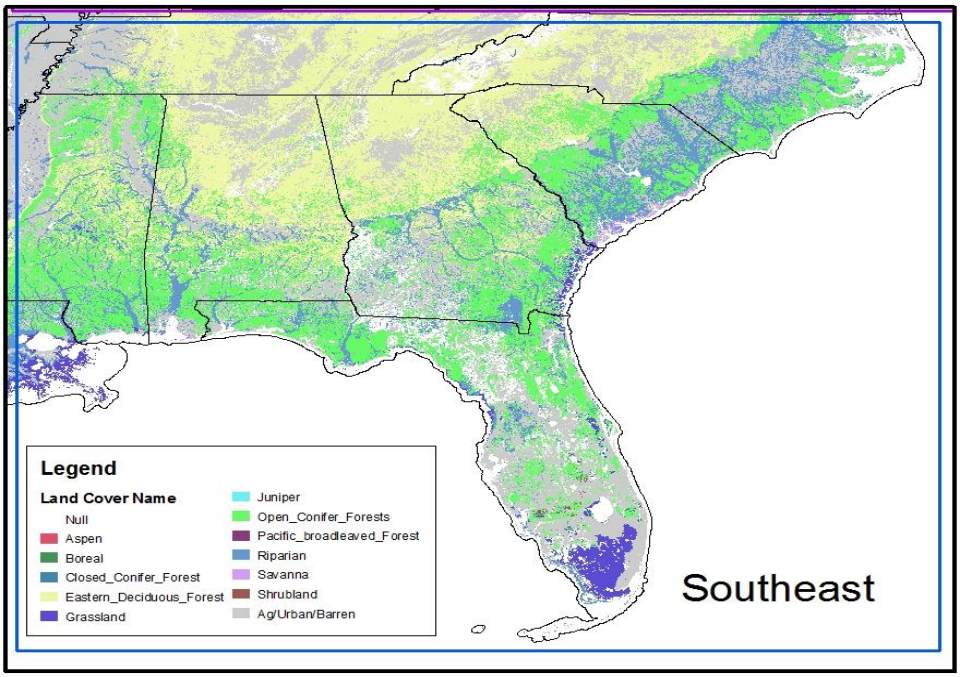

Figure 2.14: A map of the land cover types in the Southeast. The open coniferous forest, riparian, dominates the coastal area and agriculture/urban/barren land types while the eastern deciduous forest and agriculture/urban/barren land types dominate the inland area.

The land cover types present in the Southeast, seen in Figure 2.14, play a significant role in the fire activity in the region. On average, this region contains the most fire pixel detections for Terra (32.25%) and the second most for Aqua (29.54%). Its emission coefficients rank third and fourth respectively for Aqua and Terra. With the exception of Terra 2007, the emission coefficients are all greater than 0.01, the low threshold established by Ichoku and Kaufman (2005). The correlation coefficients for Aqua are good for this area of the globe while the ones for Terra are low, as seen in Table 2.18. After this initial evaluation, the QA techniques were applied to test their effect on the coefficients.

Table 2.18: Emission coefficient, in kilograms of smoke aerosols per megajoule, and correlation coefficient (C_e, R^2) values for the Southeast before any QA screening was applied. N is the total number of MODIS overpasses (Aqua, Terra) included in the analysis and the Fire Pixels (Aqua, Terra) are the total number of fire pixels detected that year. The emission and correlation coefficient values for Aqua are greater than for Terra every year.

Year	Aqua (C_e, R^2)	Terra (C_e, R^2)	N (A, T)	Fire Pixels (A, T)
2003	0.0169, 0.668	0.0111, 0.287	393, 361	8682, 5436
2004	0.0243, 0.603	0.0133, 0.301	412, 398	9622, 6518
2005	0.0202, 0.558	0.0144, 0.359	447, 447	11367, 7867
2006	0.0210, 0.672	0.0158, 0.262	474, 460	13498, 8575
2007	0.0134, 0.515	0.0076, 0.209	467, 468	14134, 9327
2008	0.0175, 0.555	0.0125, 0.299	443, 450	12106, 8576

For both satellites, the effect of the QA techniques was largely positive as most years experienced an increase in their emission coefficient and correlation coefficient values. On average, the emission coefficients for Aqua exceed those for Terra with only 2006 having Terra greater than Aqua. As seen in Table 2.19, there is little agreement between satellites and the annual variability does not agree between satellites nor does it agree with the number of fire detections.

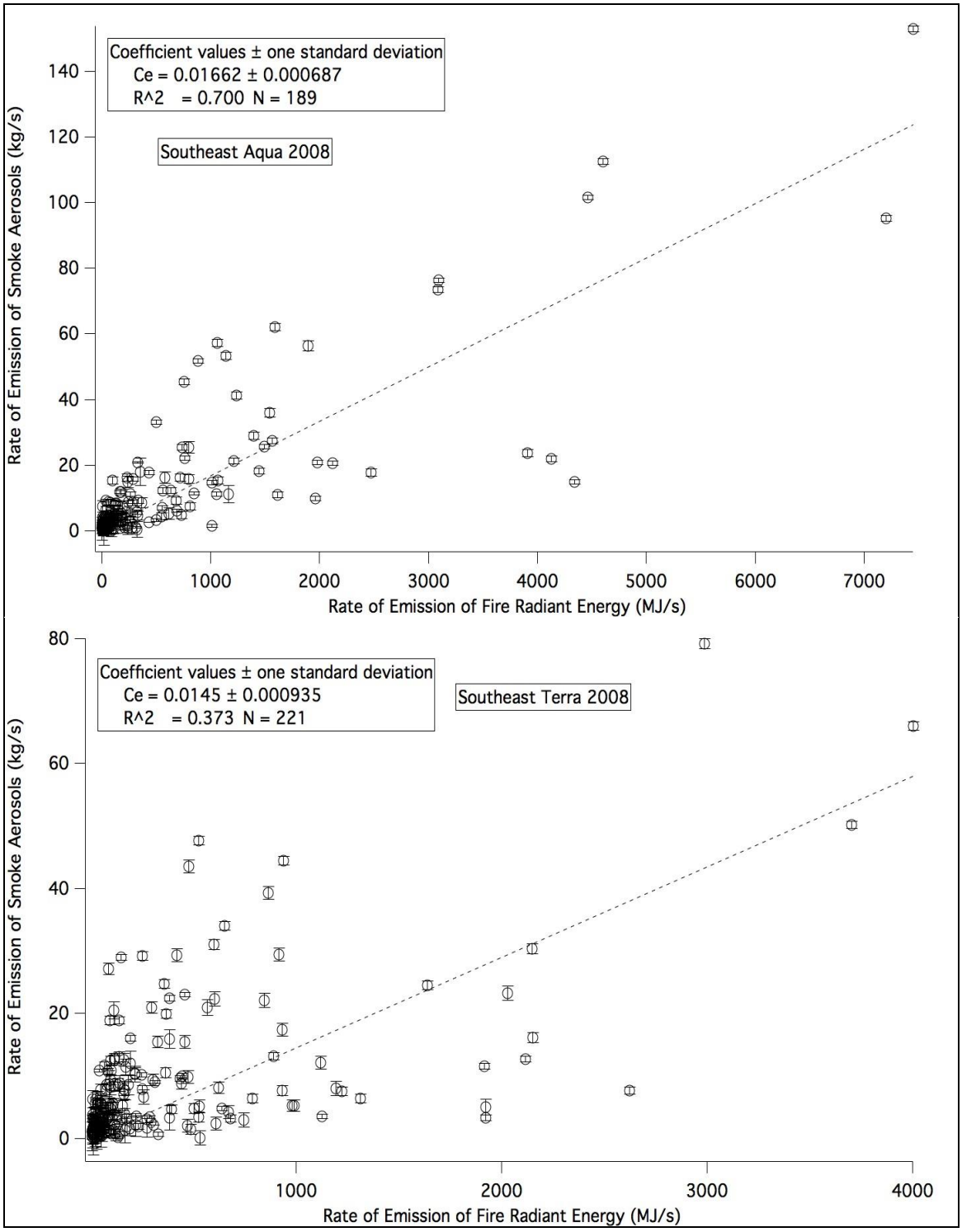

Figure 2.15: Plots of M_x versus R_{fre} for 2008. In these plots, the high R_{fre} data points, particularly for Aqua, are well correlated with the rest of the data points because of their pairing with high values of M_x. The error bars represent the standard error of the rate of release of smoke aerosols.

Most of the fire detections in this region result in low values of R_{fre}, as seen in Figure 2.15. The few higher energy detections are made by Aqua are also coupled with higher values of M_x, leading to higher emission coefficient values. This characteristic is likely the result of the prevalence of sporadic and low intensity agricultural and forest management burning in the region (Mu et al., 2011). To validate this claim, the emission coefficients for the region were calculated by land cover type.

Table 2.19: Emission coefficient, in kilograms of smoke aerosols per megajoule, and correlation coefficient (C_e, R^2) values for the Southeast with the QA techniques applied. N is the total number of MODIS overpasses (Aqua, Terra) included in the analysis and the Fire Pixels (Aqua, Terra) are the total number of fire pixels detected that year. For every year except 2006, the Aqua greater than Terra relationship held. On average, both satellites experienced and increase in their correlation coefficient values, but Terra experienced decreases in 2005 and 2006.

Year	Aqua (C_e, R^2)	Terra (C_e, R^2)	N (A, T)	Fire Pixels (A, T)
2003	0.0186, 0.746	0.0119, 0.371	161, 193	3603, 2697
2004	0.0295, 0.676	0.0230, 0.409	172, 193	3988, 3246
2005	0.0212, 0.634	0.0179, 0.339	189, 223	5277, 4000
2006	0.0212, 0.655	0.0229, 0.155	183, 230	5676, 4270
2007	0.0212, 0.743	0.0120, 0.253	192, 234	6024, 4607
2008	0.0166, 0.700	0.0145, 0.373	189, 221	5313, 3917

The land cover type with the most fire detections is agriculture/urban/barren (34.92)%, followed by open coniferous forest (32.58%), eastern deciduous forest (14.11%), riparian (8.82%), and grassland (0.95%). As seen in Table 2.20, the emission coefficient values for Aqua exhibit a class-like trend in the emission coefficient values even with annual variability. In most years, the agriculture/urban/barren land cover type has the greatest emission coefficient and therefore is in the top class. The second class is occupied by the riparian land type, followed by the two forest land types in the third class. The grassland type is in the last class due to its typically low value. The two forest types do not exhibit as much annual variability as the other land types. This is likely the

result of land management fires in these land types having similar fire activity from year to year.

Table 2.20: Emission coefficient, in kilograms of smoke aerosols per megajoule, and correlation coefficient (C_e, R^2) values for Aqua for the Southeast with the QA techniques applied. Underlined values represent those calculated from a negative R-value. There is not a clear link between one land cover type's emission coefficient and the regional emission coefficient value.

Land Type	2003 (C_e, R^2)	2004 (C_e, R^2)	2005 (C_e, R^2)	2006 (C_e, R^2)	2007 (C_e, R^2)	2008 (C_e, R^2)
Null	0.0228, 0.604	0.0429, 0.353	0.0361, 0.364	0.0322, 0.760	0.0434, 0.773	0.0316, 0.603
Eastern Deciduous Forest	0.0197, 0.659	0.0194, 0.511	0.0154, 0.619	0.0159, 0.556	0.0114, 0.359	0.0144, 0.641
Grassland	0.0253, 0.032	<u>0.0119, 0.028</u>	<u>0.0059, 0.031</u>	0.0076, 0.158	0.0078, 0.002	0.0015, 0.166
Open Coniferous Forest	0.0185, 0.657	0.0175, 0.380	0.0191, 0.460	0.0225, 0.597	0.0247, 0.845	0.0185, 0.736
Riparian	0.0135, 0.119	0.0370, 0.646	0.0341, 0.529	0.0349, 0.552	0.0123, 0.092	0.0188, 0.361
Ag/Urban/ Barren	0.0310, 0.663	0.0549, 0.871	0.0324, 0.675	0.0409, 0.738	0.0220, 0.497	0.0332, 0.765

The emission coefficients by land type for Terra (Table 2.21) exhibit many of the same characteristics as those for Aqua. Because of many of the fires in this region are prescribed burns, the reason for the emission coefficient values for Aqua exceeding those for Terra is likely related to the time of observation. While similar numbers of detection exist between the two satellites, R_{fre} and M_x are lower for Terra, suggesting that the prescribed burns have yet to reach their peak emission rates.

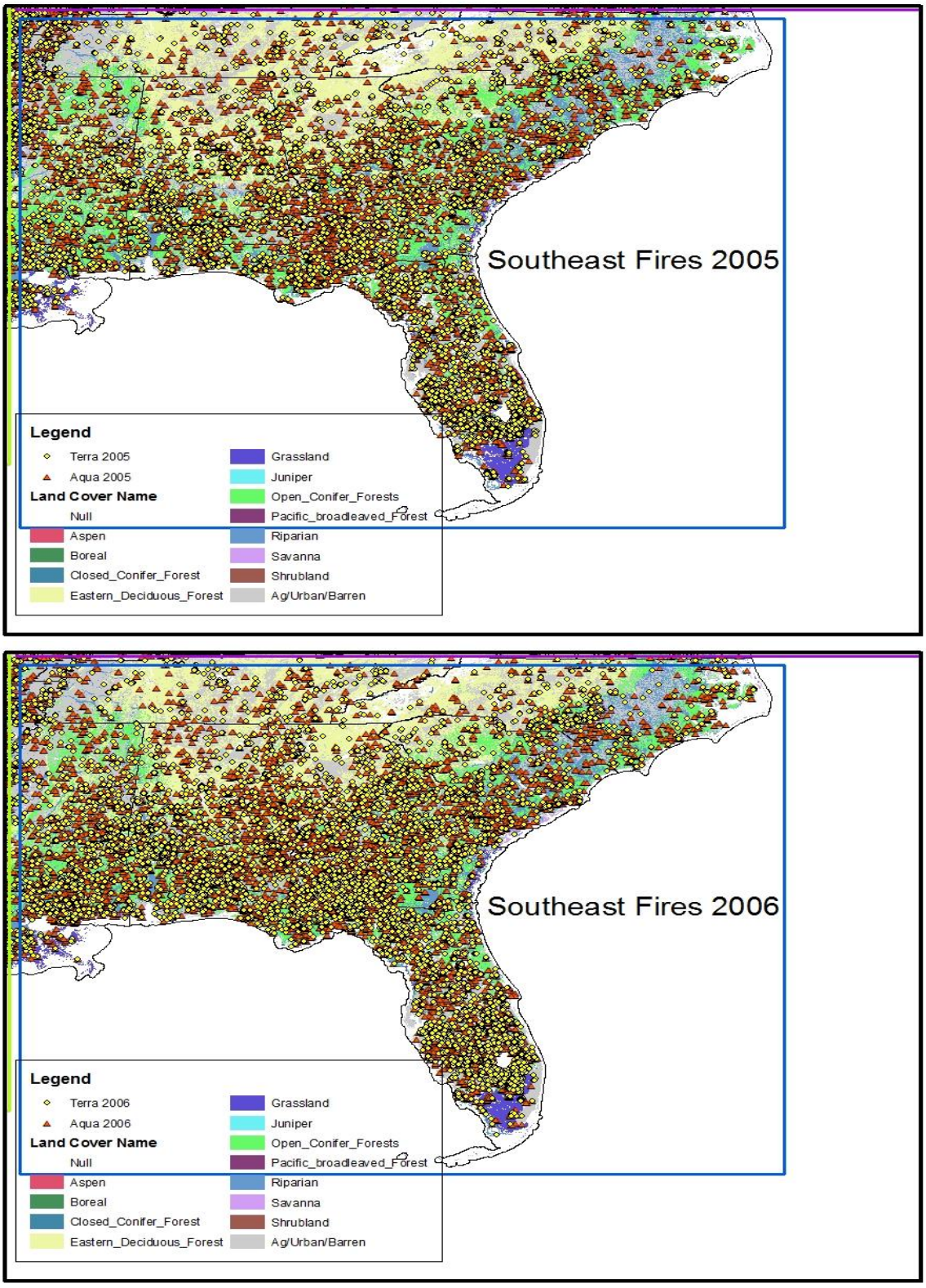

Figure 2.16: Observed fire pixel detections in the Southeast for 2005 and 2006. Minimal change in fire locations is observed in this region.

The reason for the annual variability in this region where so many of the detected fires are for land management purposes is difficult to deduce. As seen in Figure 2.16, a majority of the fire detections for both satellites occur in nearly the same locations each year. Due to the ubiquitous nature of the fire detections in the region, it is difficult to separate any wildfires from the land management fires. Additionally, the emission coefficient values do not follow the number of fire detections for the year in which they are calculated.

Table 2.21: Emission coefficient, in kilograms of smoke aerosols per megajoule, and correlation coefficient (C_e, R^2) values for Terra for the Southeast with QA applied. Underlined values represent those calculated from a negative R-value. As observed with the regional emission coefficient values, most of these emission coefficients are less than their Aqua counterpart.

Land Type	2003 (C_e, R^2)	2004 (C_e, R^2)	2005 (C_e, R^2)	2006 (C_e, R^2)	2007 (C_e, R^2)	2008 (C_e, R^2)
Null	0.0142, 0.081	0.0416, 0.361	0.0160, 0.095	0.0397, 0.491	0.0231, 0.124	0.0228, 0.605
Eastern Deciduous Forest	0.0086, 0.299	0.0149, 0.176	0.0112, 0.272	0.0152, 0.568	0.0181, 0.371	0.0144, 0.307
Grassland	0.0155, 0.060	0.0533, 0.012	0.0196, 0.033	0.0114, 0.622	0.0150, 0.371	0.0022, 0.537
Open Coniferous Forest	0.0108, 0.499	0.0164, 0.308	0.0174, 0.397	0.0147, 0.328	0.0141, 0.267	0.0128, 0.374
Riparian	0.0175, 0.362	0.0304, 0.446	0.0110, 0.059	0.0169, 0.144	0.0071, 0.363	0.0153, 0.372
Ag/Urban/ Barren	0.0201, 0.150	0.0368, 0.258	0.0274, 0.320	0.0408, 0.301	0.0279, 0.231	0.0242, 0.224

Southern Plains United States

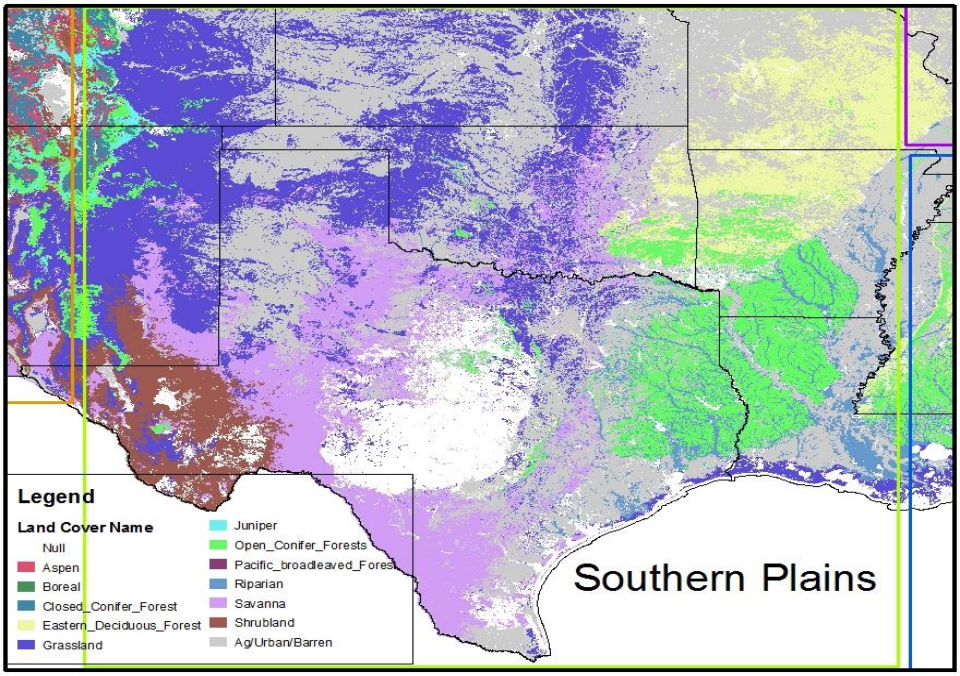

Figure 2.17: A map of the land cover types in the Southern Plains. Each land cover type present in the region covers a significant portion of the land area.

Many land cover types sharing most of the land area characterize the Southern Plains region. As seen in Figure 2.17, there is not one land type that dominates over the others. This region ranks first in number of fire detections for Aqua (32.03%) and second for Terra (28.53%) and its average emission coefficients rank first and third for Aqua and Terra. For all years, the emission coefficients in Table 2.22 are greater than 0.01, which is greater than the minimum expected value from Ichoku and Kaufman (2005). The correlation coefficients in this region, on average, are fair and coupled with a fair amount of annual variability, the QA techniques were applied in an effort to improve the correlations and investigate the variability.

Table 2.22: Emission coefficient, in kilograms of smoke aerosols per megajoule, and correlation coefficient (C_e, R^2) values for the Southern Plains before any QA screening was applied. N is the total number of MODIS overpasses (Aqua, Terra) included in the analysis and the Fire Pixels (Aqua, Terra) are the total number of fire pixels detected that year. There are an equal number of years of the emission coefficients for Aqua exceeding those for Terra as there is for Terra exceeding Aqua in this region.

Year	Aqua (C_e, R^2)	Terra (C_e, R^2)	N (A, T)	Fire Pixels (A, T)
2003	0.0218, 0.605	0.0208, 0.375	469, 430	11469, 7589
2004	0.0139, 0.421	0.0114, 0.190	461, 421	11402, 5927
2005	0.0204, 0.443	0.0192, 0.475	528, 496	15647, 9530
2006	0.0120, 0.416	0.0147, 0.334	514, 495	12784, 7861
2007	0.0152, 0.448	0.0173, 0.547	493, 457	11529, 6382
2008	0.0124, 0.359	0.0165, 0.386	572, 522	16965, 8761

The application of the QA techniques raised the value of both the emission and correlation coefficients for both satellites for every year except for the correlation coefficient for Aqua 2006. On average, the emission coefficients for Aqua exceed those for Terra, but the coefficients for Terra exceed those for Aqua four of the six years. This is the result of the years of the greatest emission coefficients for Aqua matching with the years of the lowest emission coefficient for Terra, as seen in Table 2.23.

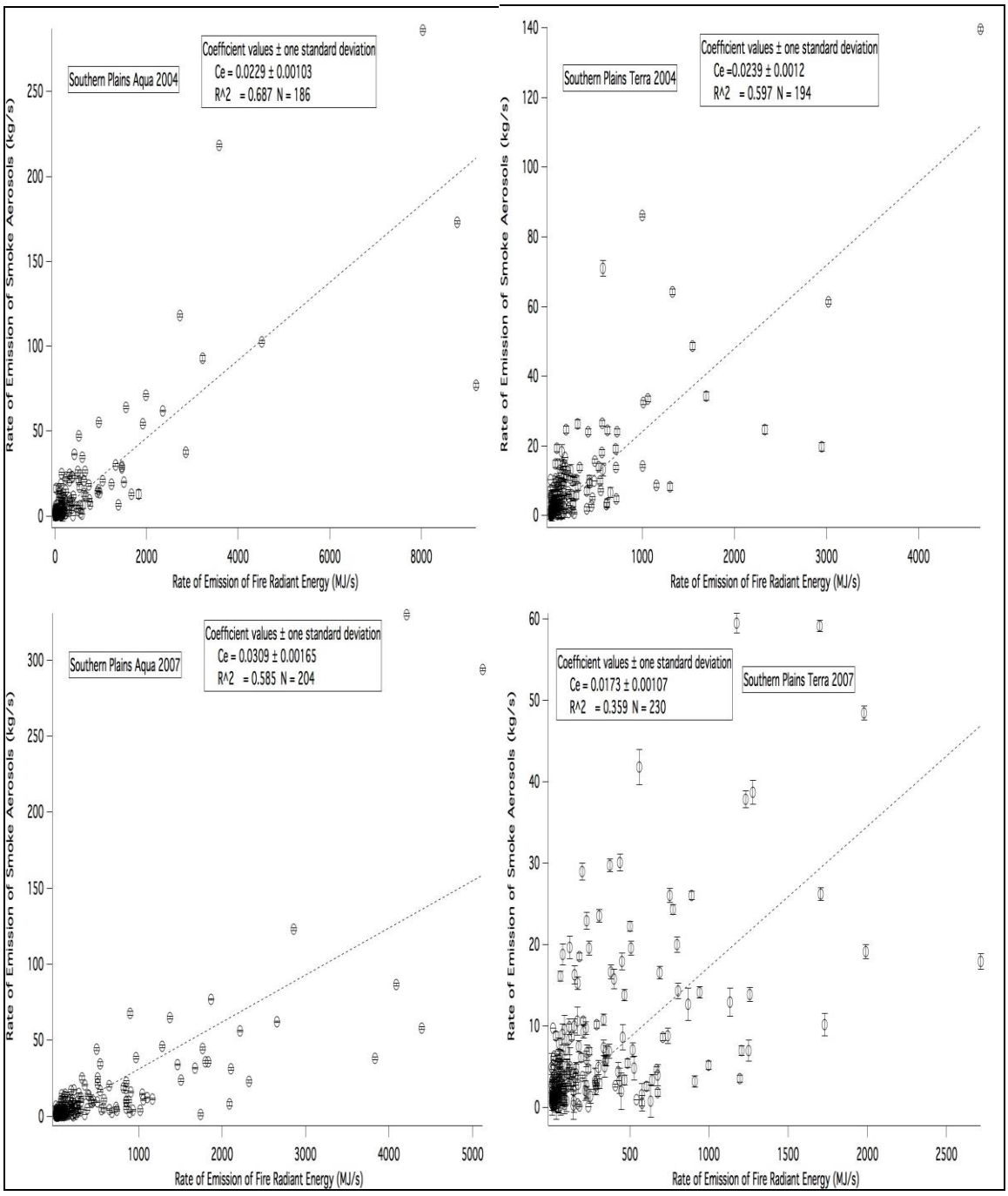

Figure 2.18: Plots of M_x versus R_{fre} for 2004 and 2007. The top two plots for Aqua and Terra 2004 have similar emission coefficients. This is an example of the diurnal nature of fires as the data points with the highest M_x value on each plot are from consecutive overpasses. Those two points drive the emission coefficient value for that year. While the Aqua plot for 2007 is similar to the one for 2004, the 2007 plot for Terra represents a year when the highest M_x value is not associated with the highest R_{fre} value. The error bars represent the standard error of the rate of release of smoke aerosols.

Aside from 2003 and 2007, the emission coefficients show good agreement between the two satellites. In the top two graphs of Figure 2.18, the data points with the highest M_x are coupled with the highest R_{fre} values of the year. These two points occur in consecutive overpasses, indicating that they are observations from the same fire. Data points such as those that appear to be outliers are prevalent in every year for both satellites. Their regularity indicates that they are representative of the normal annual fire activity. The bottom right graph in Figure 2.18 is an example of a year when this does not occur. This leads to the lowest observed emission coefficient for the region. The bottom left graph represents instances when R_{fre} is moderately high but M_x is very high. To investigate if one particular land cover type is responsible for these high energy, high aerosol data points, the emission coefficients were calculated for the land cover types in the region.

Table 2.23: Emission coefficient, in kilograms of smoke aerosols per megajoule, and correlation coefficient (C_e, R^2) values for the Southern Plains with the QA techniques applied. N is the total number of MODIS overpasses (Aqua, Terra) included in the analysis and the Fire Pixels (Aqua, Terra) are the total number of fire pixels detected that year. Most years experienced a significant increase in the correlation coefficient values but Aqua 2006 and Terra 2007 experienced decreases.

Year	Aqua (C_e, R^2)	Terra (C_e, R^2)	N (A, T)	Fire Pixels (A, T)
2003	0.0325, 0.789	0.0188, 0.423	223, 205	6005, 2821
2004	0.0229, 0.687	0.0239, 0.597	186, 194	4870, 2756
2005	0.0232, 0.828	0.0274, 0.846	260, 250	6351, 4665
2006	0.0203, 0.221	0.0204, 0.561	229, 222	4411, 3223
2007	0.0309, 0.585	0.0173, 0.359	204, 230	4897, 3038
2008	0.0286, 0.739	0.0299, 0.626	226, 255	5867, 3617

In the Southern Plains, most of the fire detections occur in the agriculture/urban/barren (35.20%) land cover type. Because there is not a clear dominant land cover type in this region (Figure 2.17), fires are detected in significant numbers in all of the land cover types present. The second greatest number of fire detections occurs

in the grassland land cover type and the ranking of the other land cover types changing from year to year.

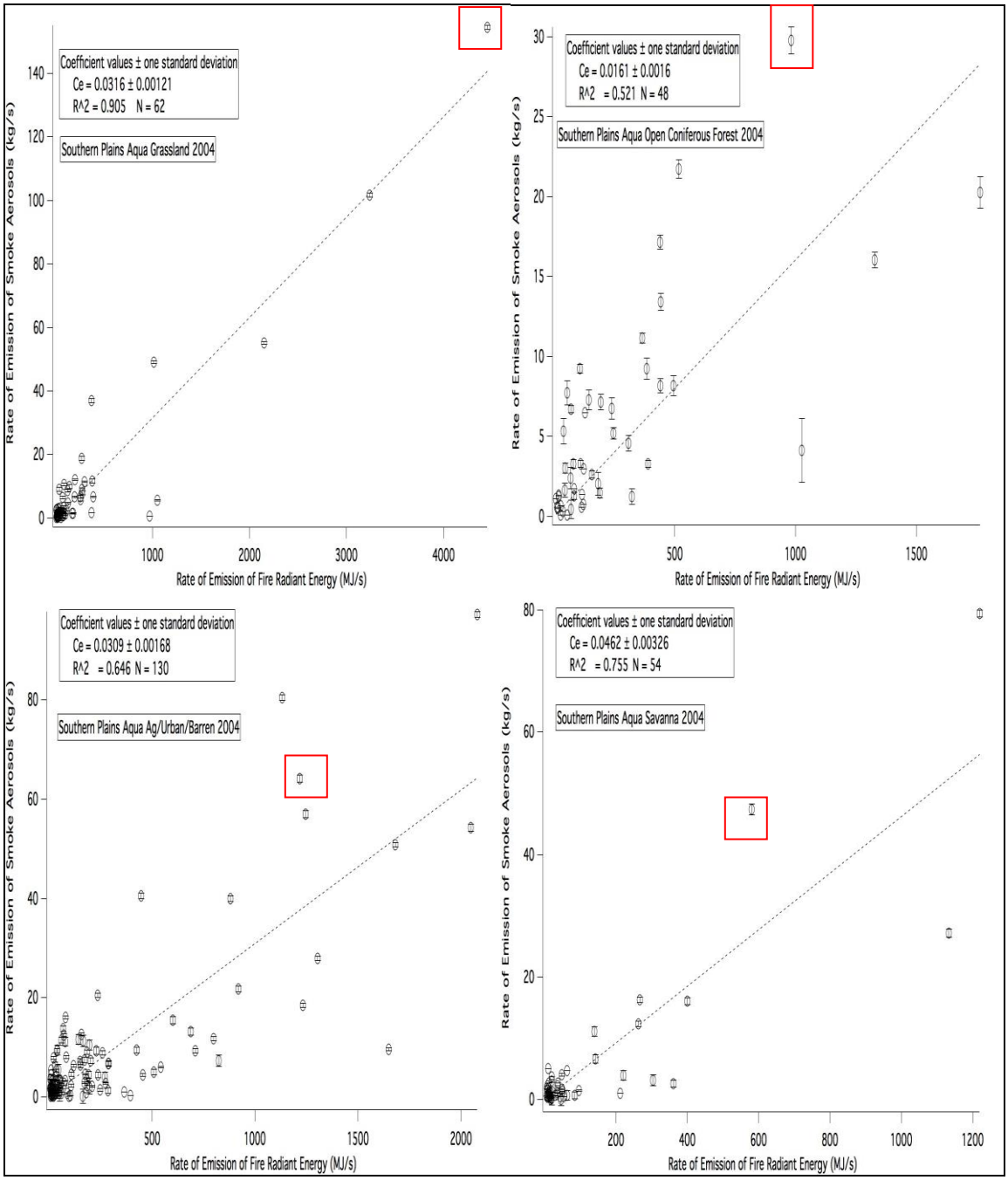

Figure 2.19: Plots of M_x versus R_{fre} for the grassland, open coniferous forest, agriculture/urban/barren, and savanna land cover types for 2004. While each and cover type contributes to the large RSA value in Figure 2.18, the grassland plot indicates it is the most influential. The error bars represent the standard error of the rate of release of smoke aerosols.

Because the emission coefficients in Table 2.24 or 2.25 do not follow a pattern based on the number of fire detections per land cover type, a deeper look is required. Figure 2.19 is a display of four land cover types for Aqua 2004 that influence its graph in Figure 2.18. The points of interest are the data point in Figure 2.18, Aqua 2004, with the greatest R_{fre} value and the data points highlighted in red in Figure 2.19. In this case, the data point in the grassland graph shows the greatest influence on the data point from Figure 2.18. However, it requires contributions from the other land types to reach the value seen in Figure 2.18. Investigation into the other high energy data points in Figure 2.18 reveals that the land cover type of greatest influence changes for each case. Therefore, no conclusion as to which land cover type is most influential can be made.

Table 2.24: Emission coefficient, in kilograms of smoke aerosols per megajoule, and correlation coefficient (C_e, R^2) values for Aqua for the Southern Plains with the QA techniques applied. The land cover type with the greatest emission coefficient value varies annually. The land cover type with the most consistent emission coefficient is the open coniferous forest.

Land Type	2003 (C_e, R^2)	2004 (C_e, R^2)	2005 (C_e, R^2)	2006 (C_e, R^2)	2007 (C_e, R^2)	2008 (C_e, R^2)
Null	0.0051, 0.013	0.0157, 0.320	0.0185, 0.494	0.0215, 0.233	0.0169, 0.466	0.0104, 0.189
Eastern Deciduous Forest	0.0290, 0.847	0.0111, 0.532	0.0288, 0.513	0.0262, 0.855	0.0252, 0.838	0.0124, 0.611
Grassland	0.0383, 0.825	0.0316, 0.905	0.0231, 0.961	0.0223, 0.411	0.0584, 0.707	0.0396, 0.832
Open Coniferous Forest	0.0157, 0.796	0.0161, 0.521	0.0157, 0.481	0.0127, 0.351	0.0104, 0.420	0.0123, 0.297
Riparian	0.0195, 0.162	0.0317, 0.338	0.0113, 0.228	0.0165, 0.311	0.0161, 0.537	0.0148, 0.204
Savanna	0.0663, 0.963	0.0462, 0.755	0.0109, 0.132	0.0148, 0.142	0.0339, 0.555	0.0307, 0.419
Ag/Urban/ Barren	0.0302, 0.456	0.0309, 0.646	0.0209, 0.446	0.0245, 0.350	0.0274, 0.253	0.0421, 0.582

Like the regional emission coefficients, annual variability is ubiquitous for both satellites in all land cover types. The land cover type with the greatest emission coefficient is inconsistent for both satellites, adding another layer of confirmation to the claim that no one land cover type is most influential in the region.

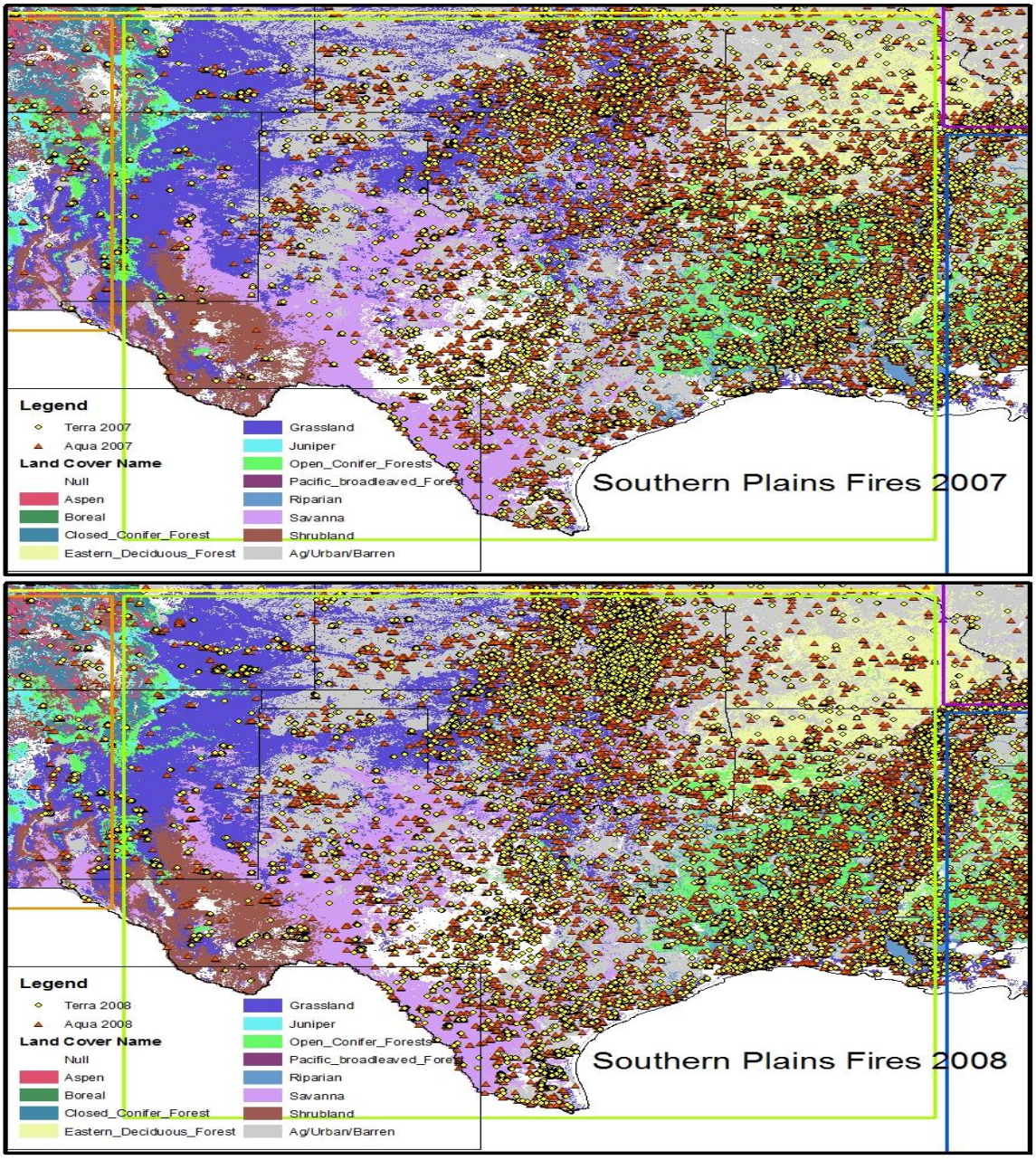

Figure 2.20: Observed fire pixel detections in the Southern Plains for 2007 and 2008. There is very little observed spatial deviation in the areas of high fire activity.

For Terra, the land cover type with the lowest emission coefficient is the open coniferous forest for every year except for 2008. For Aqua, the land cover type with the lowest emission coefficient changes from year to year, but for three of the six years, it is the open coniferous forest. As revealed in Figure 2.20, much of the fire detections in the region occur in the same areas each year. Although the locations are very similar from year to year, the number of detections changes, particularly in the grasslands of eastern Kansas. The number of fire detections in that area jumps significantly from 2007 to 2008 and there is an observed significant increase in the emission coefficient for Terra for the grassland. Despite the increase in the emission coefficient for Terra, the emission coefficient for Aqua decreases from 2007 to 2008; further evidence that no single land cover type drives the emission coefficient values for either satellite over the six years.

Table 2.25: Emission coefficient, in kilograms of smoke aerosols per megajoule, and correlation coefficient (C_e, R^2) values for Terra for the Southern Plains with QA applied. The emission coefficient values for each land type in the region exhibit varying degrees of annual variability.

Land Type	2003 (C_e, R^2)	2004 (C_e, R^2)	2005 (C_e, R^2)	2006 (C_e, R^2)	2007 (C_e, R^2)	2008 (C_e, R^2)
Null	0.0172, 0.144	0.0149, 0.334	0.0153, 0.223	0.0244, 0.297	0.0279, 0.503	0.0071, 0.074
Eastern Deciduous Forest	0.0617, 0.849	0.0179, 0.209	0.0344, 0.458	0.0179, 0.023	0.0217, 0.377	0.0341, 0.002
Grassland	0.0250, 0.354	0.0269, 0.687	0.0277, 0.916	0.0287, 0.943	0.0303, 0.735	0.0502, 0.971
Open Coniferous Forest	0.0075, 0.434	0.0119, 0.489	0.0089, 0.431	0.0085, 0.359	0.0063, 0.454	0.0077, 0.188
Riparian	0.0133, 0.378	0.0167, 0.545	0.0090, 0.182	0.0420, 0.356	0.0098, 0.116	0.0051, 0.042
Savanna	0.0698, 0.945	0.0622, 0.691	0.0445, 0.438	0.0420, 0.355	0.0246, 0.177	0.0265, 0.244
Ag/Urban/ Barren	0.0275, 0.608	0.0286, 0.386	0.0440, 0.770	0.0273, 0.493	0.0181, 0.132	0.0267, 0.309

Southwest United States

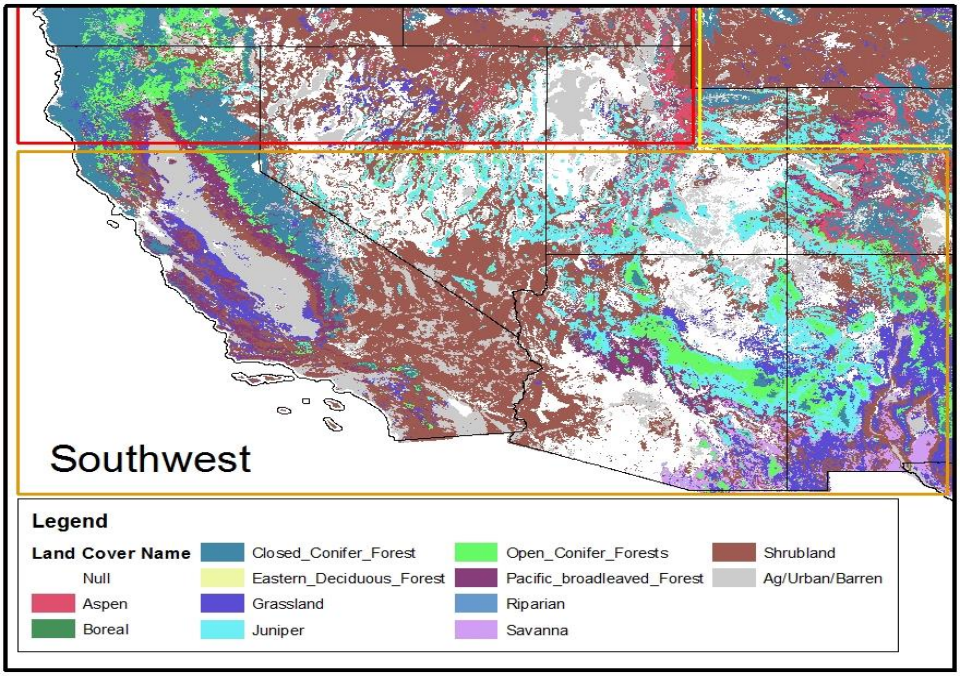

Figure 2.21: A map of the land cover types present in the Southwest. Aside from the large area of shrubland in the center of this region, much of the region is characterized by multiple land cover types intermixed over short distances.

The Southwest is another region that is characterized by diverse land cover types and a diverse geographical landscape. As seen in Figure 2.21, the dominant land cover type depends on the location in the region. On average, this region contains the second fewest fire detections for Aqua (4.50%) and the third fewest for Terra (8.37%). The emission coefficients for this region are the lowest of the regions for both satellites. All of the emission coefficients for both satellites, seen in Table 2.26, are an order of magnitude lower than the expected value from Ichoku and Kaufman (2005), with the coefficients for Aqua 2003 and 2008 two orders of magnitude lower. Coupled with low correlation coefficient values, the very low emission coefficient values emphasized the necessity of applying the QA techniques in this region.

Table 2.26: Emission coefficient, in kilograms of smoke aerosols per megajoule, and correlation coefficient (C_e, R^2) values for the Southwest before any QA screening was applied. N is the total number of MODIS overpasses (Aqua, Terra) included in the analysis and the Fire Pixels (Aqua, Terra) are the total number of fire pixels detected that year. This region is characterized by very low emission coefficient values for both satellites.

Year	Aqua (C_e, R^2)	Terra (C_e, R^2)	N (A, T)	Fire Pixels (A, T)
2003	0.0009, 0.293	0.0010, 0.349	401, 372	6858, 4626
2004	0.0013, 0.219	0.0031, 0.195	352, 347	3944, 2534
2005	0.0032, 0.635	0.0026, 0.309	379, 354	5611, 3701
2006	0.0011, 0.209	0.0015, 0.227	385, 365	4995, 3303
2007	0.0008, 0.157	0.0014, 0.394	384, 363	5674, 3830
2008	0.0021, 0.182	0.0042, 0.202	405, 372	4413, 3129

Applying the QA techniques yielded mixed results for both satellites. While average emission coefficient and correlation coefficient values increased for both satellites, the gains on the correlation coefficients was quite small, less than 0.01 (Table 2.27). The emission coefficients for Terra experienced significant increases in value, but 2006 and 2007 and all of Aqua's emission coefficients remain below the minimum expected value 0.01 (Ichoku and Kaufman, 2005).

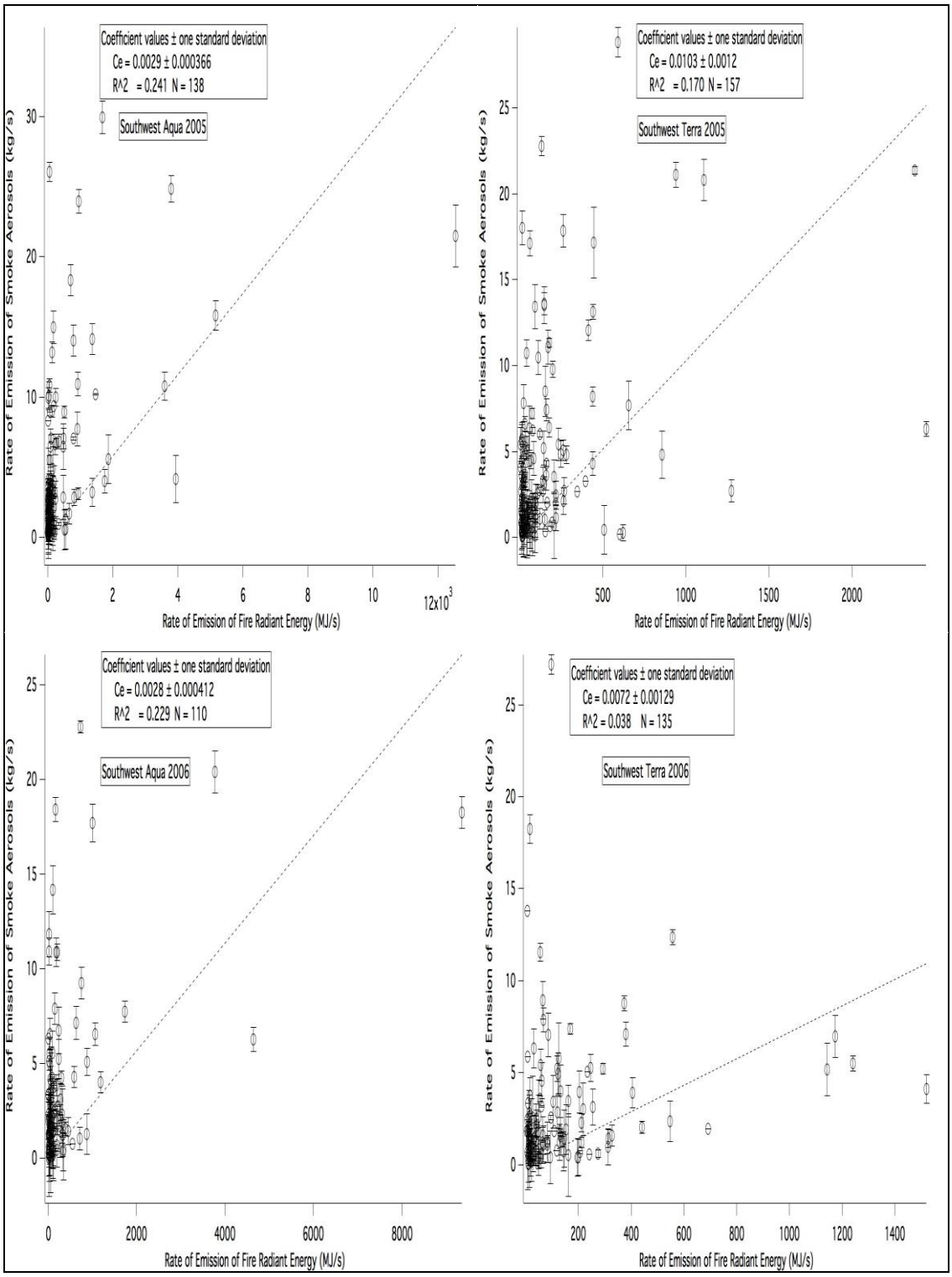

Figure 2.22: Plots of M_x versus R_{fre} for 2005 and 2006. Although the bulk of the R_{fre} and M_x values for Aqua and Terra are similar, the maximum R_{fre} values are considerably different between the two satellites. The error bars represent the standard error of the rate of release of smoke aerosols.

Data points with high to very high R_{fre} and low to very low M_x drive the emission coefficients in this region. This relationship between R_{fre} and M_x is much more pronounced in this region than in the Northwest, as the observed values for M_x are higher in the Northwest than the Southwest. This relationship is not related to the number of fire detections in the region, as the emission coefficients do not follow the same annual variability as the fire pixel counts. Remarkably, the emission coefficients for Aqua are nearly identical from 2004 to 2006; however, the other three years do not display obvious reasons for their deviations from the values from 2004 to 2006. Figure 2.22 provides insight into the nearly identical emission coefficients for Aqua in 2005 and 2006. The distributions in the two left hand graphs (Figure 2.22) are nearly identical and the decrease in the maximum R_{fre} value for both years is met with a sufficient decrease in M_x for the data point with the maximum R_{fre}. The right-hand graphs in Figure 2.22 represent Terra for the same years. Even though R_{fre} is much lower for Terra than Aqua in these graphs, M_x for the high R_{fre} values for Terra is so low that the emission coefficient for the year remains low. To investigate this phenomenon, the emission coefficients for this region were calculated by their land cover type.

Table 2.27: Emission coefficient, in kilograms of smoke aerosols per megajoule, and correlation coefficient (C_e, R^2) values for the Southwest with the QA techniques applied. N is the total number of MODIS overpasses (Aqua, Terra) included in the analysis and the Fire Pixels (Aqua, Terra) are the total number of fire pixels detected that year. The emission coefficients in this region largely remain below the expected values and continue to have low to poor correlation coefficient values.

Year	Aqua (C_e, R^2)	Terra (C_e, R^2)	N (A, T)	Fire Pixels (A, T)
2003	0.0060, 0.387	0.0130, 0.593	121, 150	1369, 1346
2004	0.0028, 0.107	0.0106, 0.294	122, 133	1006, 806
2005	0.0029, 0.241	0.0103, 0.170	138, 157	1379, 942
2006	0.0028, 0.229	0.0072, 0.038	110, 135	1156, 740
2007	0.0054, 0.663	0.0064, 0.302	133, 135	1240, 967
2008	0.0037, 0.118	0.0147, 0.316	130, 158	1367, 1103

For Aqua, the land cover type with the most fire pixel detections changes each year, with agriculture/urban/barren and shrubland having the most twice each and open coniferous forest and pacific broadleaved forest for the other two years. The land cover type with the most detections from 2004 to 2006 is agriculture/urban/barren in 2004, shrubland in 2005, and open coniferous forest in 2006. On average, the most fire pixel detections occur in the agriculture/urban/barren (26.72%) land type, followed by the open coniferous forest (19.09%), shrubland (16.66%), and pacific broadleaved forest (14.59%) land types. Therefore, the nearly identical emission coefficients for those years are not a product of the most active land cover type. For Terra, the land cover type with the most fire pixel detections is agriculture/urban/barren (36.48%) for each year. The land cover type with the second most detections changes each year but no trend with the emission coefficients for those land types are observed.

Table 2.28: Emission coefficient, in kilograms of smoke aerosols per megajoule, and correlation coefficient (C_e, R^2) values for Aqua for the Southwest with QA applied. Underlined values represent those calculated from a negative R-value. For most years and land cover types, the emission coefficient values are less than 0.01. This indicates the low emission coefficient values are a product of the region, not a land cover type.

Land Type	2003 (C_e, R^2)	2004 (C_e, R^2)	2005 (C_e, R^2)	2006 (C_e, R^2)	2007 (C_e, R^2)	2008 (C_e, R^2)
Null	0.0462, 0.098	0.0306, 0.210	0.0117, 0.079	0.0183, 0.560	0.0215, 0.096	0.0111, 0.148
Closed Coniferous Forest	0.0050, 0.317	0.0122, 0.119	0.0042, 0.058	0.0069, 0.002	0.0045, 0.818	0.0101, 0.204
Grassland	0.0134, 0.020	0.0246, 0.032	0.0215, 0.628	0.0133, 0.007	0.0085, 0.005	0.0047, 0.248
Juniper	0.0091, 0.957	0.0162, 0.321	0.0033, 0.140	0.0076, 0.012	0.0193, 0.430	0.0053, 0.000
Open Coniferous Forest	0.0049, 0.157	0.0022, 0.027	0.0089, 0.317	0.0048, 0.664	0.0094, 0.770	0.0048, 0.285
Pacific Broadleaved Forest	0.0110, 0.934	0.0038, 0.111	0.0018, 0.743	0.0106, 0.648	0.0034, 0.233	0.0033, 0.073
Shrubland	0.0018, 0.002	0.0015, 0.051	0.0085, 0.573	0.0051, 0.349	0.0056, 0.751	0.0381, 0.313
Ag/Urban/ Barren	0.0240, 0.030	0.0257, 0.091	0.0443, 0.107	0.0591, 0.371	0.0415, 0.131	0.0231, 0.001

For both Aqua and Terra, the emission coefficient values for the agriculture/urban/barren land type, seen in Tables 2.28 and 2.29, fall within the range observed in other regions. This indicates that the other land cover types in the region are responsible for the low regional emission coefficient values.

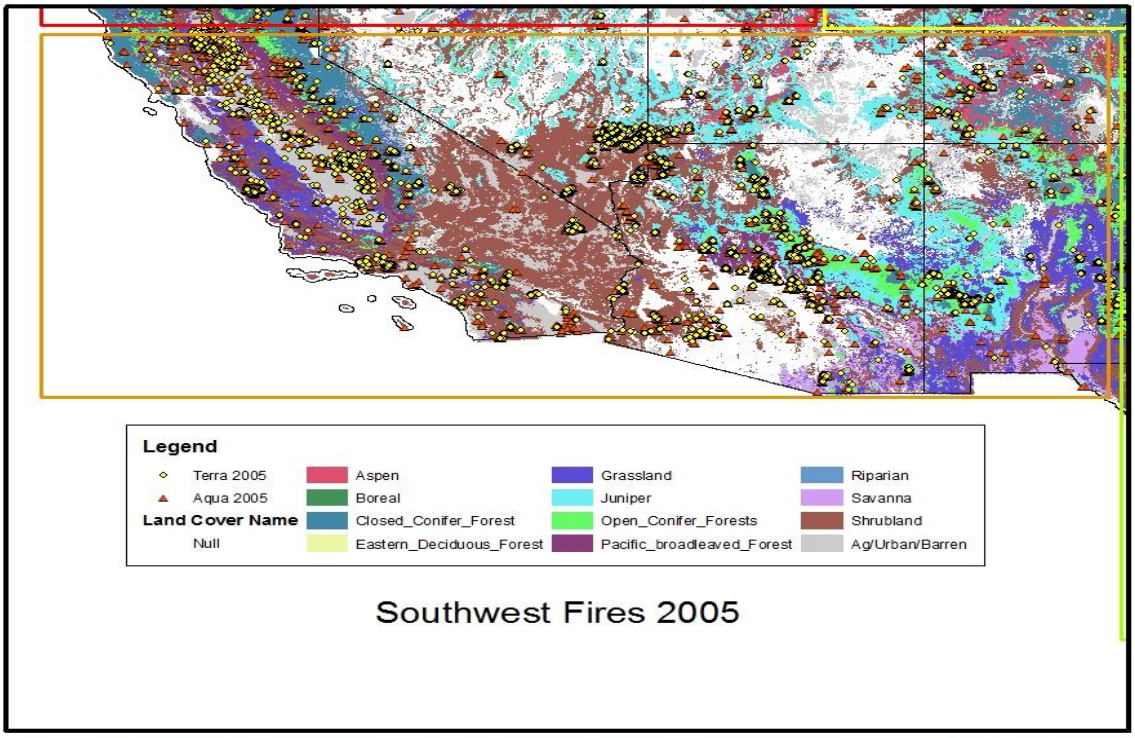

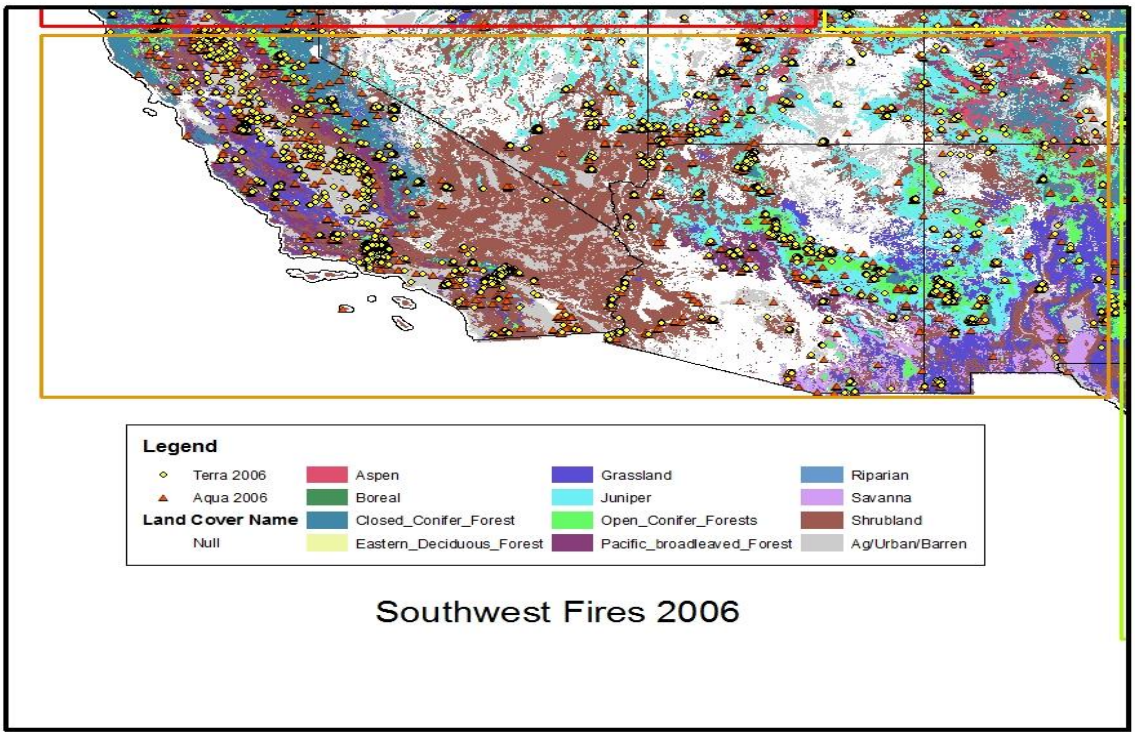

Figure 2.23: Observed fire pixel detections in the Southwest for 2005 and 2006. The only land cover type to exhibit significant spatial variability is shrubland. While similar locations burn from year to year, the most active area in the shrubland type varies annually between southern California and southern Nevada. However, this spatial variability is not reflected in the emission coefficients for this land type.

The value and subsequent influence of the emission coefficients for the other land cover types do not show significant dependence on location within the region. As seen in Figure 2.23, the fire activity in the region is spatially similar from year to year and the variability in the correlation coefficients increases the uncertainty for any conclusion. Additionally, as seen in Figure 2.24, some correlation coefficients may be overestimated due to the presence of extreme values. For example, the correlation coefficient value for the pacific broadleaved forest land cover type in 2005 is 0.743, but in Figure 2.24, the distribution of points does not appear well correlated.

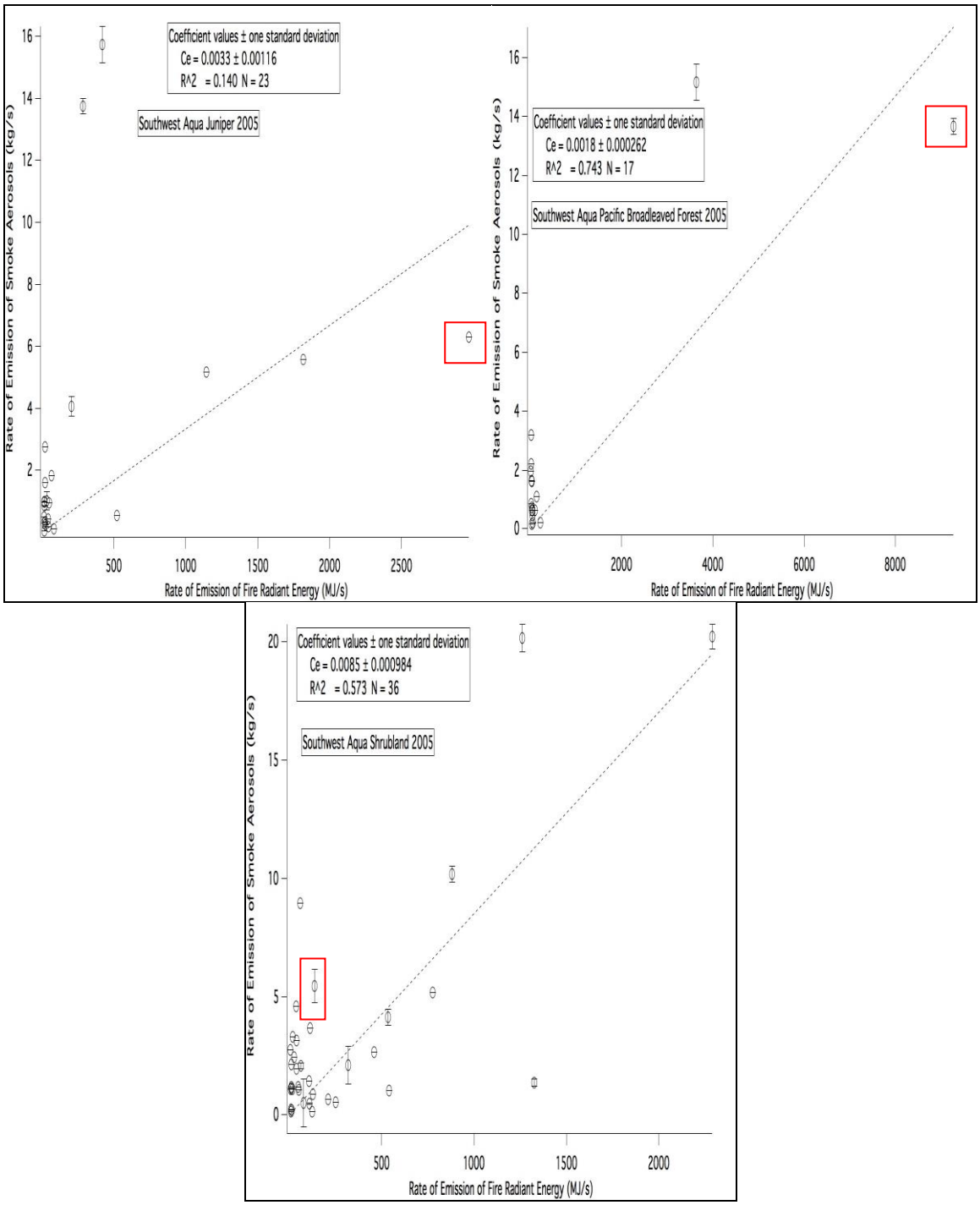

Figure 2.24: Plots of M_x versus R_{fre} for the juniper, pacific broadleaved forest, and shrubland land cover types for 2005. The highlighted points in the plots indicate the data points responsible for the extreme data point in Aqua 2005 in Figure 2.22. The error bars represent the standard error of the rate of release of smoke aerosols.

For Aqua in 2005, the pacific broadleaved forest land cover type contains the fifth highest fire detections of the land cover types in the region. In Figure 2.22, the data point with the very high R_{fre} value heavily influences the emission coefficient for Aqua 2005. In Figure 2.24, the land cover types responsible for that data point are highlighted. The pacific broadleaved forest has the most influence on the data point from Figure 2.22, with the juniper land cover type joining in. Looking at a visible image, Figure A.14, for the overpass responsible for the data point in question, there is not an obvious reason for M_x to be so low for the observed value of R_{fre}.

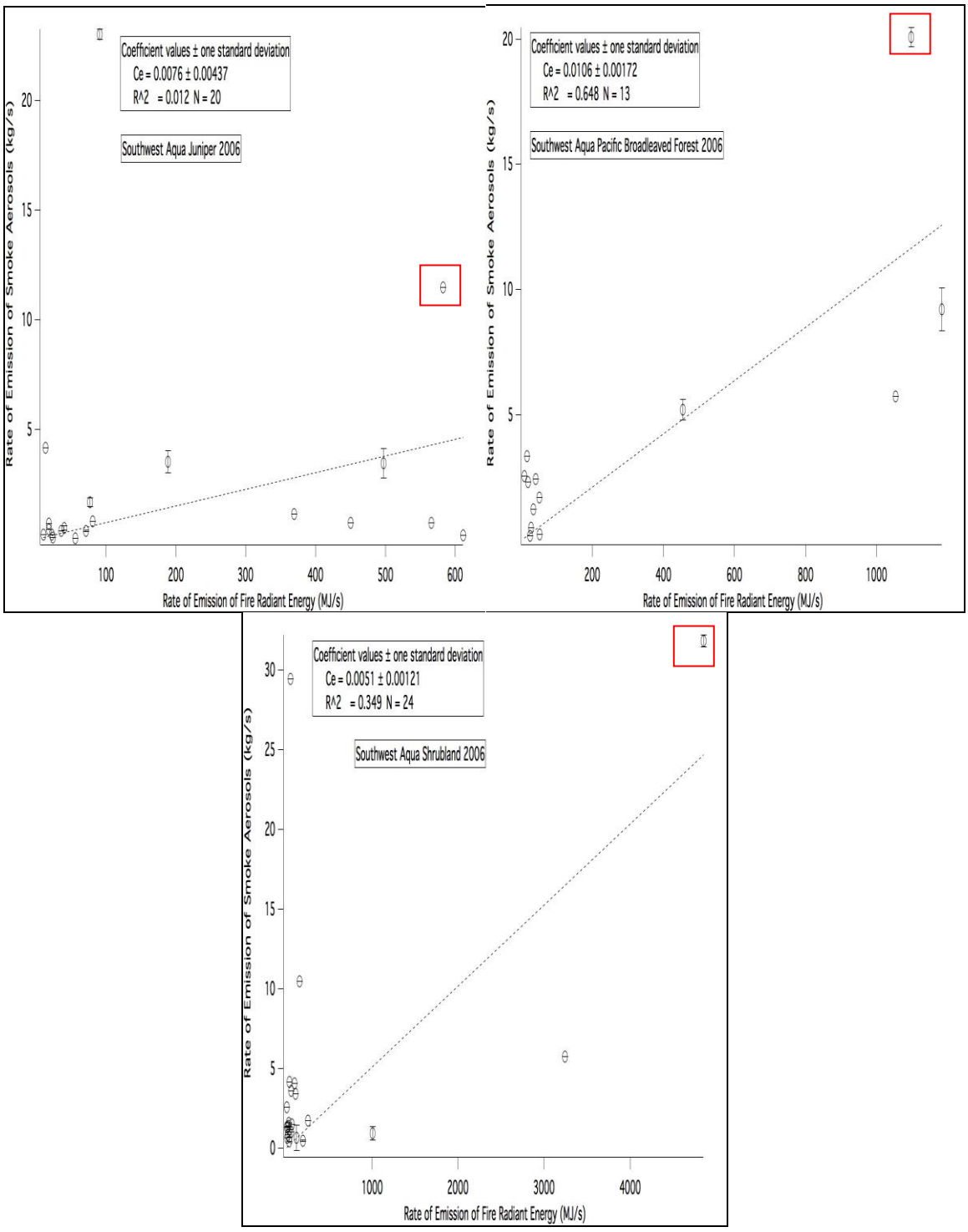

Figure 2.25: Plots of M_x versus R_{fre} for the juniper, pacific broadleaved forest, and shrubland land cover types for 2006. The highlighted points in the plots indicate the data points responsible for the extreme data point in Aqua 2006 in Figure 2.22. The error bars represent the standard error of the rate of release of smoke aerosols.

Figure 2.25 confirms that the annual variability is not contained to just one land cover type in the region. The shrubland land cover type is the most responsible for the high R_{fre}, low M_x, data point Aqua in 2006. This figure also provides an example of how the averaging process in calculating M_x can affect the reported value. The shrubland M_x on its own is nearly double the regional value.

Table 2.29: Emission coefficient, in kilograms of smoke aerosols per megajoule, and correlation coefficient (C_e, R^2) values for Terra for the Southwest with QA applied. Underlined values represent those calculated from a negative R-value. Significant annual variability is present in each land cover type. Because of the instability of the emission coefficients, no one land cover type in an indicator for the region.

Land Type	2003 (C_e, R^2)	2004 (C_e, R^2)	2005 (C_e, R^2)	2006 (C_e, R^2)	2007 (C_e, R^2)	2008 (C_e, R^2)
Null	0.0630, 0.005	0.0677, 0.065	0.0219, 0.811	0.0130, 0.101	0.0294, 0.017	0.0320, 0.202
Closed Coniferous Forest	0.0134, 0.382	0.0010, 0.028	0.0076, 0.184	0.0085, 0.027	0.0102, 0.026	0.0081, 0.463
Grassland	0.0203, 0.001	0.0501, 0.034	0.0156, 0.015	0.0174, 0.233	0.0563, 0.310	0.0244, 0.000
Juniper	0.0167, 0.113	0.0218, 0.195	0.0233, 0.422	0.0063, 0.062	0.0077, 0.640	0.0050, 0.022
Open Coniferous Forest	0.0270, 0.825	0.0065, 0.392	0.0039, 0.001	0.0053, 0.495	0.0090, 0.308	0.0118, 0.213
Pacific Broadleaved Forest	0.0065, 0.240	0.0237, 0.921	0.0108, 0.801	0.0143, 0.039	0.0045, 0.290	0.0141, 0.412
Shrubland	0.0059, 0.095	0.0041, 0.006	0.0131, 0.549	0.0049, 0.418	0.0087, 0.303	0.0340, 0.645
Ag/Urban/ Barren	0.0144, 0.564	0.0242, 0.100	0.0308, 0.047	0.0299, 0.006	0.0334, 0.041	0.0388, 0.107

2.6 Conclusion

Emission coefficients for smoke aerosols from biomass burning were calculated for the United States using fire radiative power and aerosol optical thickness measurements from MODIS. These emission coefficients were calculated for six years, starting in 2003 and ending in 2008 for the whole U.S. Six regions and thirteen land cover types were used to calculate emission coefficients at smaller spatial scales.

Two QA methods were adopted to improve estimates of the emission coefficients, one for each MODIS product. The first method limited observations of fire radiative power to scan angles of $\pm 40^{o}$. The second method eliminated retrievals of aerosol optical thickness and fire radiative power when the cloud fraction from the aerosol product was greater than zero for the target pixel. In nearly all cases, the emission and correlation coefficients were significantly improved by the implementation of these methods.

Each year of the study resulted in a different emission coefficient for every region and land cover type. Neither the spatial distribution nor number of fire pixel detections provided conclusive evidence as the driver for the annual variability. It appears that the annual variability is rooted in the values of the rate of emission of radiant energy and the rate of emission of smoke aerosols for that year.

Calculating the emission coefficients by region and by land cover type allowed for a better understanding of the fire characteristics in the United States. Most detected fires in the United States are land management fires. These fires occur in every region and are mostly found in agricultural areas, although burning of other land cover types occurs frequently. Typically, these land management fires are detected as low radiant energy fires with low to moderate rates of emission of smoke aerosols. Judging by the

good correlation coefficient values associated with the agriculture/urban/barren land type, this kind of biomass burning is well handled. The remaining detected fires in the United States are wildfires, which occur in every region and in every land cover type. Wildfires are detected in varying intensity throughout the United States. The wildfires with the highest radiant energy are typically found in the two western regions. Wildfires in the Northwest are fairly well handled, as the correlation coefficient values are moderate to good. The Southwest does not handle wildfires well, as the correlation coefficient values are low to poor. In the four remaining regions, the wildfires are not characterized by very high radiant energy and therefore are handled well.

2.7 Acknowledgements

The author would like to thank the National Science Foundation, Award 0914764, for funding this research.

The author would like to thank Charles Ichoku and Luke Ellison from NASA for supplying the base code for calculating the emission coefficients and for their insights and suggestions for improving this method.

The author would like to thank his advisor, Dr. Fok-Yan Leung, for his support and guidance during the entire research process.

References

Andreae, M. O., Merlet, P., 2001. Emission of trace gases and aerosols from biomass burning. Global Biogeochemical Cycles, 15, 955-966.

Giglio, L., Descloitres, J., Justice, C. O., Kaufman, Y. J., 2003. An enhanced contextual fire detection algorithm for MODIS. Remote Sensing of Environment, 87, 273-282.

Giglio, L., van der Werf, G. R., Randerson, J. T., Collatz, G. J., Kasibhatla, P., 2006. Global estimation of burned area using MODIS active fire observations. Atmospheric Chemistry and Physics, 6, 957-974.

Giglio, L., 2010. MODIS collection 5 active fire product user's guide version 2.4.

Freeborn, P. H., Wooster, M. J., Roberts, G., 2011. Addressing the spatiotemporal sampling design of MODIS to provide estimates of the fire radiative energy emitted from Africa. Remote Sensing of Environment, 115, 475-489.

Ichoku, C., Kaufman, Y.J., 2005. A method to derive smoke emission rates from MODIS fire radiative energy measurements. IEEE Transactions on Geoscience and Remote Sensing, 43(11), 2626-2649.

Ichoku, C., Martins, J. V., Kaufman, Y. J., Wooster, M. J., Freeborn, P. H., Hao, W. M., Baker, S., Ryan, C. A., Nordgren, B. L., 2008. Laboratory investigation of fire radiative energy and smoke aerosol emissions. Journal of Geophysical Research, 113, D14S09.

Ichoku, C., Kahn, R., Chin, M., 2012. Satellite contributions to the quantitative characterization of biomass burning for climate modeling. Atmospheric Research, 111, 1-28.

Jordan, N.S., Ichoku, C., Hoff, R.M., 2008. Estimating smoke emissions over the US Southern Great Plains using MODIS fire radiative power and aerosol observations. Atmospheric Environment, 42, 2007-2022.

Kalnay, E., Kanamitsu, M., Kistler, R., Collins, W., Deaven, D., Gandin, L., Iredell, M., Saha, S., White, G., Woolen, J., Zhu, Y., Chelliah, M., Ebisuzaki, W., Higgins, W., Janowiak, J., Mo, K. C., Ropelewski, C., Wang, J., Leetmaa, A., Reynolds, R., Jenne, R., Joseph, D., 1996. The NCAR/NCEP 40-year reanalysis project. Bulletin of the American Meteorological Society, 437-471.

Kaufman, Y. J., Tucker, C. J., Fung, I., 1990. Remote sensing of biomass burning in the tropics. Journal of Geophysical Research, 95, 9927-9939.

Kaufman, Y. J., Tanré, D., Remer, L. A., Vermote, E. F., Chu, A., Holben, B.N., 1997a. Operational remote sensing of tropospheric aerosol over land from EOS moderate resolution imaging spectroradiometer. Journal of Geophysical Research, 102, 17051-17067.

Kaufman, Y. J., Wald, A. E., Remer, L. A., Gao, B-C., Li, R.-R., Flynn, L., 1997b. The MODIS 2.1-μm channel-correlation with visible reflectance for use in remote sensing of aerosol. IEEE Transactions on Geoscience and Remote Sensing, 35, 1286-1298.

Kaufman, Y. J., Tanré, D., 1998. Algorithm for remote sensing of tropospheric aerosol from MODIS.

Kaufman, Y. J., Justice, C. O., Flynn, L. P., Kendall, J. D., Prins, E. M., Giglio, L., Ward, D. E., Menzel, W. P., Setzer, A. W., 1998. Potential global fire monitoring from EOS-MODIS. Journal of Geophysical Research, 103, 32215-32238.

Levy, R. C., Remer, L. A., Tanré, D., Mattoo, S., Kaufman, Y. J., 2009. Algorithm for remote sensing of tropospheric aerosol over dark targets from MODIS: collections 005 and 051.

Mu, M., Randerson, J. T., van der Werf, G. R., Giglio, L., Kasibhatla, P., Morton, D., Collatz, G. J., DeFries, R. S., Hyer, E. J., Prins, E. M., Griffith, D. W. T., Wunch, D., Toon, G. C., Sherlock, V., Wennberg, P. O., 2011. Daily and 3-hourly variability in global fire emissions and consequences for atmospheric model predictions of carbon monoxide. Journal of Geophysical Research, 116, D24303.

Pereira, G., Freitas, S. R., Moraes, E. C., Ferreira, N. J., Shimabukuro, Y. E., Rao, V. B., Longo, K. M., 2009. Estimating trace gas and aerosol emissions over South America: relationship between fire radiative energy released and aerosol optical depth observations. Atmospheric Environment, 43, 6388-6397.

Prins, E. M., Feltz, J. M., Menzel, W. P., Ward, D. E., 1998. An overview of GOES-8 diurnal fire and smoke results for SCAR-B and 1995 fire season in South America. Journal of Geophysical Research, 103, 31821-31835.

Remer, L. A., Kaufman, Y. J., Tanré, D., Mattoo, S., Chu, D. A., Martins, J. V., Li, R.-R., Ichoku, C., Levy, R. C., Kleidman, R. G., Eck, T. F., Vermote, E., Holben, B. N., 2005. The MODIS aerosol algorithm, products, and validation. Journal of the Atmospheric Sciences, 62, 947-973.

Roberts, G. J., Wooster, M. J., 2008. Fire detection and fire characterization over Africa using meteosat SEVIRI. IEEE Transactions on Geoscience and Remote Sensing, 46, 1200-1218.

Seiler, W., Crutzen, P. J., 1980. Estimates of gross and net fluxes of carbon between the biosphere and the atmosphere from biomass burning. Climatic Change, 2, 207-247.

Simon, M., Plummer, S., Fierens, F., Hoelzemann, J. J., Arino, O., 2004. Burnt area detection at global scale using ATSR-2: the GLOBSCAR products and their qualification. Journal of Geophysical Research, 109, D14S02.

van der Werf, G. R., Randerson, J. T., Giglio, L., Collatz, G. J., Mu, M., Kasibhatla, P. S., Morton, D. C., DeFries, R. S., Jin, Y., van Leeuven, T. T., 2010. Global fire emissions and the contribution of deforestation, savanna, forest, agricultural, and peat fires (1997-2009). Atmospheric Chemistry and Physics, 10, 11707-11735.

Wooster, M. J., Roberts, G., Perry, G. L. W., Kaufman, Y. J., 2005. Retrieval of biomass combustion rates and totals from fire radiative power observations: FRP derivation and calibration relationships between biomass consumption and fire radiative energy release. Journal of Geophysical Research, 110, D24311.

Xu, W., Wooster, M. J., Roberts, G., Freeborn, P., 2010. New GOES imager algorithms for cloud and active fire detection and fire radiative power assessment across North, South, and Central America. Remote Sensing of Environment, 114, 1876-1895.

CHAPTER 3

EVALUATION OF FIRE RADIATIVE POWER DERIVED PM EMISSIONS AND MODELED PM EMISSIONS FROM THE BLUESKY FRAMEWORK

Abstract

Particulate matter emissions from ten large fires in the 2007 Northwest United States fire season were estimated from fire radiative power (FRP) measured by the Moderate Resolution Imaging Spectroradiometer (MODIS) and the BlueSky Framework. These emissions were compared using Classification and Regression Trees (CART) to explore the meteorological, fuel characteristic, and geographical factors influencing the difference in the two methods. The MODIS and BlueSky emissions displayed fair agreement in their daily trends; however, numeric disagreement was significant. The CART analysis showed that over or under estimation of the MODIS emissions by BlueSky is driven by the fuel loadings and soil moisture and the numeric difference between MODIS and BlueSky is driven by the maximum planetary boundary layer height and soil moisture.

3.1 Introduction

Various satellite products are utilized to estimate emissions from biomass burning at different spatial scales. These products are generated globally, covering much of the last decade. Many products that calculate emissions using burned area use the following equation:

$$M = A \times B \times \alpha \times \beta \quad (1)$$

where M is the mass of biomass burned, A is the area burned, B is the fuel load, α is the fraction of above ground biomass, and β is the combustion factor (Seiler and Crutzen, 1980).

Table 3.1: Summary of recent studies estimating global emissions of gases and aerosols from biomass burning using satellite data. GFAS model utilizes a top-down approach while the remaining models utilize a bottom-up approach to estimate emissions.

Name	Author	Study Years	Satellite product used	Resolution	Area
GBA-2000	Ito and Penner	2000	SPOT 4 Burned Area	1 km	Global
GWEM	Hoelzemann et al.	2000	ATSR-2 GLOBSCAR	0.5^o	Global
GFED	van der Werf et al.	1997-2009	MODIS Burned Area	0.5^o	Global
FINN	Wiedinmyer et al.	2005-2010	MODIS Fire Detections	1 km	Global
GFAS	Kaiser et al.	2003-2011	MODIS FRP	0.5^o	Global

The global burned area product for 2000 (GBA-2000) relies on the monthly burned area derived from the VEGETATION instrument aboard the Systèm Pour l'Observation de la Terre (SPOT) 4 satellite at 1 km resolution (Ito and Penner, 2004). This method resulted in global estimates of carbon emission from open vegetation fires to be 1.4 Pg for 2000. The Global Wildland Fire Emission Model (GWEM) derives emissions using the Global

Burnt SCAR (GLOBSCAR) monthly burned area product at 1 km resolution from the Along-Track Scanning Radiometer 2 (ATSR-2) satellite sensor to produce emissions from biomass burning at 0.5^{o} resolution (Hoelzeman et al., 2004). GWEM carbon emissions were estimated to be 1.7 Pg in 2000. The Global Fire Emissions Database (GFED) derives emissions using the Moderate Resolution Imaging Spectroradiometer (MODIS) burned area product, producing global biomass burning emissions at 0.5^{o} resolution (van der Werf et al., 2010). Average carbon emissions from GFED were estimated to be 2.0 Pg per year, with 1.7 Pg estimated in 2000. The Fire INventory from NCAR (FINN) derives emissions from MODIS fire detections, producing daily estimates of emissions from biomass burning at 1 km resolution (Wiedinmyer et al., 2011). Because of their daily nature, the estimates from FINN can be readily used in air quality models. Yearly totals agree well with the other global estimates of emissions for species such as carbon monoxide and carbon dioxide. The Global Fire Assimilation System (GFAS) derives emissions from MODIS measurements of fire radiative power (FRP), producing global daily emissions from biomass burning at 0.5^{o} resolution (Kaiser et al., 2012). Average yearly carbon emissions from GFAS were estimated to be 2.07 Pg per year.

In Table 3.1 is a sample of some of the global databases related to estimation of emissions from biomass burning. Except for GFAS, the databases utilize a bottom-up approach to estimating emissions. A bottom-up approach utilizes Equation 1, or other very similar equation. The burned area information typically comes from satellite product while the land cover product comes from various sources unique to the database. Most of the databases utilize the emission factors set forth by Andreae and Merlet (2001),

except for the FINN database, which utilizes a collection of emission factors from several sources (Wiedinmyer et al., 2011). A top-down approach, which is utilized in GFAS, employs FRP to determine emissions. Using FRP almost eliminates the need for the factors on the right-hand side of Equation 1 because it is a measure of the fire size and intensity (Ichoku and Kaufman, 2005). In GFAS, the FRP is related to the emissions through a conversion factor related to the land cover classification (Kaiser et al., 2012).

The BlueSky smoke modeling framework is a modular framework that integrates existing datasets and models in a unified structure (Larkin et al., 2009). Its goal is to produce smoke trajectories and concentrations from meteorological model output and fire information. The National Center for Atmospheric Research/Penn State Mesoscale Meteorological Model (MM5) or the Weather Research and Forecasting (WRF) model supply the weather information necessary to run the framework. Fire information is supplied through the Satellite Mapping Automated Reanalysis Tool for Fire Incident Reconciliation (SMARTFIRE). It combines satellite reports from the NOAA Hazard Mapping System (HMS) and ground-based reports from the Incident Command System (ICS)-209. Fuel loading information is obtained from the Fuel Characteristic Classification System (FCCS) or from the revision by Hardy of the US National Fire Danger Rating System (NFDRS). Total consumption and time rate of consumption information is generated by the CONSUME Version 3 model, which was developed empirically from 106 pre- and post-burn plots of various vegetation types and conditions. Simple, idealized profiles are used to allocate the consumption of the fuels over time. The Fire Emissions Production Simulation (FEPS) is used to generate speciated

emissions from the fire. These emissions are dispersed through the CALPUFF dispersion model.

In this chapter, a comparison of emissions derived from MODIS measurements of FRP to emissions derived from BlueSky is presented. Ten large wildfires in Idaho and Oregon were selected from the 2007 fire season for the comparison. Classification and Regression Tree (CART) analysis is used to explore the influence of meteorological, geographical, and fuel characteristics on the emission estimates.

3.2 Method for estimating emissions using FRP and CART analysis

To calculate $PM_{2.5}$ from FRP observations by MODIS, FRP must first be converted fire radiative energy (FRE). Using the FRP measurements from both the daytime and nighttime overpasses, a profile of the daily FRP is created. Two modifications to the FRP profile are necessary to complete the profile. Because the satellites operate on Greenwich Mean Time (GMT), a conversion from GMT to local time is necessary to establish a daily profile that matches with the modeled results. A data point for midnight local time is interpolated using a linear line between the two times closest to midnight. A second data point is generated to account for the diurnal cycle in fire activity. This second point relies on the assumption that a fire is least active at sunrise, therefore its FRP value is set at zero. The area under the curve, as seen in Figure 3.1, is the daily total FRE. This emission profile is used in place of an assumed emissions profile in an effort to capture a more realistic trend in the daily fire behavior and to capture the day-to-day changes in meteorology.

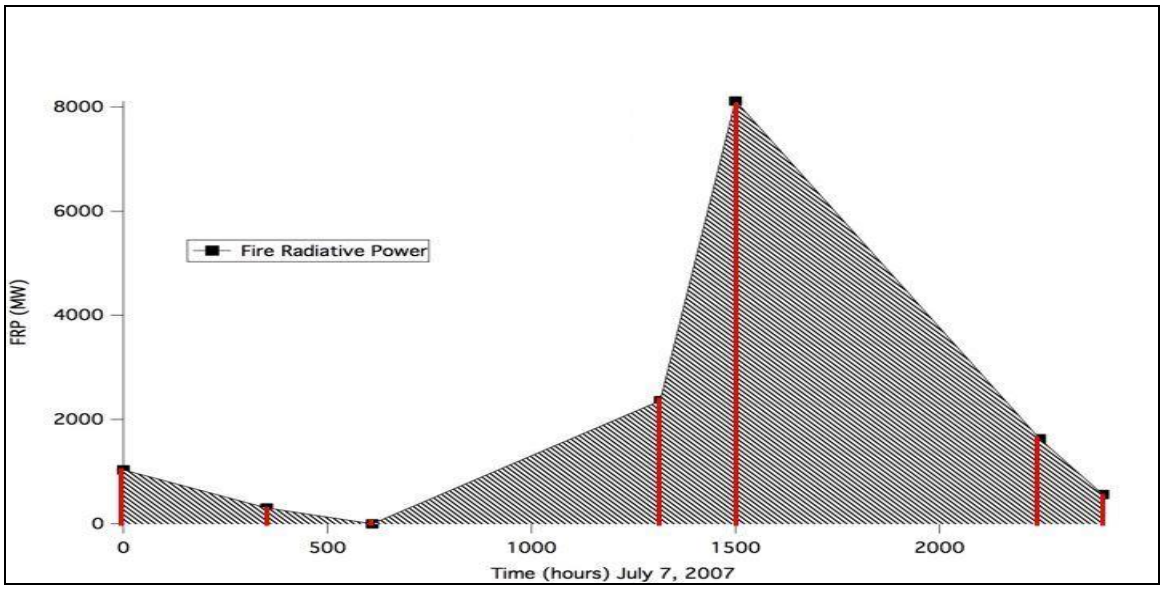

Figure 3.1: A plot of the daily FRP profile and the daily FRE for July 7, 2007. The edges of the trapezoids used to calculate FRE are highlighted in red. The diurnal profile of peak emissions in the afternoon and lowest emissions at night is quite visible.

To calculate FRE, the trapezoid rule is used calculate the area under the curve, using the time between data points as the base of the trapezoid (Boschetti and Roy, 2009). The FRE from each trapezoid is then multiplied by the emission coefficient for the satellite that made the measurement that occurred earliest in the day. For measurements made by Aqua, the emission coefficient is 0.0055 kg/MJ and for Terra, the emission coefficient is 0.0202 kg/MJ. These emission coefficients are for the Northwest region in 2007 and were chosen in place of the land cover specific emission coefficients because of the better consistency in both the value of the emission coefficients and correlation coefficients. Once the emissions are calculated for each trapezoid, the emissions are summed to provide a daily estimate of total particulate matter (TPM) emissions. To get emissions of $PM_{2.5}$, the TPM emissions are multiplied by 0.9, which is the approximate ratio of $PM_{2.5}$ to TPM in smoke (Reid et al., 2005).

CART analysis seeks to explain the variation in a response variable by multiple explanatory variables (De'ath and Fabricius, 2000). If the response variable is categorical, a classification tree is used. If the response variable is numeric, a regression tree is used. The explanatory variables can be either categorical or numeric. Trees are built by splitting the explanatory variable data until an oversized tree is grown. To achieve the best tree, the first step is to prune back the oversized tree by eliminating splits in the tree that do not result in enough improvement in the tree. The next step in finding the best tree is through cross-validation, which seeks to find the tree with the least amount of error. Cross-validation is implemented through one of two ways. The first way is through selecting a random subset of the data to build trees, then using the remaining data to calculate the error of the trees. The second way is through V-fold cross-validation, which divides the data into mutually exclusive subsets before building trees using all but one of the subsets. This process is repeated until the tree with the lowest estimated error is found.

3.3 Results and discussions

FRE-based $PM_{2.5}$ emissions from ten large wildfires in 2007 were compared to emissions modeled by the BlueSky Framework. Eight of the ten fires occur in Idaho and two occur in Oregon, as seen in Figure 3.2. These fires were chosen because of their size, location, and fuel types. Of the ten fires, six occur primarily in closed coniferous forests, three occur primarily in shrublands, and one occurs primarily in an open coniferous forest. These land cover types represent the three main land cover types in the region.

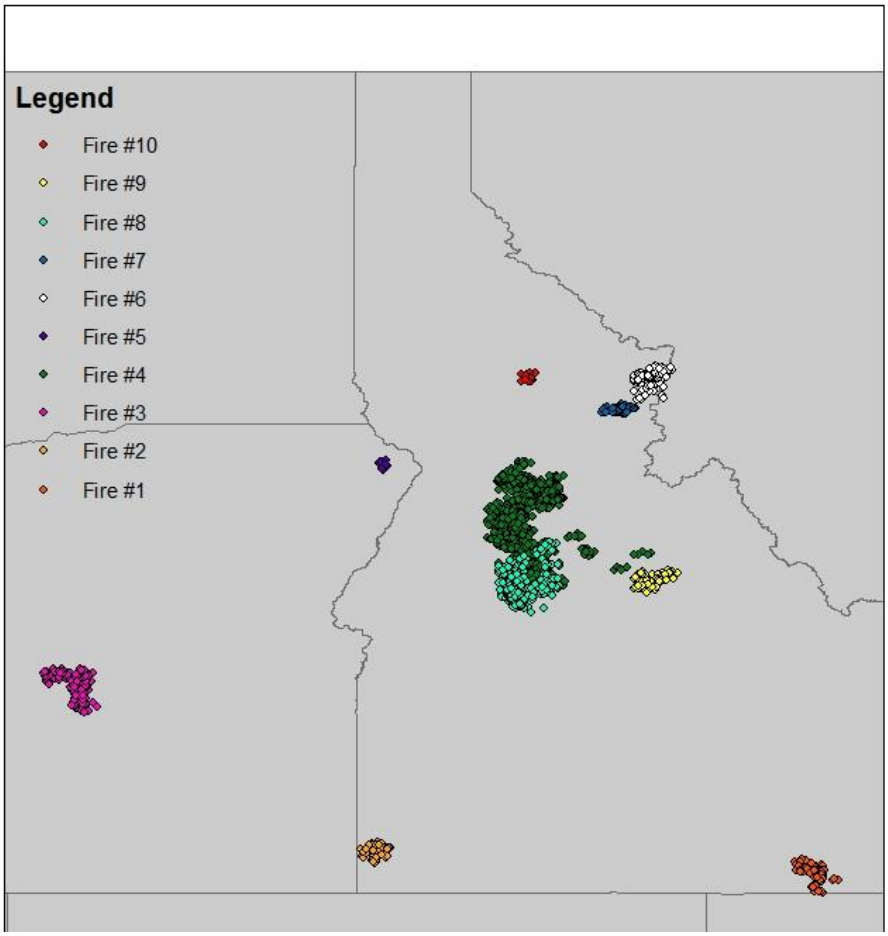

Figure 3.2: A map of the ten fires that burned during July through early September in 2007. The largest fire, fire #4 in dark green, burns longest, beginning July 14 and ending August 30.

These fires range in size and duration, with the fire #4 as the largest and longest lasting fire of the group. The emissions from these fires are modeled by the BlueSky Framework and are calculated from MODIS measurements of FRP. Missing values are present in both data sets due to either the model failing to execute or MODIS failing to detect the fire due to clouds or the fire not burning during an overpass.

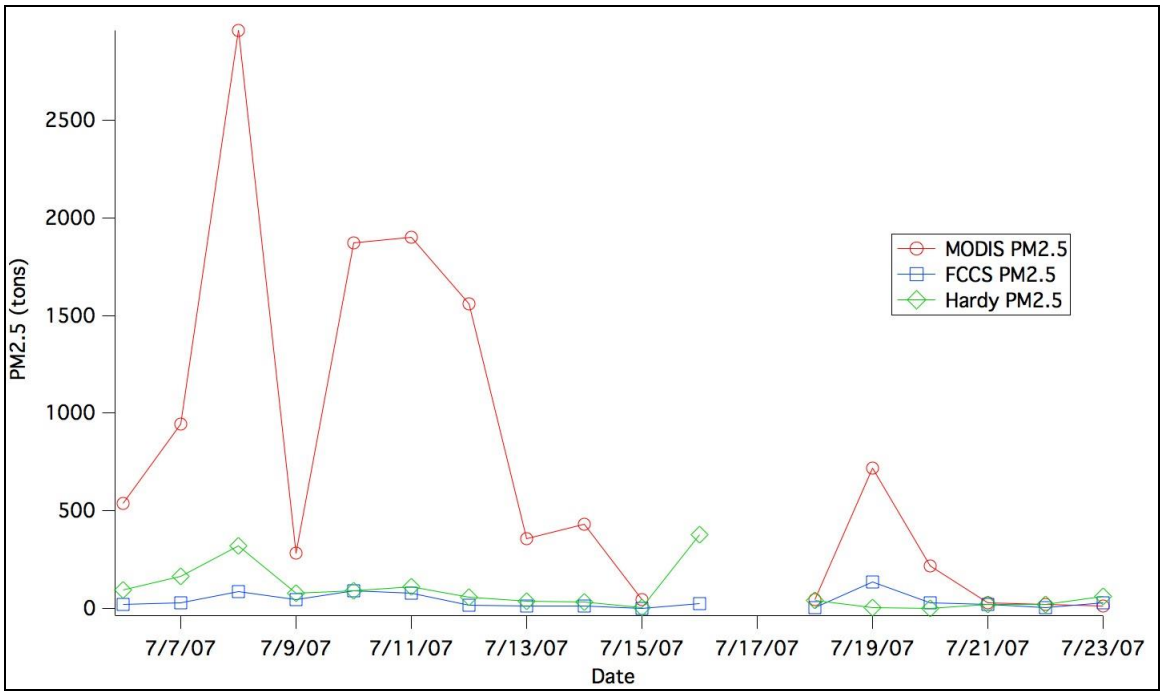

Figure 3.3: MODIS and BlueSky estimated $PM_{2.5}$ emissions for fire #1 in south central Idaho. The land cover type in which this fire burned was shrubland. MODIS emissions consistently exceed both BlueSky emission estimates.

For fire #1 in central Idaho, Figure 3.3, emissions estimated by MODIS consistently exceed those from both BlueSky runs. In almost instances, the emissions estimated by MODIS exceed the BlueSky runs by at least an order of magnitude. Because of the large difference between the emissions estimates, it is difficult to assess common trends in the data. Despite the large difference in values, the emissions follow the trend of a rise and fall from 7/6/07 to 7/9/07 and from 7/18/07 to 7/21/07. The reason for both the weak agreement and the large differences requires further exploration.

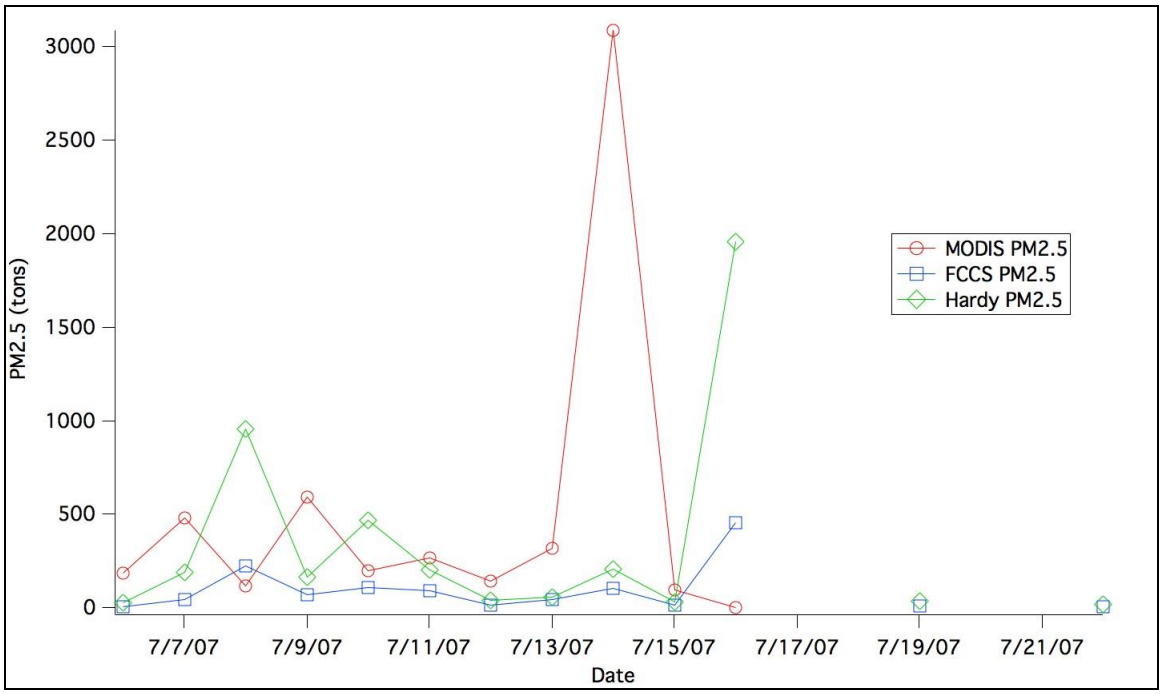

Figure 3.4: MODIS and BlueSky estimated $PM_{2.5}$ emissions for fire #2 in southwest Idaho. This fire burned in the shrubland land cover type. The large peak in emissions estimated by MODIS on 7/14 is missed by both BlueSky estimates and the Hardy peak on 7/16 is missed by MODIS and FCCS.

For fire #2 in southwest Idaho, Figure 3.4, the method of greatest estimated emissions trade daily for most of the fire duration. The most obvious trend in the data is that it appears that the modeled emissions lag behind the MODIS emissions by a day. This lag creates an alternating pattern to which method produces the greatest emissions for that day. Only the data gap on 7/17/07 is found for another fire, indicating that either the model did not execute or there was not a report of the fire activity given to drive the model. Given that the data gaps in the MODIS emissions could be the result of cloud obscuration, it cannot be concluded that the fire was not burning during the days of no emissions.

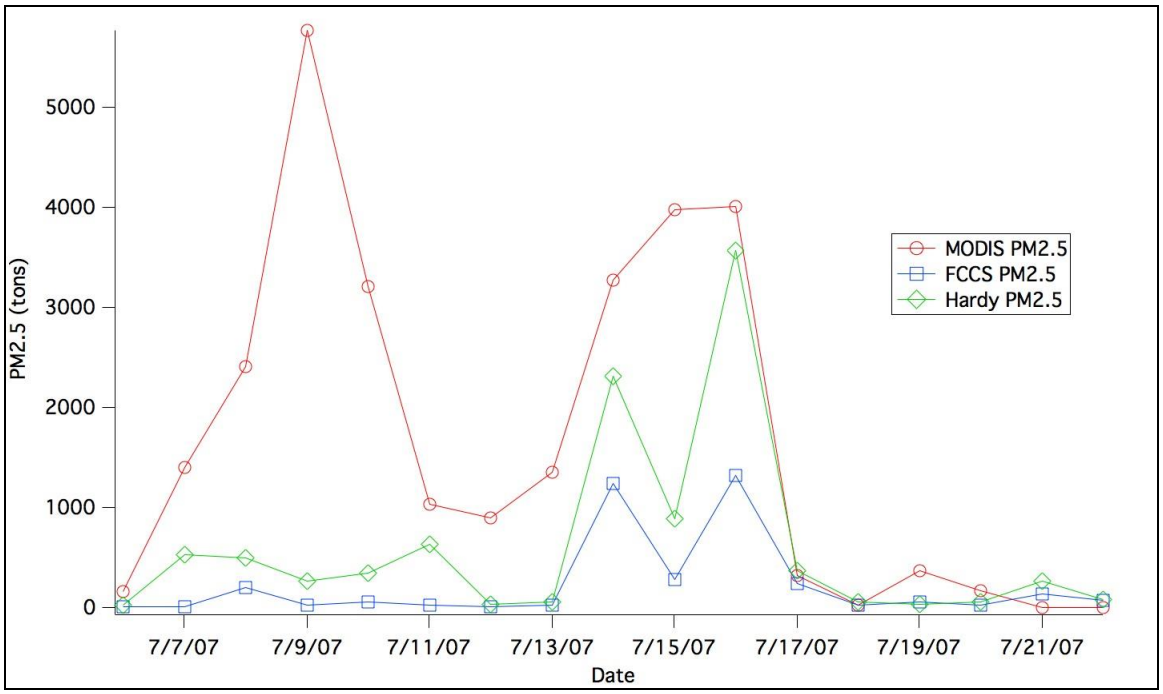

Figure 3.5: MODIS and BlueSky estimated $PM_{2.5}$ emissions for fire #3 in central Oregon. This fire burned primarily in the open coniferous forest land cover type. The elevated emissions period from 7/13 to 7/17 is reasonably correlated between MODIS and Hardy.

For fire #3 in central Oregon, Figure 3.5, the estimated emissions from MODIS consistently exceed those from BlueSky. Prior to 7/13/07, there is very little agreement between the MODIS and BlueSky emissions. Starting on 7/13/07, there is fair agreement as all three methods show the large increase in emissions followed by the large drop in emissions on 7/17/07. If the MODIS emissions are to be believed, the significant under prediction of emissions by BlueSky is a significant miss by the framework. Of the two vegetation drivers for BlueSky, the emissions from Hardy perform best for this fire.

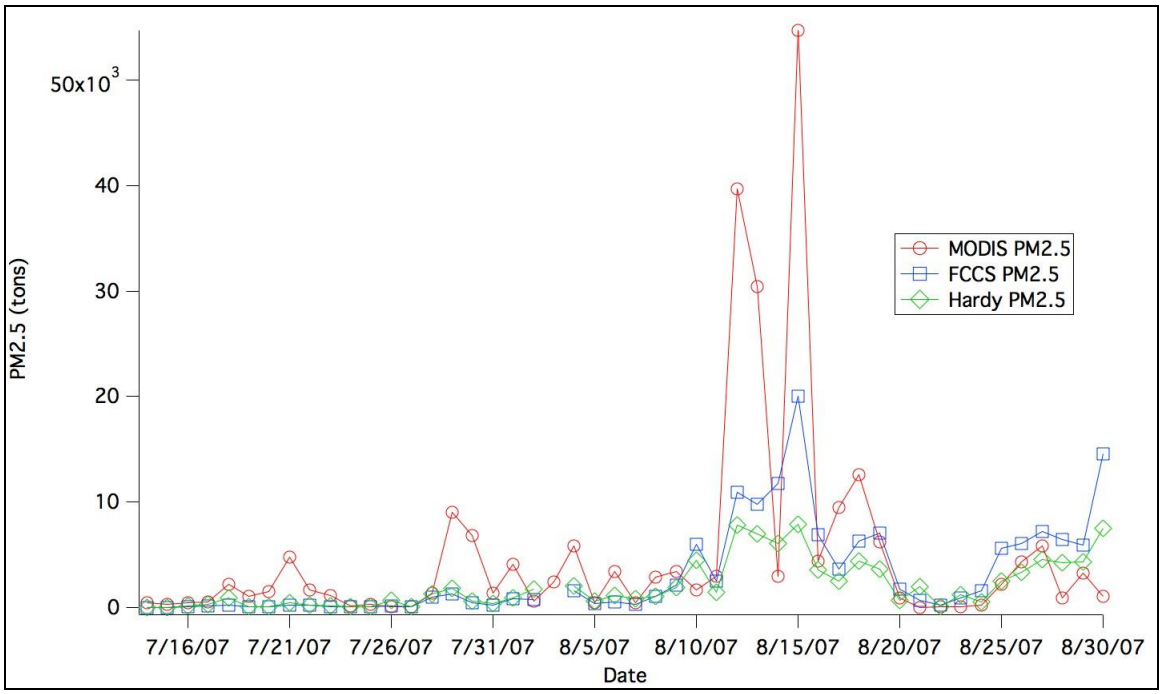

Figure 3.6: MODIS and BlueSky estimated $PM_{2.5}$ emissions for fire #4 in central Idaho. The primary land cover type in which the fire burned was the closed coniferous forest. The emission estimates by all three methods are best correlated during the final ten days of the fire.

For fire #4 in central Idaho, Figure 3.6, most of the daily estimated emissions from MODIS exceed those from BlueSky. All three methods capture the large increase in emissions from 8/11/07 through 8/20/07. Leading up to 8/11/07, there is fair agreement between the three methods for most days, however, the trend of MODIS exceeding BlueSky continues. The difference between the emissions from 8/11/07 to 8/20/07 is very significant as the MODIS emissions are two to three times those from BlueSky for the first half of the time period. Beginning on 8/19/07, the methods show good agreement in both the trend in emissions and the quantity of emissions. Also in this period begins a trend observed in the remaining fires: one or both of the BlueSky emissions frequently exceeding the MODIS emissions.

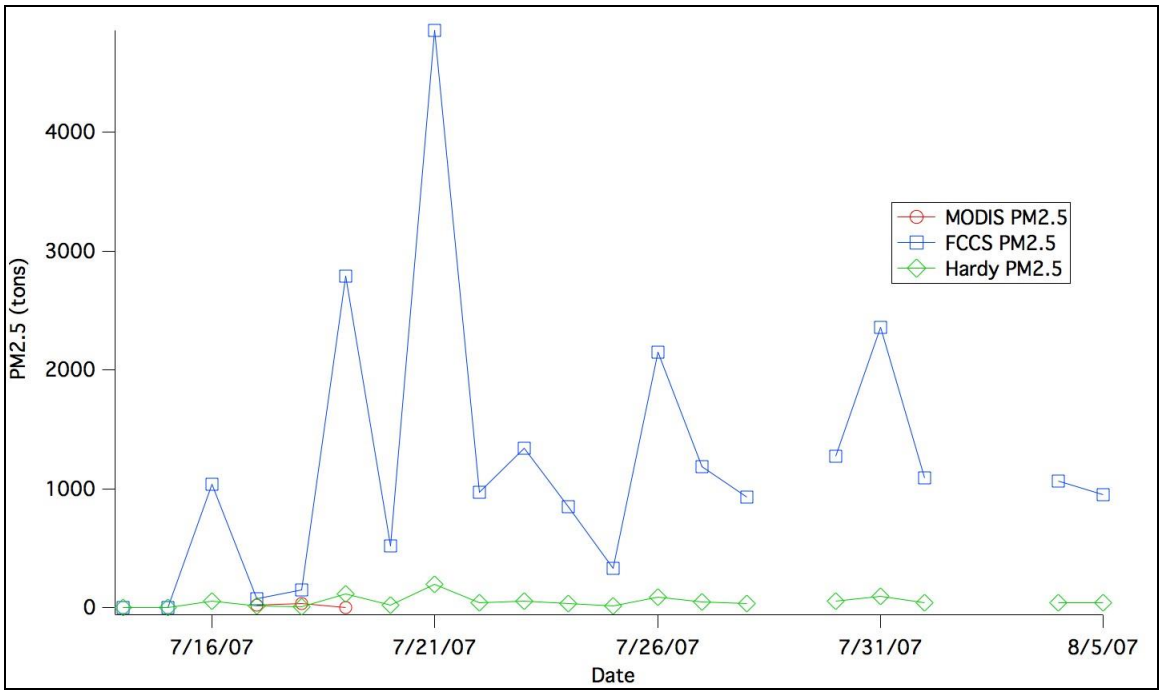

Figure 3.7: MODIS and BlueSky estimated $PM_{2.5}$ emissions for fire #5 in northeast Oregon. This fire burned in the closed coniferous forest type. MODIS observed burning for only three days of the fire, with limited correlation with the BlueSky estimates.

For fire #5 in northeast Oregon, Figure 3.7, only three days of this fire are observed by MODIS. This fire highlights the most glaring issue with using satellites to estimate emissions: cloud obscuration. For the three days, MODIS emissions were exceeded by both BlueSky results. MODIS and Hardy showed good agreement for those three days, but the FCCS exceeded both all three days. The FCCS results are much higher than the other methods, which is the opposite trend from most of the other fires. The large difference in the emission values between the two BlueSky models is a result of vastly different fuel loading values.

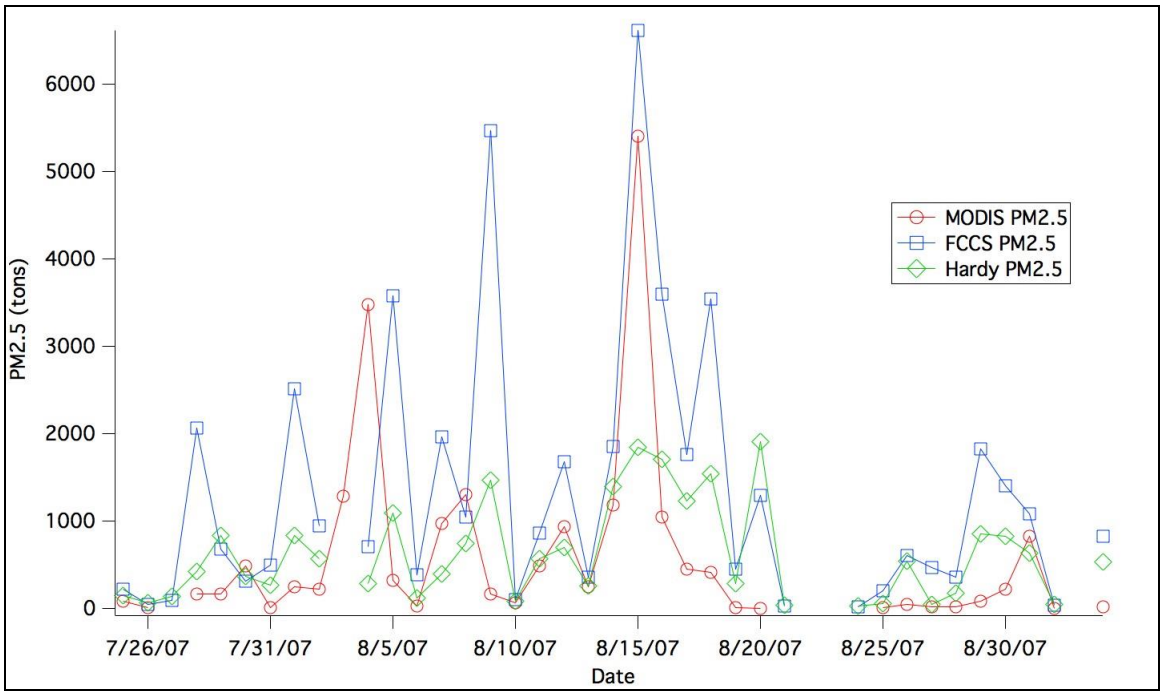

Figure 3.8: MODIS and BlueSky estimated $PM_{2.5}$ emissions for fire #6 in northeast Idaho. This fire burned in the closed coniferous forest land type. The saw tooth pattern to the FCCS estimates does not correlate well with the Hardy or MODIS estimates.

For fire #6 in northeast Idaho, Figure 3.8, the method with the highest daily estimated emissions is BlueSky FCCS for nearly every day. There is very little agreement between the methods for both the emission trends and magnitude. The best agreement occurs from 8/10/07 to 8/15/07, as there is a rise and fall from 8/10 to 8/13, followed by a dramatic rise from 8/13 to 8/15. Aside from those few days, MODIS and BlueSky show opposite trends, with lagged increases and decreases and significant differences in the quantity emitted. Data gaps may represent little to no fire activity as they span similar days.

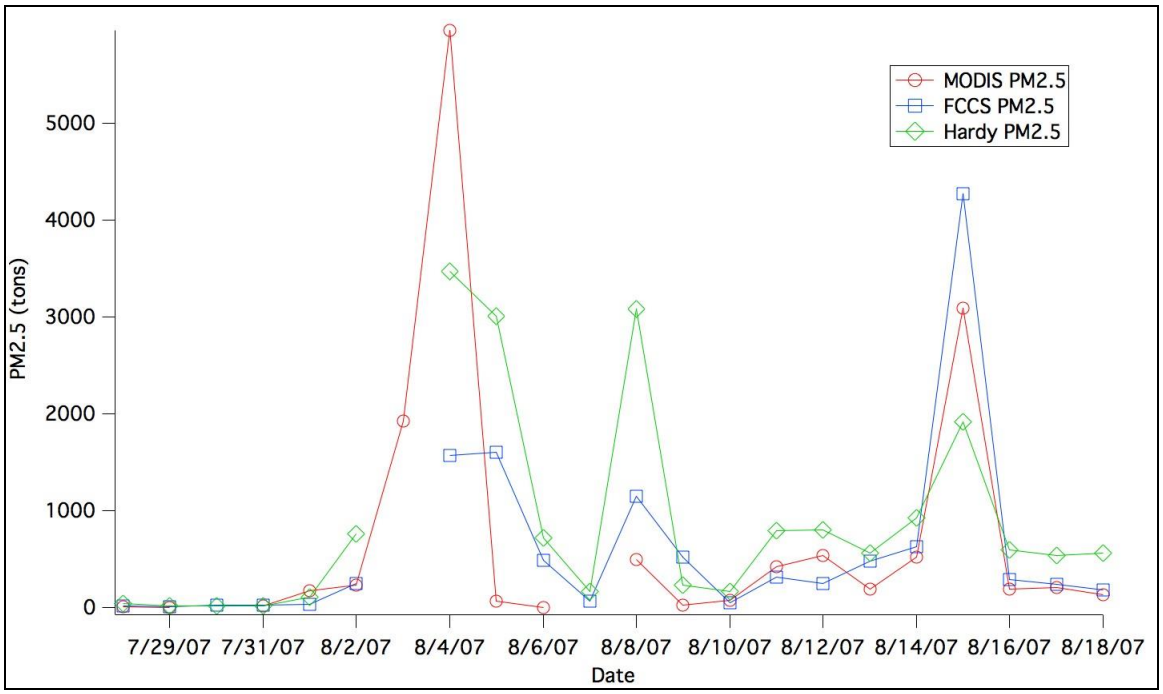

Figure 3.9: MODIS and BlueSky estimated $PM_{2.5}$ emissions for fire #7 in northeastern Idaho. This fire burned in the closed coniferous forest land cover type. While all three methods display reasonable agreement, the randomness of the estimates during the high emission days limits the overall agreement between the methods for this fire.

For fire #7 in northeastern Idaho, Figure 3.9, the method with the highest daily estimated emissions is, on average, BlueSky Hardy. All three methods agree on the overall trend in the emissions over the duration of the fire. There is disagreement on the magnitude of the highest emission days, with each method estimating the greatest emissions once for each of the three peaks. The BlueSky data gap on 8/3/07 is one that occurs frequently in theses fires, therefore it is likely the result of the framework failing to execute. The MODIS data gap on 8/7/07 could be the product of cloud cover or undetectable fire activity, as the BlueSky emissions are low for that day.

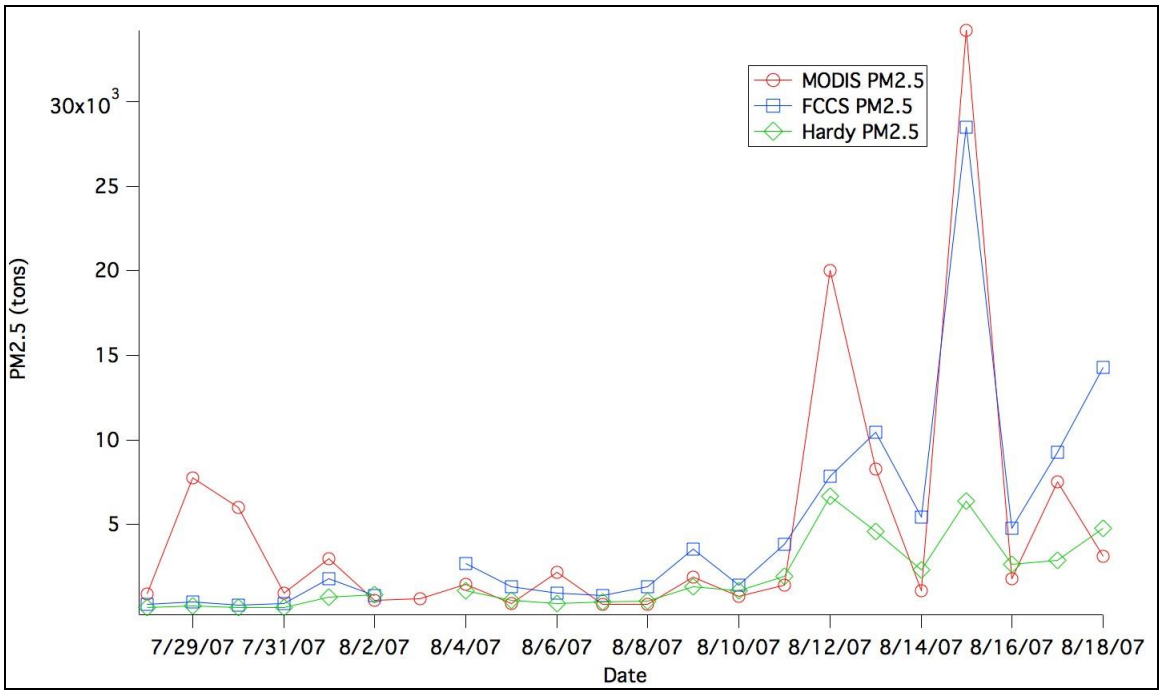

Figure 3.10: MODIS and BlueSky estimated $PM_{2.5}$ emissions for fire #8 in central Idaho. This fire burned in the closed coniferous forest land cover type. The high emissions day on 8/15/07 is well correlated between MODIS and FCCS.

For fire #8 in central Idaho, Figure 3.10, the method with the highest daily estimated emissions alternates between the three methods daily. Starting 7/31/07, there is good agreement on the overall trend in emissions for this fire. The increase in emissions at the end of the fire period is fairly well agreed upon, with Hardy estimating much lower emissions than MODIS or FCCS. At the beginning of the fire period, MODIS is estimating considerably more emissions than BlueSky. This type of relationship occurs in several of the other fires, so while noteworthy, it is not unique to this fire.

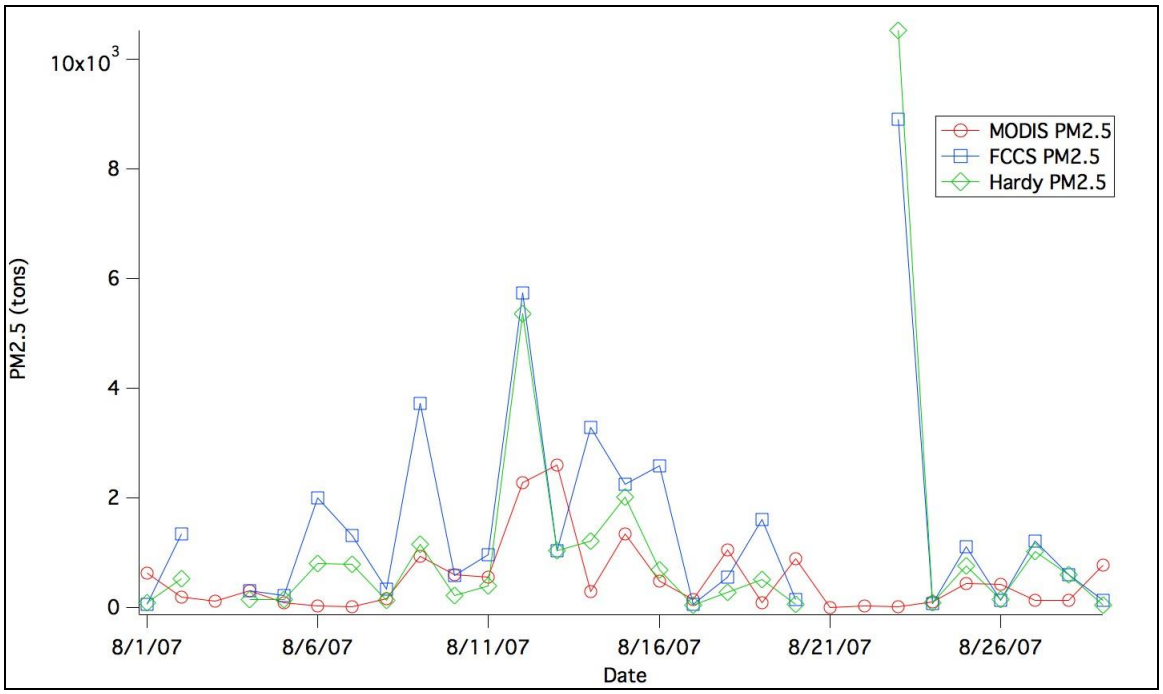

Figure 3.11: MODIS and BlueSky estimated $PM_{2.5}$ emissions for fire #9 in central Idaho. This fire burned primarily in the closed coniferous forest but also in the shrubland land cover type. The contributions from a mixed-type fire may be the driver for the overall lack of agreement between the three methods.

For fire #9 in central Idaho, Figure 3.11, the method with the highest daily estimated emissions alternates between MODIS and BlueSky FCCS. There is very little agreement between the three methods for the daily trends in emissions. There are several days where there is good agreement between FCCS and Hardy, but the agreement typically lasts for only one or two days. The emissions from MODIS show very little agreement with the trends and quantity of emissions from BlueSky. It is not obvious why there is such little agreement; therefore more investigation into the external factors that may be influencing the emission estimates is required.

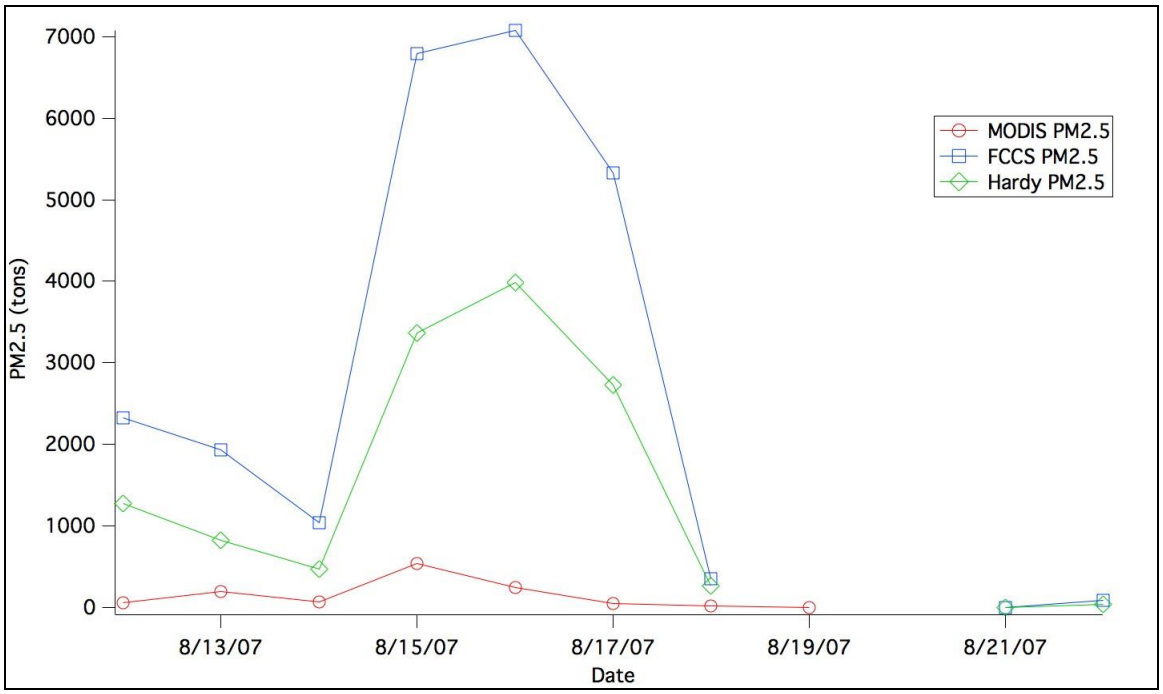

Figure 3.12: MODIS and BlueSky estimated $PM_{2.5}$ emissions for fire #10 in northern Idaho. This fire burned in a closed coniferous forest. As seen with other fires, the difference in the estimated emissions by Hardy and FCCS is significant. The estimates from MODIS estimates are uncharacteristically low for this fire.

For fire #10 in northern Idaho, Figure 3.12, the estimated emissions from MODIS are much less than those from BlueSky. The BlueSky emissions follow the same trend in the emissions activity but diverge significantly on the quantity. Due to its timing and location, the MODIS emissions from this fire may be underestimated due to smoke and or cloud obscuration of the FRP measurements. There also could be external factors at play that could be influencing the disagreement between MODIS and BlueSky.

For all days of concurrent MODIS and BlueSky estimates of emissions, the absolute difference between the MODIS and BlueSky emissions is calculated. This absolute difference becomes the response variable for use in a regression tree. The response variable for use in a classification tree is a categorical variable based on whether the difference between the MODIS and BlueSky emissions is positive or negative. To

ease evaluation of these estimates, it is assumed that the MODIS emissions are the "true" emissions, where positive differences are underestimations and negative differences are overestimations. In order to explore the differences between MODIS and BlueSky, Table 3.2 lists the eighteen exploratory variables from meteorology, geography, and land cover that are used.

Table 3.2: The exploratory variables for the CART analysis to test the influence of meteorology, fuel characteristics, and geography on the daily emissions.

Meteorology	Fuel characteristics	Geography
Max Temperature	Fuel Load 1hr	Elevation
Max Wind Speed	Fuel Load 10hr	Soil Moisture
Max PBL Height	Fuel Load 100hr	
Min Temperature	Fuel Load 1Khr	
Min Wind Speed	Fuel Load 10Khr	
Wind Direction	Fuel Load GT10Khr	
	Fuel Moisture 1hr	
	Fuel Moisture 10hr	
	Fuel Moisture 100hr	
	Fuel Moisture 1Khr	

The meteorology is supplied through the framework from the WRF model and both the Hardy and FCCS land cover data are supplied through the framework. The elevation data was obtained from the United States Geological Survey: (USGS) National Map at 1 arc second resolution. The soil moisture data was obtained from approximate sites from the Snowpack Telemetry (SNOTEL) network (Leavesley et al., 2010).

A classification tree is generated to explain the variation in the response variable tied to whether the difference between the MODIS emissions and the BlueSky Hardy emissions is positive or negative. The relative cost of this tree is 0.703, which indicates that this tree contains 70.3% of the error experienced if there was no model to predict if the difference in emissions is positive or negative. Looking at the tree in Figure 3.13, the

key variables in predicting a positive or negative difference are daily soil moisture, maximum daily wind speed, maximum daily temperature, minimum daily wind speed, and wind direction. As seen in Table 3.3, the variables that are in the classification tree do not appear in order of the most important variables. This indicates that while important, their inclusion in the tree does not produce the tree with the lowest relative cost.

Table 3.3: The variable importance table from the classification tree. The variable importance value is a measure of its performance as a surrogate to the primary split relative to the best performing variable.

Variable	Importance
SOILMOISTURE	100
MINTEMP	90.71215
FUEL1KHR	74.32278
FUEL10KHR	74.32278
FUEL10HR	69.25401
FUEL100HR	69.25401
WINDDIR	41.30581
MAXPBL	37.04954
MINWINDSP	35.17903
MAXTEMP	32.63135
MAXWINDSP	27.34346
ELEVATION	6.82564
FUELGT10KHR	0
FUEL1HR	0
MOISTURE1KHR	0
MOISTURE100HR	0
MOISTURE1HR	0
MOISTURE10HR	0

Of the 195 cases used to generate the Hardy classification tree, the tree is able to correctly 78.02% of the negative cases and 75.96% of the positive cases. This results in an overall successful prediction rate of 76.92%.

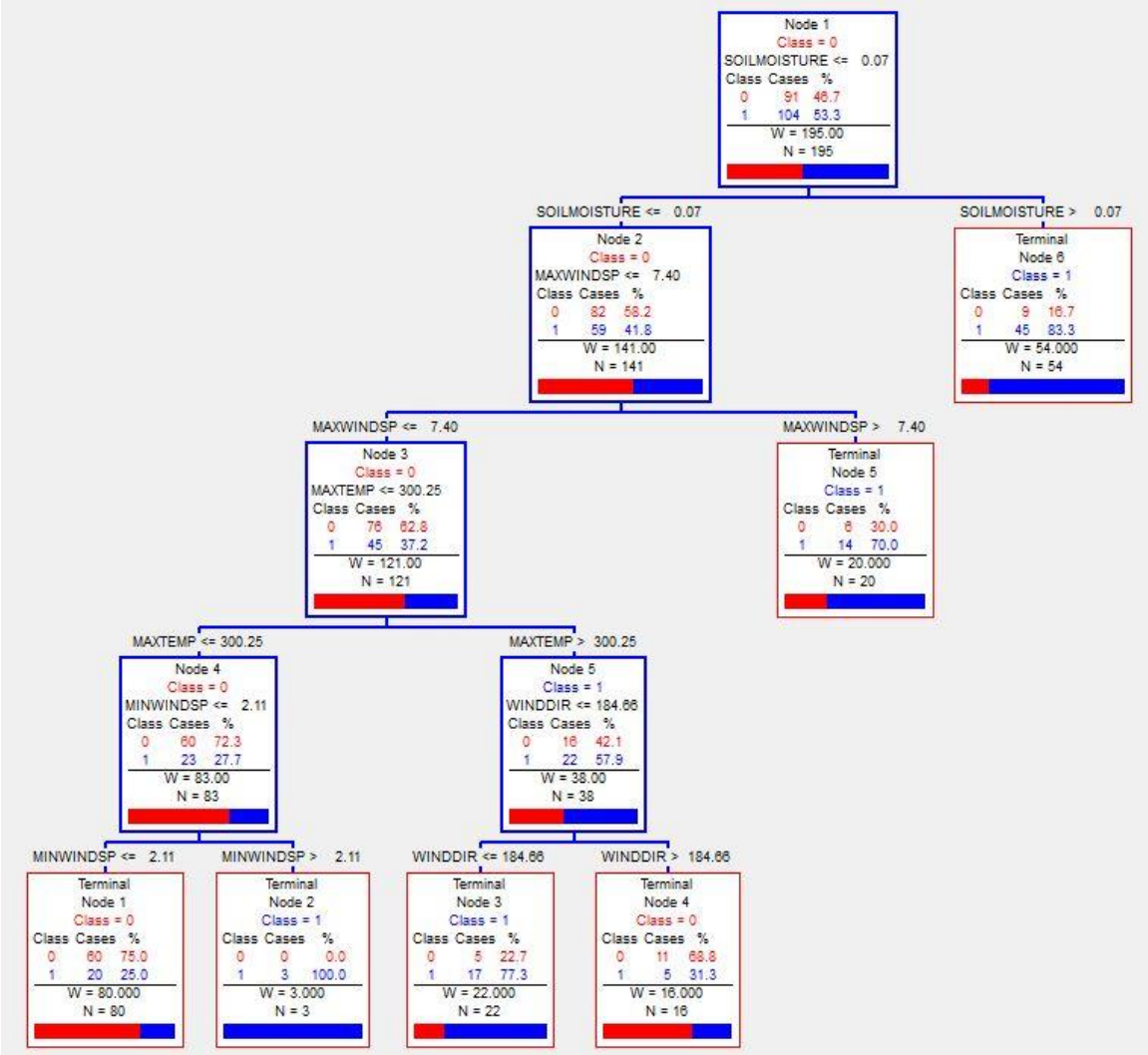

Figure 3.13: The classification tree built from the Hardy dataset. Class 0 is for when BlueSky emission estimates exceed the MODIS emission estimates and Class 1 is for when MODIS exceeds those by BlueSky.

The Hardy classification tree was used to predict whether the difference between the MODIS and FCCS BlueSky emissions would be positive or negative. The FCCS emissions contained the same number of test cases as the Hardy emissions. Using the Hardy tree, the tree is able to correctly predict 71.85% of the negative cases and 76.09% of the positive cases. This results in an overall successful prediction rate of 73.85%.

Using the successful prediction rates from both fuel loading datasets, the classification tree generated from the Hardy data set is a good predictor of which method,

MODIS or BlueSky, will be the greatest for the given conditions. The variable importance table shows that collectively, the fuel loading is the driver for the over or under estimation of emissions by BlueSky.

From the same data, a regression tree was built using the difference between MODIS and the Hardy BlueSky emissions estimates. The relative cost for this tree is 0.8698 and R-squared value of 0.6532. Comparing the tree in Figure 3.14 to the variable importance table (Table 3.4) the most important variables are represented in both locations. Only the maximum planetary boundary layer (PBL) height and soil moisture are present in the regression tree, which follows with the variable importance table. These two variables contribute collectively to the numeric difference, with the maximum PBL height contributing more strongly than the soil moisture. From the variable importance table, the remaining variables are not strong contributors to the difference between MODIS and BlueSky Hardy.

Table 3.4: The variable importance table from the regression tree. The top two variables in the table are the only two variables that appear in the best-fit tree.

Variable	Importance
MAXPBL	99.99999
SOILMOISTURE	22.35072
MINWINDSP	5.00163
FUEL1KHR	1.69561
FUEL1HR	1.69555
FUEL10KHR	1.69555
WINDDIR	1.49853
ELEVATION	0.3566
MINTEMP	0.00824
MAXTEMP	0.0082
MAXWINDSP	0
FUEL10HR	0
FUEL100HR	0
MOISTURE100HR	0
FUELGT10KHR	0
MOISTURE1KHR	0
MOISTURE1HR	0
MOISTURE10HR	0

Because of the high relative cost value and the moderate R-squared value, the regression analysis of the difference between MODIS and BlueSky Hardy emissions is inconclusive. When the BlueSky FCCS emissions were applied to the Hardy regression tree, the resulting R-squared value was 0.2494, which is considerably less than the Hardy R-squared value. This shows that the regression tree does not explain the difference between the MODIS and BlueSky emissions well.

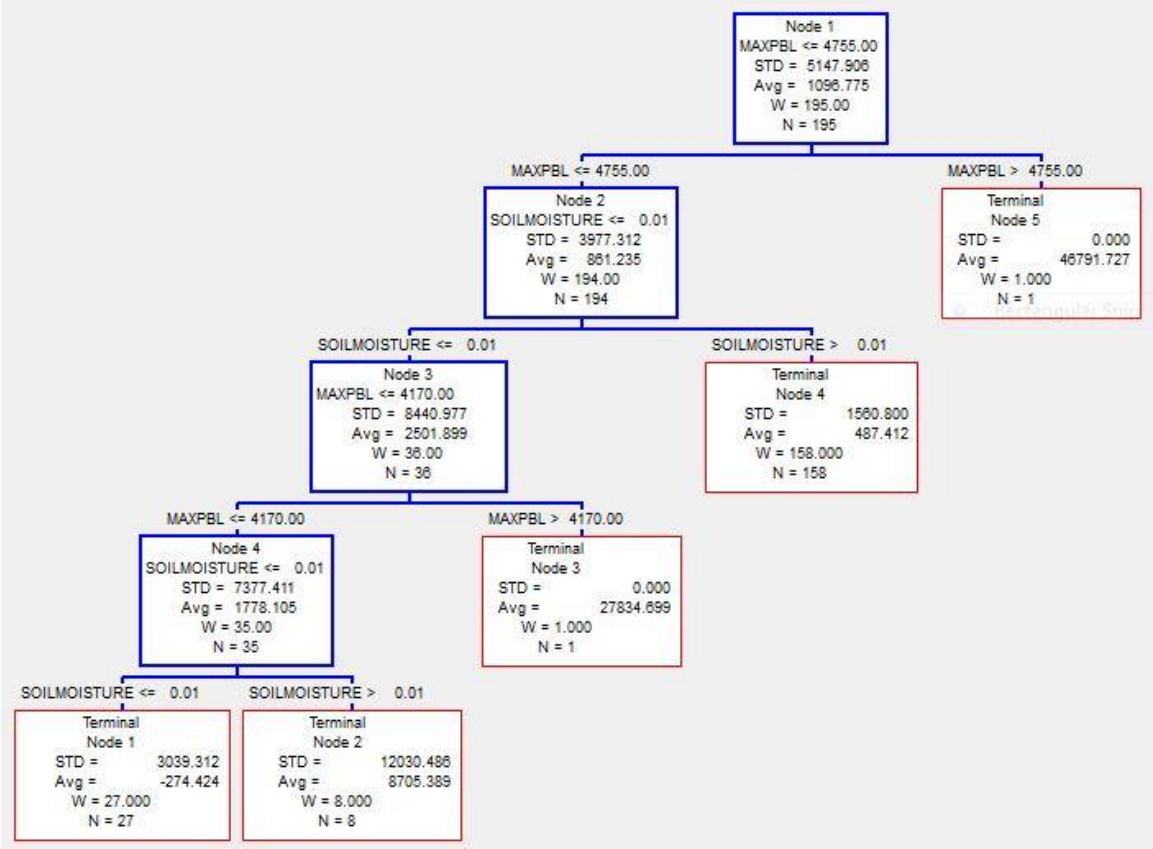

Figure 3.14: The regression tree built from the Hardy dataset. The regression tree terminal nodes contain a node-specific average and standard deviation of the numeric difference between MODIS and Hardy.

Looking at the variable importance tables and trees for both the classification and regression analysis collectively provides valuable insight. Fuel loadings are present in both variable importance tables, which indicates they play a significant role in determining the BlueSky emissions. The high values of relative importance in Table 3.3 compared to Table 3.4 suggests that while the correct fuel loading is crucial in determining an over or under estimation, it is not as important in determining the numeric difference. Soil moisture is very important in both analyses, indicating that it heavily influences the numeric value of the emissions. The meteorological variables also play important roles in both analyses. Looking at the relative importance of the maximum

PBL height, its role is much more prominent in determining the numeric difference than an over or under estimation. From a meteorological standpoint, the maximum height of the PBL provides insight into the general conditions near the surface. Using that, the maximum PBL height serves as a proxy for the other meteorological variables and is most responsible for the numeric difference. The other meteorological variables do play a strong role in determining an over or under estimation as they have significant values in Table 3.3 and feature in the classification tree.

3.4 Conclusions

Emissions of $PM_{2.5}$ were estimated using MODIS measurements of FRP and modeled using the FCCS and Hardy land cover maps by BlueSky for ten fires in Idaho and Oregon during the summer wildfire season in 2007. These fires were among the largest fires for that season and burned July into September.

Overall, there is little numeric agreement between the emissions from MODIS and BlueSky, with frequent instances of large differences in the emissions. There is fair agreement in the trend of emissions from most fires despite the differences in the amount of emissions estimated during the fire's lifetime. From the CART analysis, the drivers for the over or under estimation of emissions by BlueSky are the collective fuel loadings and soil moisture. The numeric difference is driven by the meteorological conditions, with a significant contribution from soil moisture. The presence of the meteorological conditions as a driver for the numeric difference between the emissions estimates legitimizes our assumptions regarding the daily emissions profile.

Significant gaps remain between top-down and bottom-up methods to estimating emissions from biomass burning. The most significant factors separating the value of the emissions from two methods are fuel loading, soil moisture, and meteorology. While bottom-up methods utilize fuel loading in their algorithms, evidence suggests that it is a factor that requires improvement. Soil moisture and meteorological data are absent from most methods. The feasibility of incorporating soil moisture and meteorology into global estimates of emissions and their impact requires further investigation.

3.5 Acknowledgments

The author would like to thank the National Science Foundation, Award 0914764, for funding this research.

The author would to thank Dr. Joseph Vaughn, Soumita Kundu, and Levi Golston for their insights regarding the BlueSky framework and assistants in data compilation.

The author would like to thank his advisor, Dr. Fok-Yan Leung, for his support and guidance during the entire research process.

References

Boschetti, L., Roy, D. P., 2009. Strategies for the fusion of satellite fire radiative power with burned area data for fire radiative energy derivation. Journal of Geophysical Research, 114, D20302.

De'ath, G., Fabricius, K. E., 2000. Classification and regression trees: a powerful yet simple technique for ecological data analysis. Ecology, 81 (11), 3178-3192.

Hoelzemann, J. J., Shultz, M. G., Brasseur, G. P., Granier, C., 2004. Global wildland fire emission model (GWEM): evaluating the use of global area burnt satellite data. Journal of Geophysical Research, 109, D14S04.

Ichoku, C., Kaufman, Y.J., 2005. A method to derive smoke emission rates from MODIS fire radiative energy measurements. IEEE Transactions on Geoscience and Remote Sensing, 43(11), 2626-2649.

Ito, A., Penner, J. E., 2004. Global estimates of biomass burning emissions based on satellite imagery for the year 2000. Journal of Geophysical Research, 109, D14S05.

Kaiser, J. W., Heil, A., Andreae, M. O., Benedetti, A., Chubarova, N., Jones, L., Morcette, J.-J., Razinger, M., Shultz, M. G., Suttie, M., van der Werf, G. R., 2012. Biomass burning emissions estimated with a global fire assimilation system based on observed fire radiative power. Biogeosciences, 9, 527-554.

Larkin, N. K., O'Neill, S. M., Solomon, R., Raffuse, S., Strand, T., Sullivan, D. C., Krull, C., Rorig, M., Peterson, J. L., Ferguson, S. A., 2009. The BlueSky smoke modeling framework. International Journal of Wildland Fire, 18, 906-920.

Leavesley, G., David, O., Garen, D., Goodbody, A., Lea, J., Marron, J., Perkins, T., Strobel, M., Tama, R., 2010. A modeling framework for improved agricultural water-supply forecasting.

Reid, J. S., Koppmann, R., Eck, T. F., Eleuterio, D. P., 2005. A review of biomass burning emissions part II: intensive physical properties of biomass burning particles. Atmospheric Chemistry and Physics, 5, 799-825.

Seiler, W., Crutzen, P. J., 1980. Estimates of gross and net fluxes of carbon between the biosphere and the atmosphere from biomass burning. Climatic Change, 2, 207-247.

Simon, M., Plummer, S., Fierens, F., Hoelzemann, J. J., Arino, O., 2004. Burnt area detection at global scale using ATSR-2: the GLOBSCAR products and their qualification. Journal of Geophysical Research, 109, D14S02.

van der Werf, G. R., Randerson, J. T., Giglio, L., Collatz, G. J., Mu, M., Kasibhatla, P. S., Morton, D. C., DeFries, R. S., Jin, Y., van Leeuven, T. T., 2010. Global fire emissions and the contribution of deforestation, savanna, forest, agricultural, and peat fires (1997-2009). Atmospheric Chemistry and Physics, 10, 11707-11735.

Wiedinmyer, C., Akagi, S. K., Yokelson, R. J., Emmons, L. K., Al-Saadi, J. A., Orlando, J. J., Soja, A. J., 2011. The fire inventory from NCAR (FINN): a high resolution global model to estimate the emissions from open burning. Geoscientific Model Development, 4, 625-641.

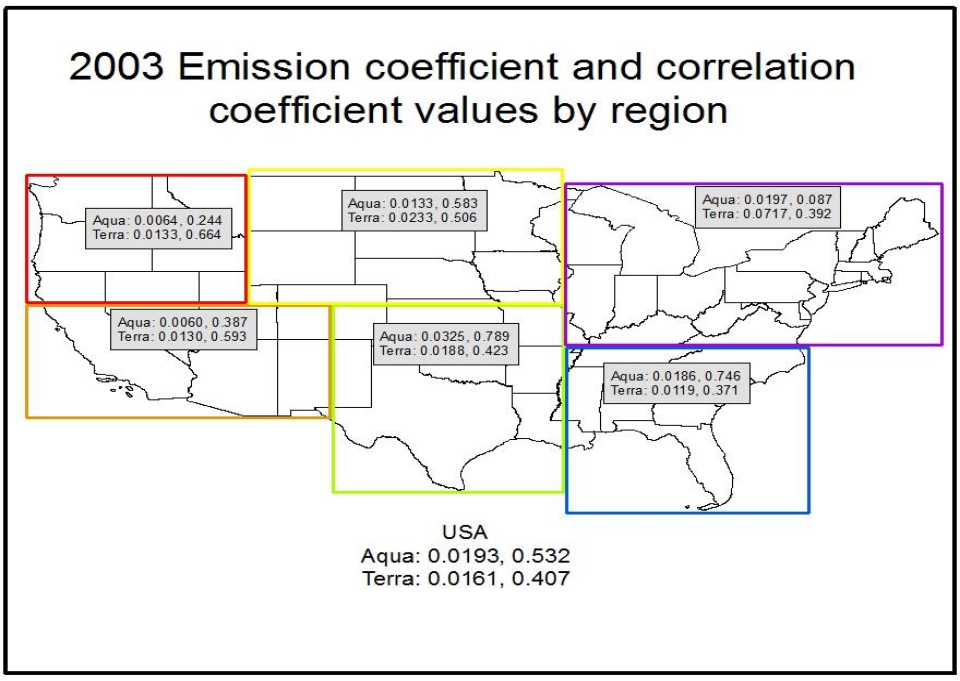

Figure A.1: U.S. and regional emission coefficients for 2003

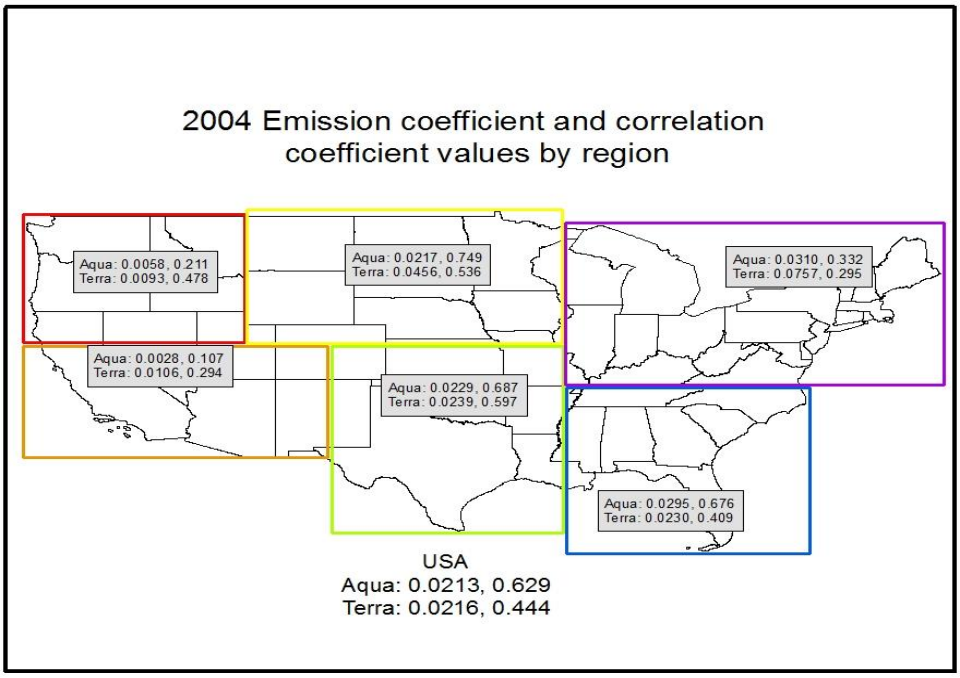

Figure A.2: U.S. and regional emission coefficients for 2004

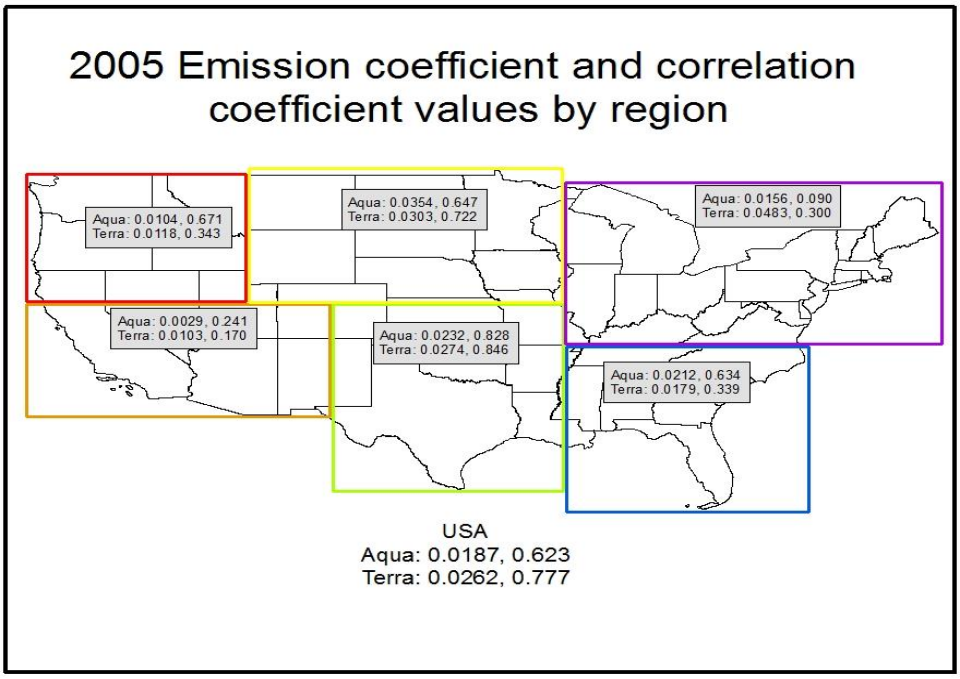

Figure A.3: U.S. and regional emission coefficients for 2005

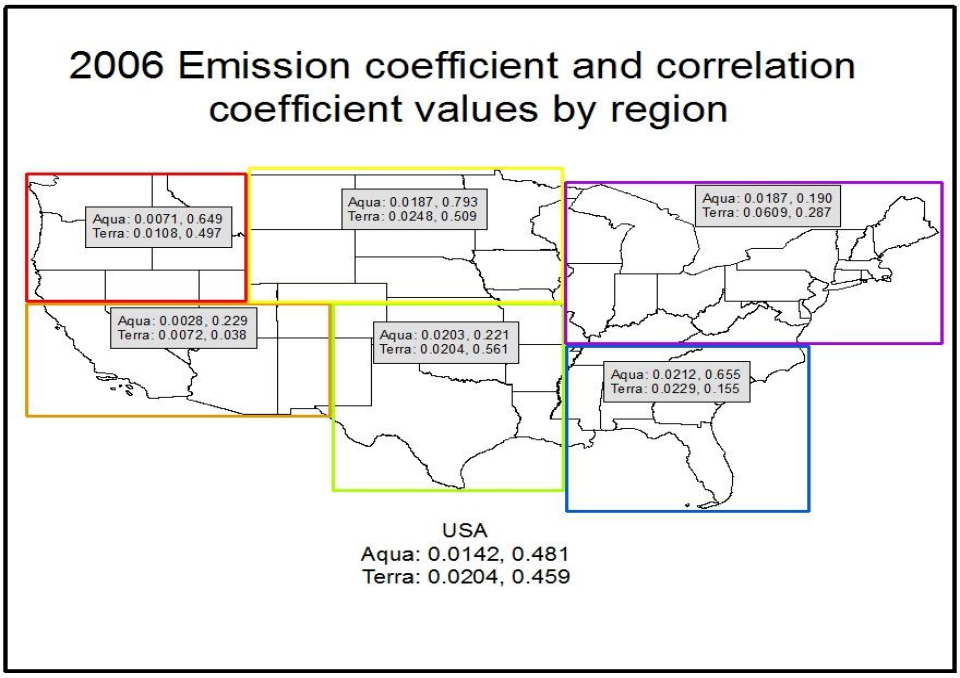

Figure A.4: U.S. and regional emission coefficients for 2006

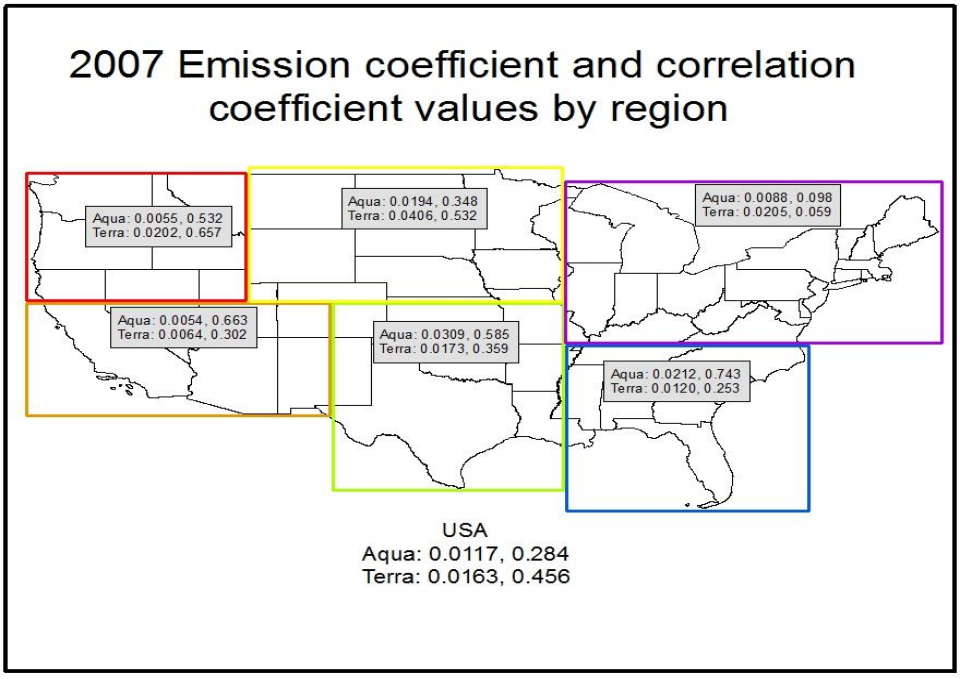

Figure A.5: U.S. and regional emission coefficients for 2007

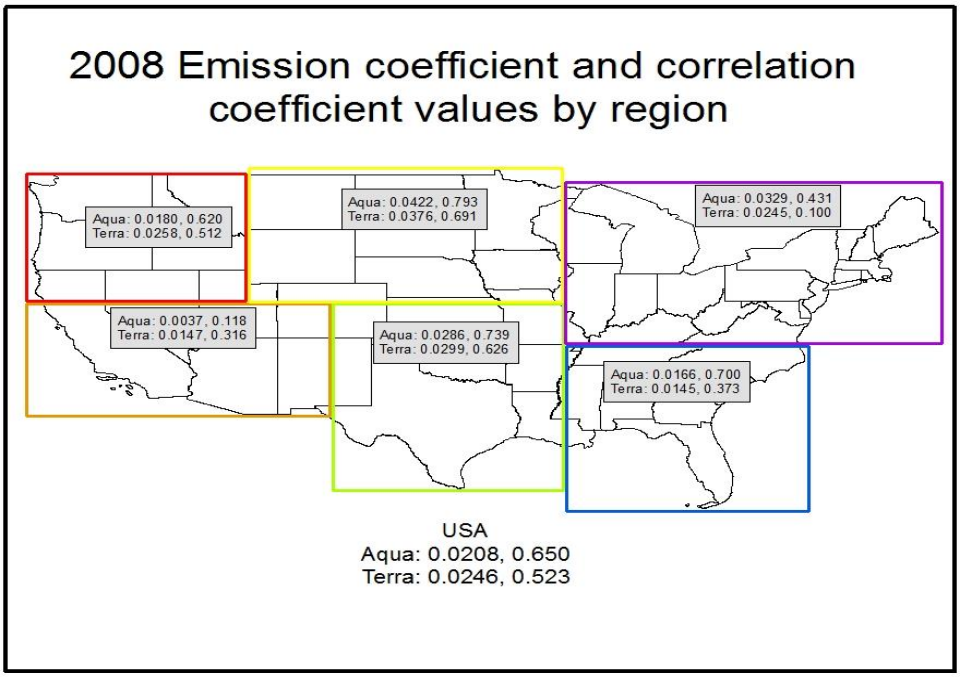

Figure A.6: U.S. and regional emission coefficients for 2008

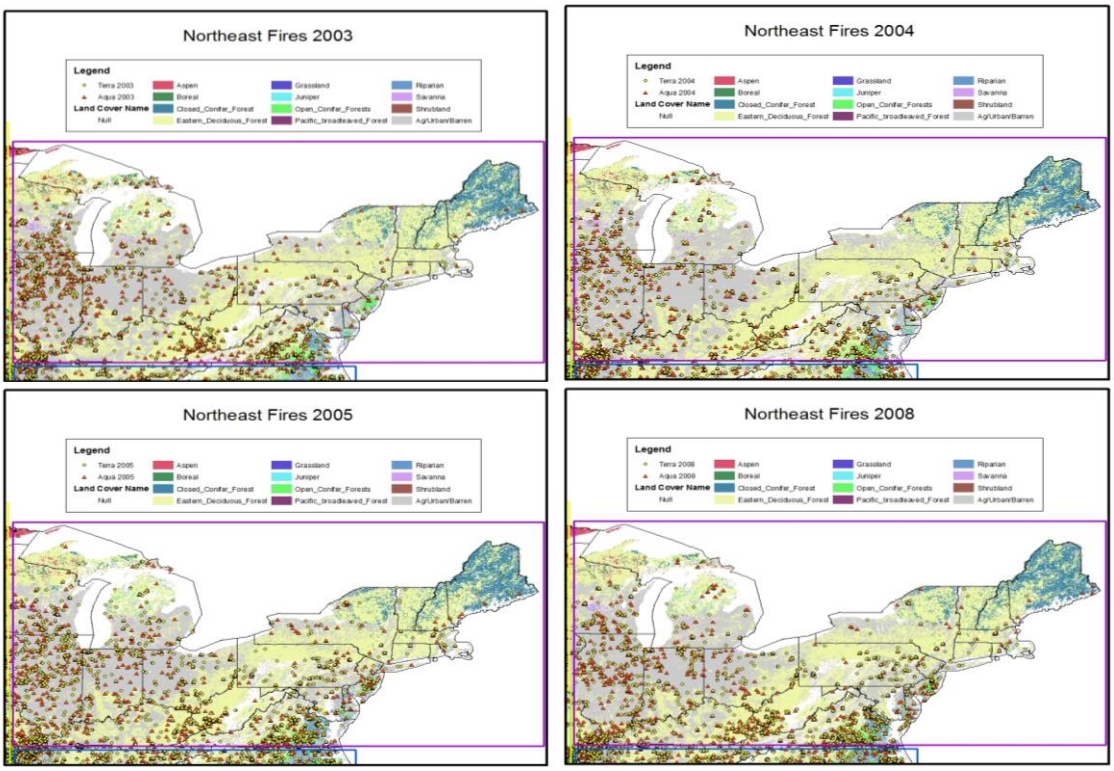

Figure A.7: Northeast fire detections for 2003, 2004, 2005, and 2008.

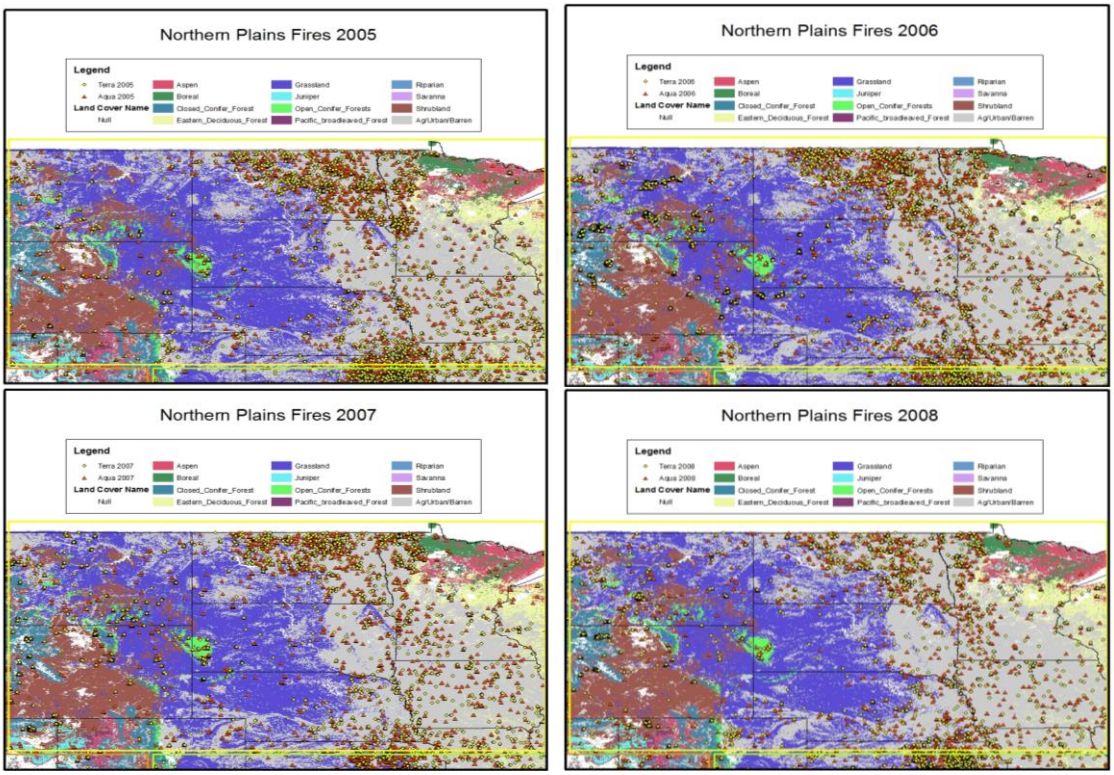

Figure A.8: Northern Plains fire detections for 2005, 2006, 2007, and 2008.

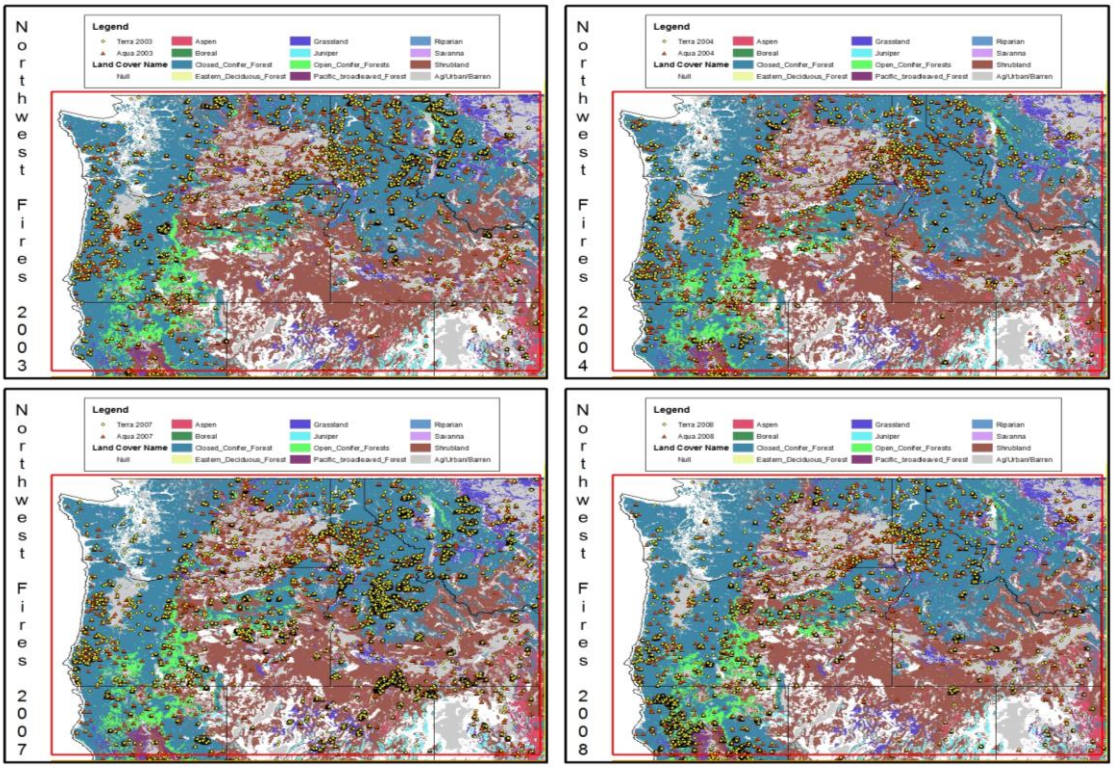

Figure A.9: Northwest fire detections for 2003, 2004, 2007, and 2008.

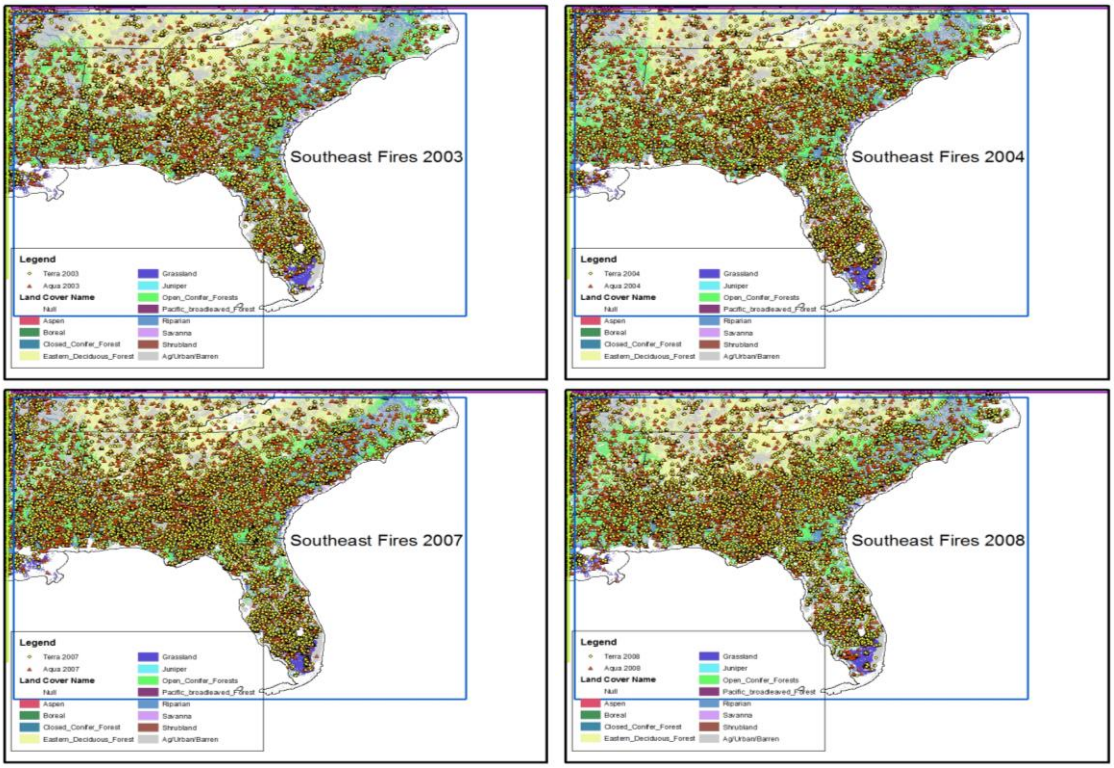

Figure A.10: Southeast fire detections for 2003, 2004, 2007, and 2008.

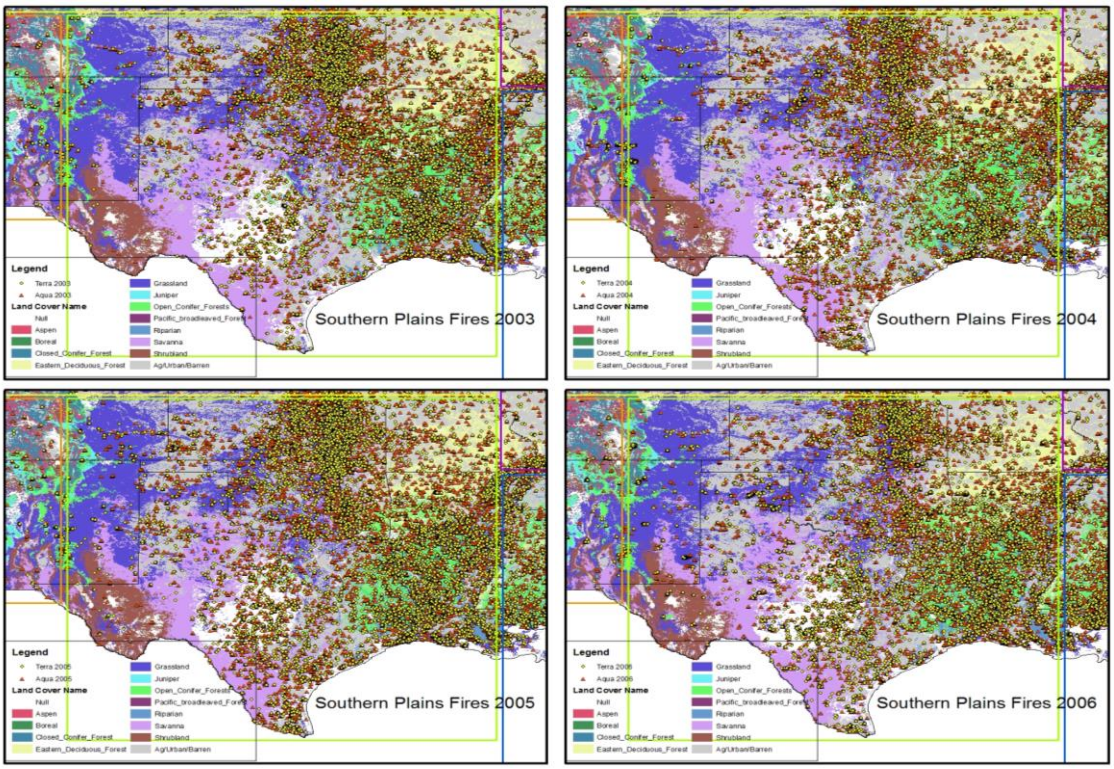

Figure A.11: Southern Plains fire detections for 2003, 2004, 2005, and 2006.

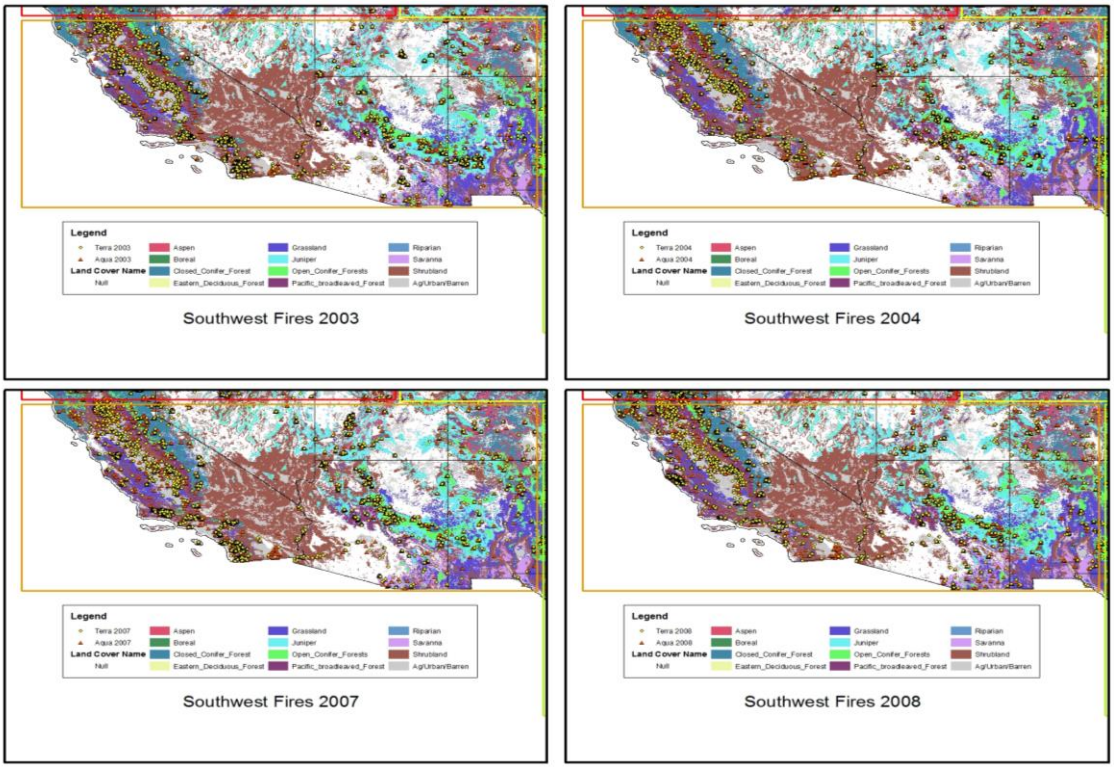

Figure A.12: Southwest fire detections for 2003, 2004, 2007, and 2008.

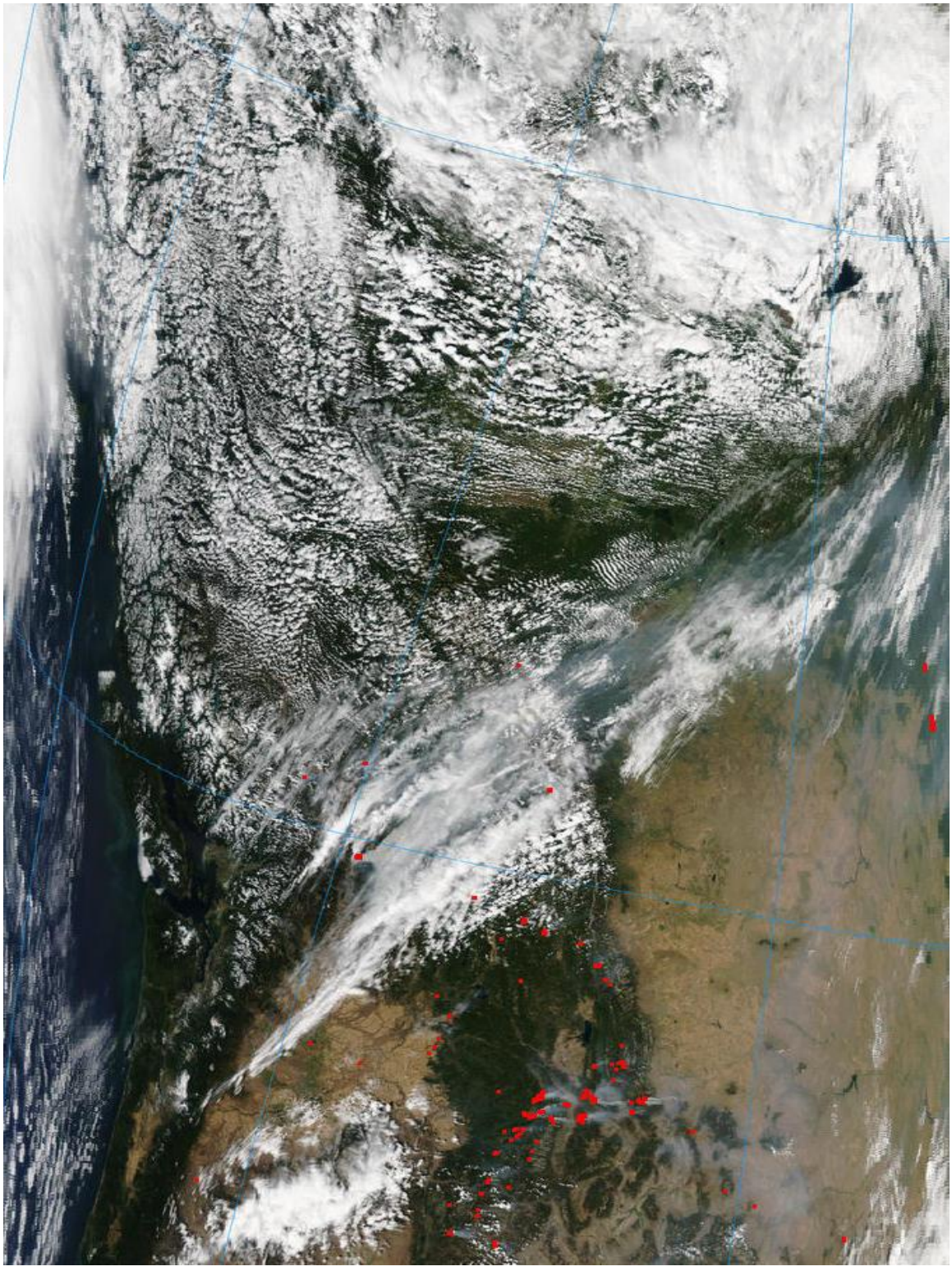

Figure A.13: Aqua visible image with overlaid fire detections for Julian day 231 in 2003. Very low M_x is calculated despite very high R_{fre}.

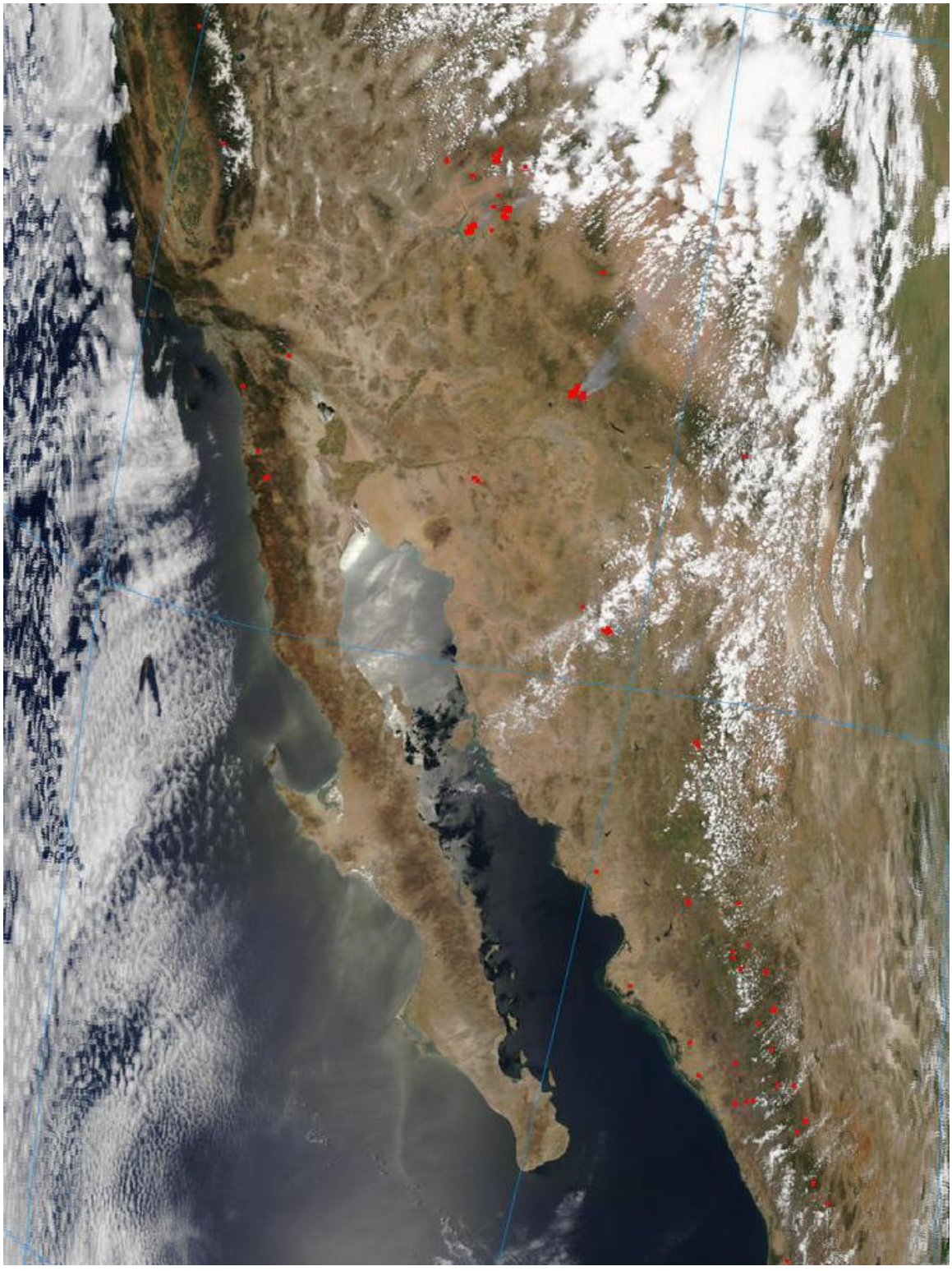

Figure A.14: Aqua visible image with overlaid fire detections for Julian day 179 in 2005. Very low M_x is calculated despite very high R_{fre}.

Table A.1: US Aqua fire pixel detections and number of data points by land cover types (fire pixels, N)

Land Type	2003 (FP, N)	2004 (FP, N)	2005 (FP, N)	2006 (FP, N)	2007 (FP, N)	2008 (FP, N)
Null	618, 162	749, 157	1008, 193	1109, 180	1249, 177	934, 181
Aspen	16, 9	11, 6	10, 6	20, 9	36, 7	17, 10
Boreal	30, 8	5, 2	12, 7	9, 3	19, 6	3, 2
Closed Coniferous Forest	2163, 86	579, 57	703, 67	2075, 90	2314, 80	2240, 93
Eastern Deciduous Forest	1350, 125	1273, 102	1235, 136	1674, 145	1607, 140	1292, 123
Grassland	1548, 138	2174, 117	2357, 143	1030, 153	1060, 135	2014, 133
Juniper	74, 16	59, 14	126, 25	76, 23	131, 25	74, 20
Open Coniferous Forest	2290, 223	2312, 191	2814, 242	3555, 261	3223, 235	3407, 239
Pacific Broadleaved Forest	53, 18	110, 26	117, 18	79, 20	150, 22	422, 31
Riparian	526, 126	508, 85	715, 138	930, 148	810, 112	638, 126
Savanna	587, 53	474, 62	613, 87	240, 69	399, 62	523, 82
Shrubland	333, 63	197, 62	431, 71	513, 64	926, 80	312, 70
Ag/Urban/ Barren	8563, 426	8239, 452	8122, 500	6266, 453	6991, 457	7544, 428

Table A.2: US Terra fire pixel detections and number of data points by land cover types (fire pixels, N)

Land Type	2003 (FP, N)	2004 (FP, N)	2005 (FP, N)	2006 (FP, N)	2007 (FP, N)	2008 (FP, N)
Null	626, 164	577, 168	815, 214	981, 227	960, 215	849, 197
Aspen	13, 8	8, 5	14, 8	11, 6	14, 6	6, 4
Boreal	10, 4	4, 3	4, 2	7, 3	17, 4	0, 0
Closed Coniferous Forest	1358, 98	527, 66	418, 54	1081, 80	1497, 74	1373, 89
Eastern Deciduous Forest	599, 107	681, 128	777, 138	840, 148	850, 150	891, 156
Grassland	540, 116	504, 102	1064, 125	767, 123	404, 150	876, 140
Juniper	89, 31	66, 15	51, 18	44, 16	57, 17	22, 9
Open Coniferous Forest	1681, 216	1587, 205	1961, 252	2921, 268	2171, 248	2182, 250
Pacific Broadleaved Forest	46, 18	62, 18	26, 14	37, 20	174, 30	223, 39
Riparian	295, 90	371, 102	491, 144	495, 130	580, 136	436, 122
Savanna	232, 62	268, 48	394, 78	174, 62	237, 68	282, 70
Shrubland	188, 61	111, 53	279, 61	323, 59	465, 71	172, 59
Ag/Urban/ Barren	3872, 491	3632, 510	5609, 557	4416, 523	4505, 546	4342, 533

Table A.3: Northeast Aqua fire pixel detections and number of data points by land cover types (fire pixels, N)

Land Type	2003 (FP, N)	2004 (FP, N)	2005 (FP, N)	2006 (FP, N)	2007 (FP, N)	2008 (FP, N)
Null	44, 25	19, 14	23, 16	21, 13	33, 15	31, 22
Eastern Deciduous Forest	139, 39	89, 27	186, 44	143, 40	125, 36	122, 40
Open Coniferous Forest	17, 6	28, 9	26, 8	21, 10	22, 10	19, 8
Riparian	5, 4	9, 4	5, 5	17, 6	0, 0	9, 6
Savanna	3, 3	5, 4	5, 4	0, 0	3, 3	3, 3
Ag/Urban/ Barren	520, 78	380, 71	478, 94	357, 76	466, 101	399, 72

Table A.4: Northeast Terra fire pixel detections and number of data points by land cover types (fire pixels, N)

Land Type	2003 (FP, N)	2004 (FP, N)	2005 (FP, N)	2006 (FP, N)	2007 (FP, N)	2008 (FP, N)
Null	32, 19	18, 13	58, 39	38, 29	54, 30	56, 33
Eastern Deciduous Forest	72, 32	50, 23	108, 37	112, 40	101, 38	147, 55
Open Coniferous Forest	19, 10	7, 6	37, 21	8, 6	15, 11	39, 18
Riparian	6, 6	0, 0	4, 3	9, 6	4, 3	18, 8
Savanna	3, 3	0, 0	0, 0	4, 3	4, 3	0, 0
Ag/Urban/ Barren	485, 97	462, 102	832, 132	696, 115	721, 112	736, 118

Table A.5: Northern Plains Aqua fire pixel detections and number of data points by land cover types (fire pixels, N)

Land Type	2003 (FP, N)	2004 (FP, N)	2005 (FP, N)	2006 (FP, N)	2007 (FP, N)	2008 (FP, N)
Null	41, 17	33, 18	36, 14	33, 17	20, 10	10, 5
Eastern Deciduous Forest	56, 9	48, 14	29, 11	29, 12	19, 13	11, 6
Grassland	215, 45	229, 37	356, 30	342, 40	164, 40	245, 32
Open Coniferous Forest	77, 11	15, 6	5, 3	83, 13	7, 6	17, 6
Shrubland	82, 14	6, 4	29, 9	120, 10	24, 9	17, 7
Ag/Urban/ Barren	1269, 85	1133, 87	892, 91	957, 105	771, 76	601, 79

Table A.6: Northern Plains Terra fire pixel detections and number of data points by land cover types (fire pixels, N)

Land Type	2003 (FP, N)	2004 (FP, N)	2005 (FP, N)	2006 (FP, N)	2007 (FP, N)	2008 (FP, N)
Null	21, 9	6, 4	17, 9	38, 11	19, 10	12, 5
Eastern Deciduous Forest	15, 8	30, 10	23, 8	23, 9	19, 8	14, 6
Grassland	120, 39	85, 24	104, 23	234, 27	60, 28	94, 28
Open Coniferous Forest	28, 9	6, 4	0, 0	68, 12	14, 6	0, 0
Shrubland	42, 9	14, 8	14, 7	62, 8	7, 6	11, 6
Ag/Urban/ Barren	576, 86	474, 75	694, 80	653, 93	517, 106	356, 81

Table A.7: Northwest Aqua fire pixel detections and number of data points by land cover types (fire pixels, N)

Land Type	2003 (FP, N)	2004 (FP, N)	2005 (FP, N)	2006 (FP, N)	2007 (FP, N)	2008 (FP, N)
Null	13, 8	24, 14	14, 7	78, 17	169, 24	27, 17
Closed Coniferous Forest	1609, 68	528, 48	643, 50	2039, 77	2345, 65	1998, 78
Grassland	48, 17	36, 14	29, 16	50, 18	88, 12	48, 11
Open Coniferous Forest	107, 23	78, 20	46, 14	196, 32	153, 27	546, 42
Pacific Broadleaved Forest	6, 4	25, 6	0, 0	17, 9	0, 0	101, 12
Shrubland	118, 26	83, 29	146, 29	243, 25	470, 37	159, 38
Ag/Urban/ Barren	346, 67	405, 67	308, 61	365, 58	389, 60	384, 65

Table A.8: Northwest Terra fire pixel detections and number of data points by land cover types (fire pixels, N)

Land Type	2003 (FP, N)	2004 (FP, N)	2005 (FP, N)	2006 (FP, N)	2007 (FP, N)	2008 (FP, N)
Null	25, 13	9, 7	21, 12	33, 11	85, 22	26, 15
Closed Coniferous Forest	1068, 74	443, 52	408, 46	1058, 65	1667, 56	1336, 70
Grassland	20, 8	26, 17	37, 15	31, 13	57, 15	27, 16
Open Coniferous Forest	64, 19	44, 18	17, 10	69, 22	89, 17	290, 30
Pacific Broadleaved Forest	6, 4	11, 6	0, 0	16, 10	0, 0	69, 14
Shrubland	65, 24	46, 22	118, 25	212, 31	192, 29	73, 27
Ag/Urban/ Barren	318, 74	284, 76	277, 70	230, 69	194, 68	167, 62

Table A.9: Southeast Aqua fire pixel detections and number of data points by land cover types (fire pixels, N)

Land Type	2003 (FP, N)	2004 (FP, N)	2005 (FP, N)	2006 (FP, N)	2007 (FP, N)	2008 (FP, N)
Null	167, 62	226, 47	306, 71	625, 74	548, 59	391, 60
Eastern Deciduous Forest	494, 59	538, 63	560, 79	843, 76	941, 80	714, 70
Grassland	33, 13	24, 11	29, 13	79, 21	64, 18	77, 13
Open Coniferous Forest	1153, 96	1149, 105	1373, 126	1930, 126	1783, 129	1702, 116
Riparian	255, 71	299, 56	427, 85	629, 94	576, 84	412, 75
Ag/Urban/ Barren	1002, 116	1087, 127	1688, 138	1302, 137	1434, 141	1336, 131

Table A.10: Southeast Terra fire pixel detections and number of data points by land cover types (fire pixels, N)

Land Type	2003 (FP, N)	2004 (FP, N)	2005 (FP, N)	2006 (FP, N)	2007 (FP, N)	2008 (FP, N)
Null	208, 55	261, 74	276, 74	391, 98	343, 82	320, 76
Eastern Deciduous Forest	318, 58	394, 74	431, 81	461, 82	458, 85	578, 102
Grassland	14, 7	9, 6	13, 9	46, 16	27, 9	57, 14
Open Coniferous Forest	797, 99	904, 101	1084, 130	1090, 153	1307, 150	1172, 129
Riparian	169, 52	244, 62	264, 79	288, 87	431, 95	281, 74
Ag/Urban/ Barren	979, 153	1144, 162	1773, 189	1531, 187	1494, 192	1333, 175

Table A.11: Southern Plains Aqua fire pixel detections and number of data points by land cover types (fire pixels, N)

Land Type	2003 (FP, N)	2004 (FP, N)	2005 (FP, N)	2006 (FP, N)	2007 (FP, N)	2008 (FP, N)
Null	225, 75	371, 68	456, 75	278, 62	406, 70	377, 74
Eastern Deciduous Forest	545, 49	436, 29	349, 37	459, 45	406, 42	226, 33
Grassland	1053, 73	857, 62	986, 82	449, 74	679, 69	1258, 80
Open Coniferous Forest	959, 72	582, 48	703, 81	762, 74	581, 56	607, 62
Riparian	233, 56	140, 28	217, 56	234, 59	163, 33	187, 57
Savanna	544, 45	454, 54	551, 77	232, 60	402, 55	500, 72
Ag/Urban/ Barren	2079, 140	1536, 130	2034, 179	1234, 140	1500, 132	1825, 137

Table A.12: Southern Plains Terra fire pixel detections and number of data points by land cover types (fire pixels, N)

Land Type	2003 (FP, N)	2004 (FP, N)	2005 (FP, N)	2006 (FP, N)	2007 (FP, N)	2008 (FP, N)
Null	298, 64	257, 64	341, 76	437, 75	408, 71	393, 72
Eastern Deciduous Forest	157, 30	180, 33	163, 35	158, 40	168, 36	78, 27
Grassland	316, 52	353, 51	870, 77	408, 60	241, 58	659, 78
Open Coniferous Forest	552, 62	473, 64	676, 86	631, 80	556, 71	470, 72
Riparian	101, 35	118, 36	202, 64	168, 55	116, 41	122, 47
Savanna	208, 52	245, 45	383, 72	162, 54	219, 62	276, 66
Ag/Urban/ Barren	911, 139	766, 126	1451, 165	898, 140	929, 150	1094, 155

Table A.13: Southwest Aqua fire pixel detections and number of data points by land cover types (fire pixels, N)

Land Type	2003 (FP, N)	2004 (FP, N)	2005 (FP, N)	2006 (FP, N)	2007 (FP, N)	2008 (FP, N)
Null	4, 4	11, 9	95, 20	11, 8	16, 9	16, 9
Closed Coniferous Forest	265, 21	8, 6	49, 12	53, 13	45, 15	143, 23
Grassland	25, 7	5, 5	28, 13	18, 11	40, 11	26, 10
Juniper	65, 12	43, 12	135, 23	57, 20	59, 20	72, 18
Open Coniferous Forest	243, 36	83, 16	191, 31	215, 28	185, 28	143, 29
Pacific Broadleaved Forest	42, 13	98, 22	128, 17	60, 13	165, 20	289, 27
Shrubland	127, 24	93, 27	222, 36	119, 24	270, 30	100, 23
Ag/Urban/ Barren	334, 61	262, 69	187, 64	183, 55	183, 65	172, 65

Table A.14: Southwest Terra fire pixel detections and number of data points by land cover types (fire pixels, N)

Land Type	2003 (FP, N)	2004 (FP, N)	2005 (FP, N)	2006 (FP, N)	2007 (FP, N)	2008 (FP, N)
Null	19, 15	24, 14	68, 21	27, 18	16, 12	11, 9
Closed Coniferous Forest	233, 22	49, 8	27, 11	52, 12	33, 18	121, 21
Grassland	25, 18	13, 10	19, 11	31, 14	21, 13	17, 12
Juniper	80, 26	58, 12	55, 17	36, 11	41, 13	18, 6
Open Coniferous Forest	191, 32	123, 23	89, 24	89, 17	112, 23	98, 27
Pacific Broadleaved Forest	35, 11	50, 12	28, 13	22, 11	175, 29	226, 30
Shrubland	84, 23	38, 19	130, 31	70, 21	216, 34	53, 25
Ag/Urban/ Barren	381, 81	290, 89	287, 92	174, 69	226, 70	294, 98

GLOSSARY

ABBA – Automated Biomass Burning Algorithm

ATSR-2 – Along Track Scanning Radiometer

AVHRR – Advanced Very High Resolution Radiometer

AOT – Aerosol optical thickness

BSF – BlueSky Framework

CART – Classification and Regression Trees

C_e – MODIS derived emission coefficient

EOS – Earth Observing Satellites

FCCS 2 – Fuel Characteristic Classification System Version 2

FEPS – Fire Emissions Production Simulation

FRE – Fire radiative energy (MJ)

FRP – Fire radiative power (MW)

FINN – Fire Inventory for NCAR

GBA-2000 – Global Burned Area for 2000

GFAS – Global Fire Assimilation System

GFED – Global Fire Emissions Database

GLOBSCAR - Global Burnt SCAR monthly burned area dataset

GMT – Greenwich Mean Time

GOES – Geostationary Operational Environmental Satellites

GWEM – Global Wildland fire Emissions Model

HMS – NOAA Hazard Mapping System

MODIS – Moderate Resolution Imaging Spectroradiometer

MM5 – National Center for Atmospheric Research/Penn State Mesoscale Meteorological Model

M_x – rate of emission of species x

N – the total number of MODIS overpasses

NASA – National Aeronautic and Space Agency

NCEP/NCAR – National Center for Environmental Prediction/Nation Center for Atmospheric Research

NDVI – Normalized Difference Vegetation Index

NFDRS – US National Fire Danger Rating System

PBL – Planetary Boundary Layer

PM – Particulate Matter

R_{fre} – rate of emission of fire radiant energy

SEVRI – Spinning Enhanced Visible and Infra-Red Imager

SMARTFIRE – Satellite Mapping Automatic Reanalysis Tool for Fire Incident Reconciliation

SNOTEL - Snowpack Telemetry

SPOT 4 – Systèm Pour l'Observation de la Terre 4

USGS – United States Geological Survey

VIIRS – Visible Infrared Imaging Radiometer Suite

WRF – Weather Research and Forecasting Model